Probing the Solid-Liquid Interface using Single-Molecule Dynamics

By Nathaniel Nelson

B.S, University of Florida – 2009

A thesis submitted to the Faculty of the Graduate School of the University of Colorado in partial fulfillment of the requirement for the degree of Doctor of Philosophy

Department of Chemical and Biological Engineering

2014

This thesis entitled:

Probing the Solid-Liquid Interface using Single-Molecule Dynamics

written by Nathaniel Steele Nelson

has been approved for the Department of Chemical and Biological Engineering

_____

Daniel K. Schwartz

_____

Andrew Goodwin

*Date*_____

The final copy of this thesis has been examined by the signatories, and we Find that both the content and the form meet acceptable presentation standards Of scholarly work in the above mentioned discipline.

Abstract

Nelson, Nathaniel Steele (PhD, Chemical and Biological Engineering Department)

Probing the Solid-Liquid Interface Using Single Molecule Dynamics

Thesis directed by Professor Daniel K. Schwartz

Molecular interactions with solid-liquid interfaces have long been studied through macroscopic observations. There were, however, only a limited number of ways to observe true molecular phenomena leading to a wide discrepancy between theoretical models and experimental results. The work presented here uses total internal reflection fluorescence (TIRF) microscopy to image individual molecules at the solid-liquid interface as they undergo the dynamic processes of adsorption, diffusion, and desorption.

Studying these dynamic behaviors at the single-molecule level allowed great insight into the macroscopically observed hydrophobic effect as well as the Hofmeister effect. The hydrophobic effect was probed by looking at the response of individual molecules to surfaces with varying alkyl chain lengths. These experiments showed that surface residence time increased and mobility decreased with increasing alkyl chain length despite all of the surfaces having the same nominal hydrophobicity. Experiments using the salts NaF and NaSCN dissolved in water along with a fatty acid probe molecule were conducted to examine the Hofmeister effect at the molecular level. These experiments showed a dramatic change in adsorption rate of the hydrophobic probe onto a hydrophobic surface, but minimal change in diffusion or desorption rate.

We used the knowledge that molecular probes interact with specific surface chemistries very differently to develop a super-resolution imaging technique called MAPT (mapping using accumulated probe trajectories). MAPT created images of a surface using each molecular behavior

(e.g. diffusion) as a contrast mechanism. These images were first used to show variations in hydrophobicity on a photopatterned self-assembled monolayer. MAPT images also allowed us to differentiate between the 2D Brownian motion of a molecule on a surface and intermittent 3D flights through solution.

Finally, we developed a technique for identifying surface chemistry using dynamic molecular interactions using an unsupervised Gaussian mixture modeling algorithm. This algorithm identifies regions on a surface that share similar molecular behaviors which can then be compared to the behaviors observed on surfaces of known chemistry. These identifications allow, for the first time, one to create true maps of surface chemistry.

Acknowledgements

I would like to thank the sources of funding that supported my graduate studies including the U.S. Department of Energy Basic Energy Sciences, Chemical Science, Geosciences, and Biosciences Division (DE-SC0001854) and the US National Science Foundation (CHE 0841116)

I would also like to thank my many colleagues and mentors for the many thought provoking conversations and the generous guidance they have provided throughout my research. In particular Dr. Robert Walder proved to be a great guide through my early years as a graduate student. His expertise in physics was invaluable to the advancement of this research.

Finally, I wanted to express my sincerest appreciation for my adviser Dr. Dan Schwartz. His excellent leadership motivated me to continue with my research and made my time at the University of Colorado as enjoyable as possible.

List of Figures

List of Tables

Chapter 1: Introduction

The purpose of this chapter is to provide a fundamental background for observations detailed in this work. A brief introduction to adsorption, diffusion, and desorption is presented accompanied by a brief sampling of techniques that can be used to measure these events. Then, observations by the Schwartz group and others are described to provide context for the experiments presented in this dissertation as part of the broader scientific literature with particular emphasis on single-molecule techniques. Finally, a description of the experimental setup and procedures used in this work is provided to give the reader a picture of how each experiment was performed.

1.1 – Surface/Molecular interactions

The primary focus of this dissertation is measuring the way fluorescent molecules, dissolved in water, interact with a solid interface. These molecules serve as probes into the nature of a wide range of fundamental chemical phenomena such as the hydrophobic effect, specific ion effects, and diffusion. A molecule's interaction with the surface can be separated into three distinct parts; adsorption, surface diffusion, then finally desorption. Each of these three events has been studied in great detail through a wide variety of techniques which are detailed in this chapter.

1.1.1 – Adsorption

When a molecule in solution approaches a surface it experiences a free energy landscape that is markedly different from that in solution. In the case of hydrophobic surfaces in water, there is a change in density of the water which creates a slight barrier to adsorption[1, 2]. An example free

energy diagram as a function of distance from the solid surface is presented in figure 1.1. The adsorption rate for molecules in solution is controlled by the height of the free energy barrier ΔG_{ads}. Adsorption at low molecular surface coverage is controlled by the adsorbate's interaction with the surface as well as how the surface and solvent interact[3]. Adsorption at higher coverages can be impacted by the amount and type of molecules already adsorbed to the surface.

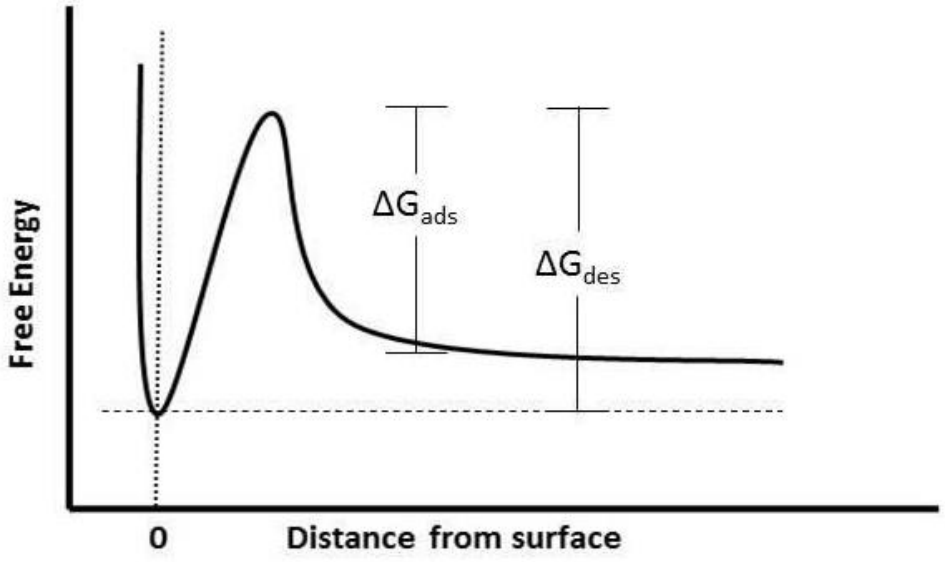

Figure 1.1 – Example free energy diagram for a hydrophobic molecule dissolved in water as a function of distance from a hydrophobic surface.

1.1.2 – Diffusion

Once a molecule has adsorbed to the interface it may undergo diffusion. One method of molecular diffusion can be thought of as Brownian motion in two dimensions[4, 5]. The free energy diagram of this diffusive mode is shown in figure 1.2. The energy barriers to move across the surface are smaller than the energy barrier for the molecule to completely detach from the surface. Another

mechanism for diffusion is where molecules either partially or totally detach from the surface, diffuse in three dimensions for a short period and quickly reattach to the surface[5, 6]. This "flying" mode of diffusion is typically much faster than two dimensional Brownian motion. Using single-molecule methods it is possible to distinguish individual molecular steps and determine frequency of steps and diffusion coefficients for each type of molecular diffusion occurring on the surface.

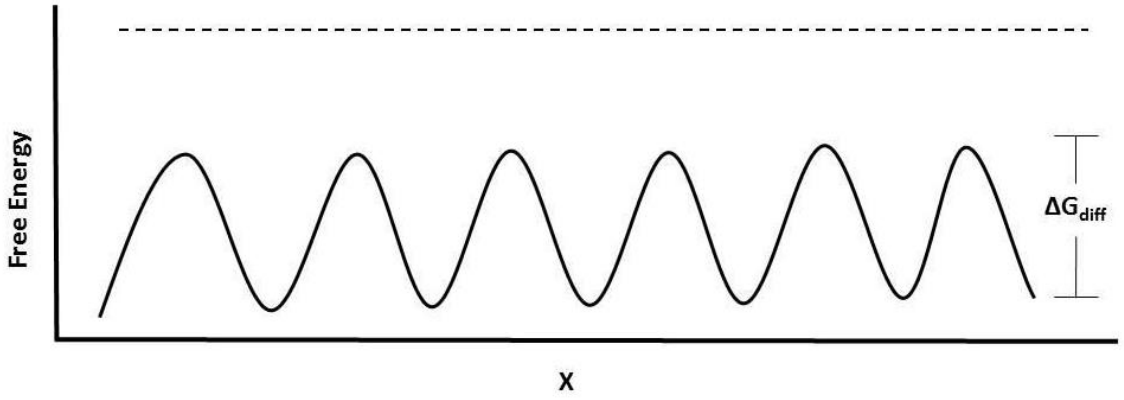

Figure 1.2 – Free energy profile for diffusion across a surface. Dashed line represents ΔG_{des}.

1.1.3 – Desorption

The final stage of a molecule's lifetime on a surface is desorption. This is where a molecule overcomes the energy barrier for reentry into solution shown in Figure 1.1 as ΔG_{des}. In the case of hydrophobic solutes, the barrier to desorption is generally much higher than the barrier to adsorption. The free energy difference between the molecule in solution and the molecule on the surface manifests as the partition coefficient between the two phases while the barrier height controls the kinetics. The time between adsorption and desorption is called the surface residence time. It is important to note that not all molecules interacting with the surface experience the same

free energy profile. Some adsorption sites may be stronger than others leading to a higher ΔG_{des}. This higher energy barrier for desorption will lead to longer surface residence times and consequently more molecules on those regions of the surface.

1.2 – Surface analysis techniques

A significant number of experimental techniques exist that probe molecular interactions with the surface. The first methods were ensemble averaged bulk measurements such as adsorption isotherms calculated by measuring the amount of material adsorbed to a macroscopic surface or fluorescence recovery after photobleaching (FRAP) measurements to study surface diffusion. Adsorption isotherms present surface coverage as a function of pressure or bulk fluid concentration at constant temperature. One way to measure an adsorption isotherm is to employ a quartz crystal microbalance. These microbalances are capable of detecting adsorption at very dilute concentrations and can be used with varying surface chemistry to analyze the adsorption of molecules on various surfaces[7, 8].

FRAP involves photobleaching an area of a surface that has a homogeneous coverage of fluorescent molecules then calculating diffusion coefficients by examining how quickly the non-photobleached molecules diffuse into the photobleached region[9]. This method is excellent at determining average diffusion coefficients for a surface, but has difficulty determining exact mechanisms for diffusion. Another disadvantage is that FRAP does not have very high spatial resolution, making examining surface with micron scale heterogeneities difficult.

More recent approaches attempt to avoid these problems by examining the molecules themselves. One such method is fluorescence correlation spectroscopy or FCS. FCS analyzes the time a

fluorescent probe molecules spend in a sample volume at very high time resolution. Using mathematical models, the user can calculate diffusion coefficients for these molecules through this sample volume. Surface diffusion is studied by simply locating this sample volume at the interface. Recent evidence suggests that this approach does not perform well when molecules exhibit more complex behavior, such as adsorbing and desorbing from the surface being studied.

1.3 – Studying Surfaces with Single Molecules

1.3.1 - Single-molecule Force Spectroscopy

An exceptionally powerful tool for obtaining thermodynamic information about single molecule interactions with a surface is single-molecule force spectroscopy (SMFS)[10, 11]. This technique uses a cantilever with a single molecular probe attached to the tip to probe the association and dissociation forces between the tethered molecule and the surface in question. Figure 1.3 shows a schematic for the SMFS device.

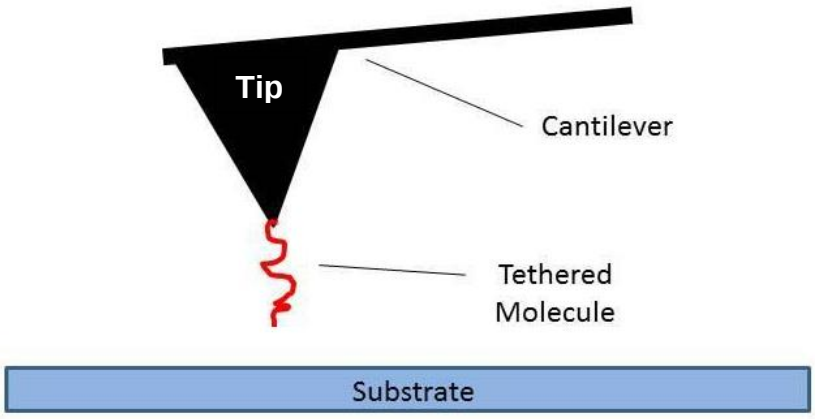

Figure 1.3 – Schematic for single-molecule force spectroscopy device.

One of the premier experiments employing SMFS was the study of hydrophobic interactions between two tethered hexadecane molecules. In these experiments Ray et.al. discovered that the

dissociation energy between two hexadecane molecules was ~41±6 kJ/mol[12]. This was significantly lower than what would be expected for cavitation in water which was one of the proposed reasons for the hydrophobic effect. These experiments also revealed that the hexadecane molecules exhibited an elongated side-by-side association rather than being globular and entangled when adjacent.

While these experiments can provide great insight into fundamental phenomena, such as the hydrophobic effect, they are unable to probe molecular diffusion or spontaneous adsorption and desorption events.

1.3.2 - Fluorescence Correlation Spectroscopy

As discussed above, one of the most commonly used single-molecule experimental techniques is fluorescence correlation spectroscopy (FCS). FCS aims to study the time a fluorescent molecule spends in a very small sample volume by studying the time correlation in the fluorescence signal from that volume[13, 14]. The experimental setup for FCS is shown in figure 1.4. Fluorophores in the sample volume are excited using a laser and fluorescence signal is collected through the microscope objective using a photon multiplier tube. This autocorrelation function for the fluorescence signal is calculated to determine how much time a molecule spends in the sample volume and from that, diffusion coefficients can be calculated[14]. The fluorescence signal has very high time resolution, detecting diffusive events on millisecond time scales.

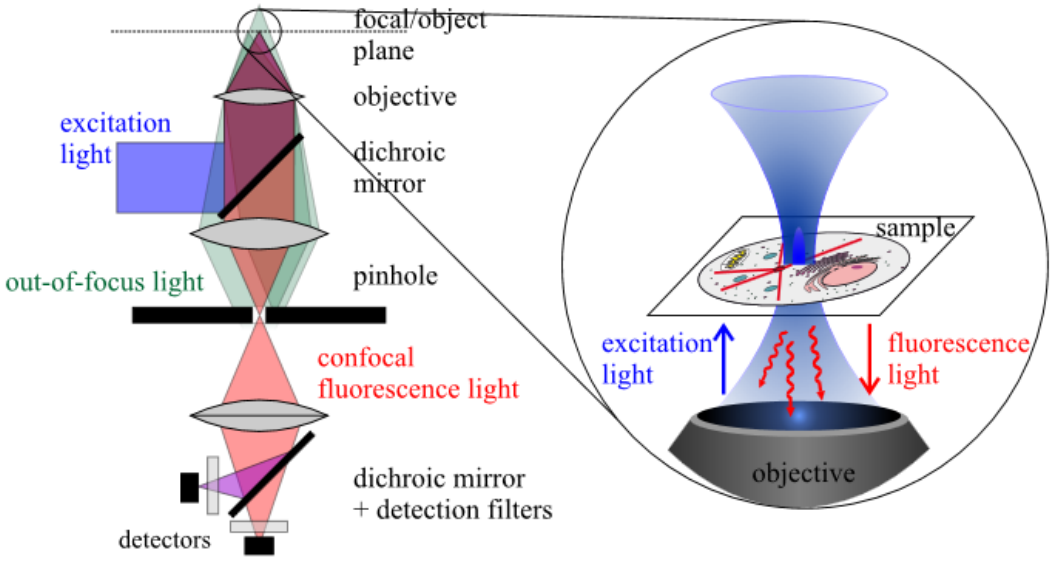

Figure 1.4 – Principle of a confocal microscope[14]

FCS can be a surface sensitive technique by setting the sample volume such that it is located at the surface. In one such experiment researchers analyzed the diffusion of fluorescently labeled polymers on a hydrophobic surface in the presence of various types of dissolved salts[15]. These experiments showed that the observed diffusion coefficient of these polymers had a strong dependence on the specific type of ions in solution. Diffusive behavior roughly followed the Hofmeister series for anions where fluoride ions are known to increase hydrophobic attraction (slowing diffusion) and thiocyanate ions are seen to decrease hydrophobic attraction (speeding diffusion). Unfortunately, the technique is susceptible to misinterpretation of data caused by molecules exiting the volume through means other than lateral diffusion (e.g. desorption) which can yield results that do not accurately represent the true dynamics of the molecules at the interface.

1.3.3 - Single-Molecule TIRF microscopy

Total Internal Reflection Fluorescence (TIRF) microscopy is a technique that uses the total internal reflection of light at an interface that has an index of refraction mismatch. This reflection causes fluorphores near the surface to be excited where fluorphores more than ~100nm away from the surface are not. This generates signal from the surface without the high fluorescence background seen in typical fluorescence setups and with such low background it is possible to identify individual fluorescent molecules as diffraction limited spots. Early experiments using single-molecule TIRF microscopy have produced a number of interesting results. In one such experiment, Honciuc et. al. analyzed the diffusion of fluorescently labeled plamitic acid on fused silica by tracing the molecular trajectories as the probes moved across the surface[4]. These experiments revealed two modes of diffusion, the first being small-scale Brownian motion in two dimensions and the other being large "jumps" which was later revealed to be three dimensional desorption mediated diffusion[5, 6]. An example trajectory from these experiments is shown in figure 1.5. The trajectory in figure 1.5.a clearly experiences periods of 2D Brownian motion separated by large jumps, with some jumps being over 1μm in length. The inset figure (figure 1.5.b) shows the apparent trajectory for an immobilized molecule, effectively demonstrating the spatial resolution for these experiments. This inset also demonstrates that the large and small diffusive steps are not just random noise.

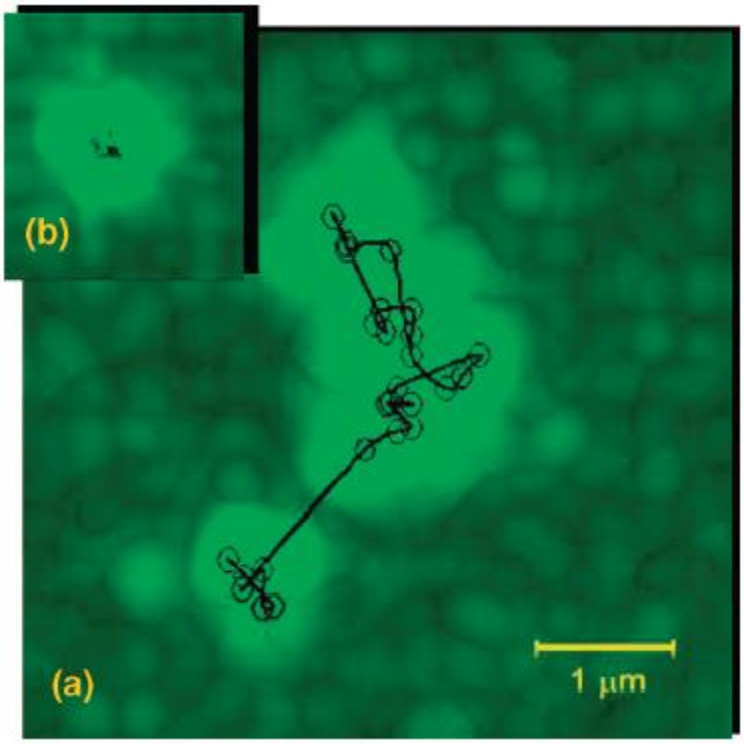

Figure 1.5 - (a) fl-PA molecule tracked for 58 s on the FS surface; the trajectory coordinates are marked by line-connected empty circles. The composite image consists of 29 overlaid frames, each integrated over a 2 s time interval. (b) The apparent trajectory of a stationary molecule on the same scale as in part a, illustrating the effective lateral resolution of the experiment.[4]

This work also used Arrhenius analysis to determine that jumps had a significant activation barrier (~50kJ/mol) while the 2D surface Brownian motion activation barrier was less than ~10 kJ/mol. These activation barriers were hypothesized to be due to the hydrogen bonding between the fused silica surface and the acid group on the fatty acid probe.

Another experiment by Honciuc et.al. used the same TIRF technique, but used it to observe activation barriers for fatty acid attachment to a hydrophilic surface instead of surface diffusion. These experiments demonstrated that the adsorption of molecules to fused silica was controlled by

the solvent/surface interaction and not just the probe/surface interaction with the activation barrier for attachment varying between ~5kJ/mol in hexadecane to ~20kJ/mol in water. It was hypothesized that this apparent activation energy is the energy required to remove a solvent molecule from the surface allowing a probe molecule to adsorb[3].

These experiments are just some of the many studies performed using TIRF. The following chapters detail the results obtained through the use of this technique and their scientific importance.

1.4– Methods

1.4.1 – TIRF Microscopy Setup

The Schwartz group began studying how molecules interact with the surface using total internal reflection fluorescence (TIRF) microscopy. This microscopy technique allows for the detection of individual molecules by creating an evanescent field at the interface between the substrate and the sample volume (Fig. 1.6). This evanescent field only excites a very small volume near the surface which significantly decreases the background fluorescence from solution that is generated by epifluorescence techniques[16, 17]. This decreased background coupled with highly sensitive electron multiplied charge coupled device (EMCCD) cameras allows the user to detect individual molecules as diffraction limited spots.

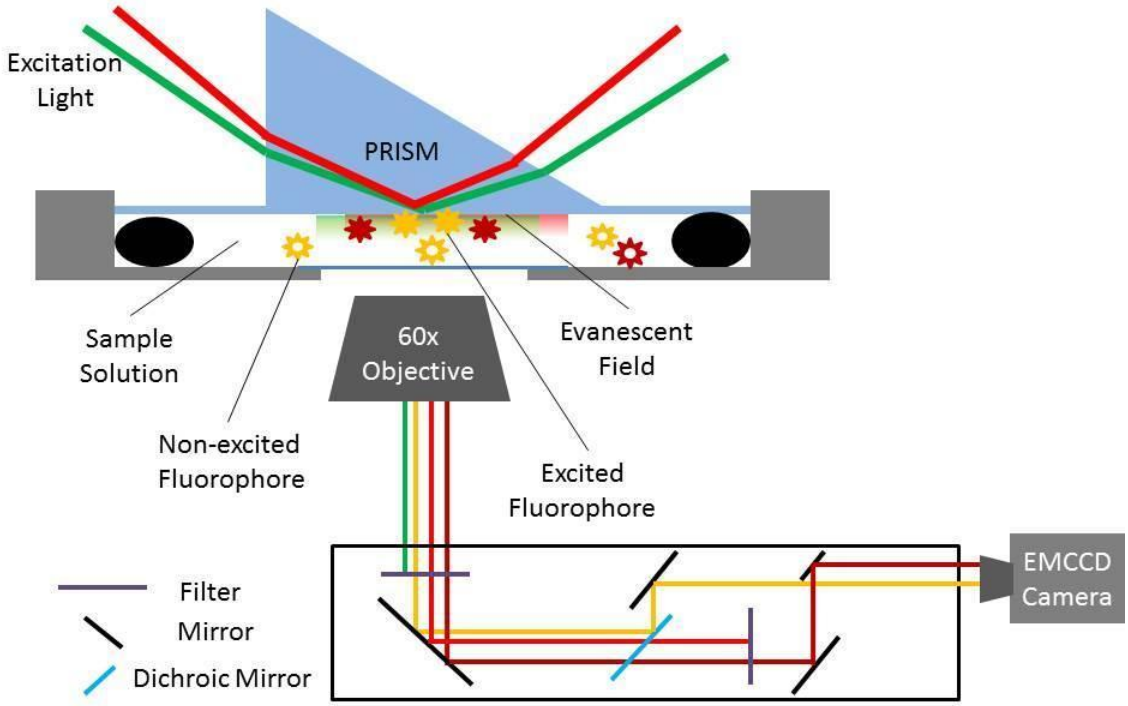

Figure 1.6 – Schematic of the prism-based TIRF microscope.

A schematic of our prism-based TIRF microscope is shown in figure 1.6. This diagram illustrates the excitation light, substrate, fluorescently excited volume, sample fluid, objective, and the optical path which allows for visualization of multiple fluorescence emission wavelengths. The optical splitter is useful for Forster resonance energy transfer (FRET) experiments as well as any experiment involving fluorescence in multiple wavelengths.

Single-molecule TIRF microscopy has several limitations in the type of sample being analyzed. First, the substrate must be of higher refractive index than the sample fluid. Second, both the sample fluid and the substrate must be free from fluorescent contamination with acceptable contamination levels <1 pM. Finally, fluorescent probe molecules can only be studied at surface

concentrations of ~0.1/um^2. Despite these limitations a wealth of information has been obtained from this technique ranging from confirming multi-mode diffusion, to the analysis of protein aggregation at an interface[5, 18, 19].

1.4.2 - Molecular Tracking

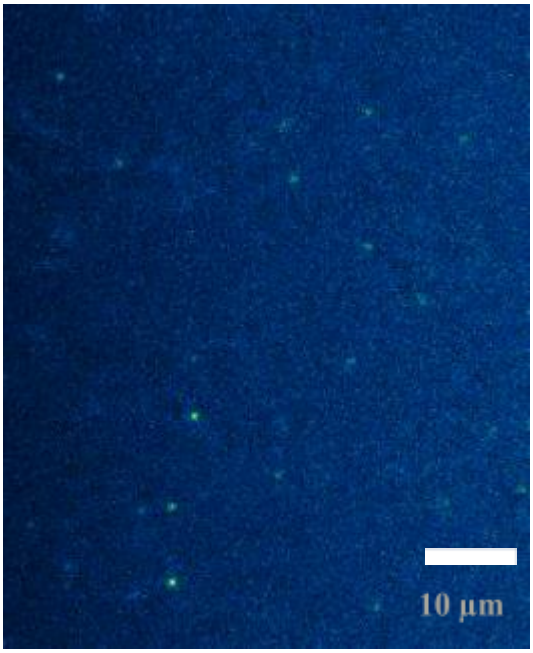

Figure 1.7 – Example image obtained from TIRF microscopy of an OTES surface. Bright spots (green) are individual fluorescently labeled C12 fatty acid molecules.

An example image obtained from a single-molecule TIRF experiment is shown in figure 1.7. Each diffraction limited spot is an individual fluorescent probe molecule. In this experiment the surface is a octadecyltriethoxy silane (OTES) monolayer on fused silica and the probe molecules are fluorescently labeled dodecanoic acid (C12). In a typical experiment a time series of these images is acquired at 5 frames per second (exposure time 200ms/frame) for 200 seconds. Each diffraction limited spot is localized on each frame with a precision of ~50nm. A diffraction limited spot

within 1um of a diffraction limited spot from the previous frame is considered the same molecule. This tracking generates trajectories for each molecule on the surface from when it adsorbs to when it desorbs. A sample molecular trajectory is diagramed in figure 1.8.

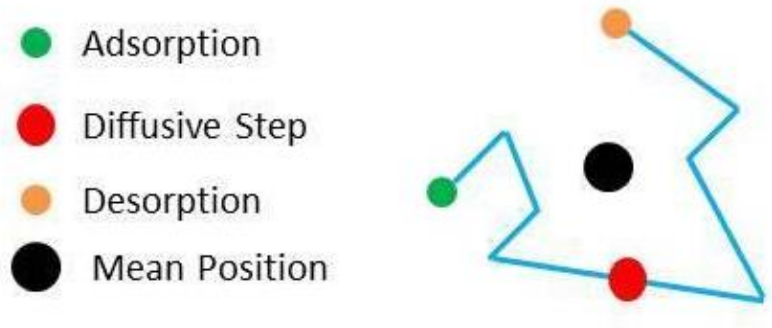

Figure 1.8 – Schematic of a sample molecular trajectory. Adsorption event (green), diffusive step lengths (blue vectors) and nominal location (red), desorption site (orange) and mean position (black) are shown. Each end of a blue vector shows the location where the molecule was observed on a frame.

The adsorption position is the first location a molecule is observed during an experiment. Diffusive steps are calculated as the distance a molecule moves from one frame to the next with the location of the step defined as the midpoint between each location. The desorption location is the final position where a molecule is observed in an experiment. A molecule's average location on the surface over the entire trajectory is used to localize surface residence time.

1.4.3 – Surface Functionalization

Controlling surface chemistry has been essential in performing the experiments presented here. In order to do this while accommodating the requirements for TIRF experiments it was necessary to use self-assembled monolayers (SAMs). SAMs were deposited on our transparent fused silica substrate in order to modify its surface chemistry from the native hydroxyl moieties. These layers present a uniform monolayer of a desired chemistry and are relatively robust under our experimental conditions. In order to form a SAM, fused silica wafers were first cleaned in hot piranha solution (30% H_2O_2/70% H_2SO_4 by volume at 70°C) for one hour followed by UV-ozone cleaning for another hour. This removed any organic contamination on the surface of the fused silica exposing only the native oxide. Wafers were then exposed to SAM precursor molecules, such as octadecyltriethoxy silane (OTES), which react with the hydroxyl groups on the surface forming a covalently bound layer of close-packed C18 chains[20-22].

Organic SAMs can be degraded by exposure to UV light which enabled the creation of controlled micron scale patterns using contact photomasks[22]. The degraded portions of these SAMs are native oxide which is available for another SAM chemistry to be deposited. Each subsequent chapter in this work contains a detailed description of the exact deposition process used for the surface being studied.

1.5 - References

1. Thomas, A. S.; Elcock, A. H., Molecular Dynamics Simulations of Hydrophobic Associations in Aqueous Salt Solutions Indicate a Connection between Water Hydrogen Bonding and the Hofmeister Effect. *J. Am. Chem. Soc.* **2007,** 129, (48), 14887-14898.

2. Nelson, N.; Schwartz, D. K., Specific Ion (Hofmeister) Effects on Adsorption, Desorption, and Interfacial Diffusion. *J. Phys. Chem. Lett.* **2013,** 4, 4064.

3. Honciuc, A.; Howard, A. L.; Schwartz, D. K., Single Molecule Observations of Fatty Acid Adsorption at the Silica/Water Interface: Activation Energy of Attachment. *J. Phys. Chem. C* **2009,** 113, (6), 2078-2081.

4. Honciuc, A.; Harant, A. W.; Schwartz, D. K., Single-Molecule Observations of Surfactant Diffusion at the Solution-Solid Interface. *Langmuir* **2008,** 24, (13), 6562-6566.

5. Walder, R.; Nelson, N.; Schwartz, D. K., Single Molecule Observations of Desorption-Mediated Diffusion at the Solid-Liquid Interface. *Physical Review Letters* **2011,** 107, (15), 156102.

6. Skaug, M. J.; Mabry, J.; Schwartz, D. K., Intermittent molecular hopping at the solid-liquid interface. *Physical Review Letters* **2013,** 110, (25), 256101.

7. Höök, F.; Rodahl, M.; Brzezinski, P.; Kasemo, B., Energy dissipation kinetics for protein and antibody-antigen adsorption under shear oscillation on a quartz crystal microbalance. *Langmuir* **1998,** 14, (4), 729-734.

8. Roach, P.; Farrar, D.; Perry, C. C., Interpretation of protein adsorption: surface-induced conformational changes. *J. Am. Chem. Soc.* **2005,** 127, (22), 8168-8173.

9. Axelrod, D.; Koppel, D.; Schlessinger, J.; Elson, E.; Webb, W., Mobility measurement by

analysis of fluorescence photobleaching recovery kinetics. *Biophys. J.* **1976,** 16, (9), 1055-1069.

10. Rief, M.; Oesterhelt, F.; Heymann, B.; Gaub, H. E., Single molecule force spectroscopy on polysaccharides by atomic force microscopy. *science* **1997,** 275, (5304), 1295-1297.

11. Dudko, O. K.; Hummer, G.; Szabo, A., Theory, analysis, and interpretation of single-molecule force spectroscopy experiments. *Proceedings of the National Academy of Sciences* **2008,** 105, (41), 15755-15760.

12. Ray, C.; Brown, J. R.; Akhremitchev, B. B., Single-molecule Force Spectroscopy Measurements of "Hydrophobic Bond" between Tethered Hexadecane Molecules. *The Journal of Physical Chemistry B* **2006,** 110, (35), 17578-17583.

13. Thompson, N. L., Fluorescence correlation spectroscopy. In *Topics in fluorescence spectroscopy*, Springer: 1999; pp 337-378.

14. Krieger, J.; Tóth, K.; Langowski, J., Fluorescence correlation spectroscopy. **2001**.

15. Yang, Q.; Zhao, J., Hofmeister effect on the interfacial dynamics of single polymer molecules. *Langmuir* **2011,** 27, (19), 11757-11760.

16. Axelrod, D., Total internal reflection fluorescence microscopy in cell biology. *Traffic* **2001,** 2, (11), 764-774.

17. Axelrod, D.; Burghardt, T. P.; Thompson, N. L., Total internal reflection fluorescence. *Annual review of biophysics and bioengineering* **1984,** 13, (1), 247-268.

18. Langdon, B. B.; Kastantin, M.; Schwartz, D. K., Apparent activation energies associated with protein dynamics on hydrophobic and hydrophilic surfaces. *Biophys. J.* **2012,** 102, (11), 2625-2633.

19. Langdon, B. B.; Kastantin, M.; Walder, R.; Schwartz, D. K., Interfacial Proteinâ€“Protein Associations. *Biomacromolecules* **2013,** 15, (1), 66-74.

20. Walba, D. M.; Liberko, C. A.; Korblova, E.; Farrow, M.; Furtak, T. E.; Chow, B. C.; Schwartz, D. K.; Freeman, A. S.; Douglas, K.; Williams, S. D., Self-assembled monolayers for liquid crystal alignment: simple preparation on glass using alkyltrialkoxysilanes. *Liquid crystals* **2004,** 31, (4), 481-489.

21. Ulman, A., Formation and structure of self-assembled monolayers. *Chemical Reviews* **1996,** 96, (4), 1533-1554.

22. Malone, S. M.; Schwartz, D. K., Polar and azimuthal alignment of a nematic liquid crystal by alkylsilane self-assembled monolayers: Effects of chain-length and mechanical rubbing. *Langmuir* **2008,** 24, (17), 9790-9794.

Chapter 2: Single Molecule Dynamics on Hydrophobic Self-Assembled Monolayers

2.1 – Abstract

The interactions between adsorbate molecules and hydrophobic surfaces are of significant interest due to their importance in a variety of biological and separations processes. However, it is challenging to extrapolate macroscopic ensemble-averaged force measurements to molecular-level phenomena. Using total internal reflection fluorescence microscopy to image individual molecules at hydrophobic solid-aqueous interfaces, we directly observed dynamic behavior associated with the interactions between fluorescently-labeled dodecanoic acid (our probe molecules) and self-assembled monolayers (SAM) comprised of *n*-alkyltriethoxysilanes with systematically increasing chain length (from *n*=4–18). In all cases, we observed at least two characteristic surface residence times and two diffusive modes, suggesting the presence of multiple distinct adsorbed populations. In general, the mean surface residence time increased and the mobility decreased with increasing SAM chain length, consistent with stronger probe-surface interactions. However, these trends were not primarily due to changes in characteristic residence times or diffusion coefficients associated with the individual populations but rather to a dramatic increase in the fraction associated with the long-lived slow-moving population(s) on long-chain SAMs. In particular, on longer (16-18 carbon) alkylsilane monolayers the probe molecule exhibited far fewer desorption-mediated "flights" than on short (4-6 carbon) monolayers. Additionally, probes on the longer chain surfaces were much more likely to exhibit extended surface residence times as opposed to short transient surface visits.

2.2 – Introduction

Hydrophobic interactions govern a wide variety of physical phenomena including protein folding[1] and surfactant self-assembly[2]. The current understanding of the hydrophobic effect generally states that it is caused by entropic and enthalpic penalties for creating an interface between water and non-polar surfaces[3]. Typically, intermolecular interactions (Coulomb, van der Waals, hydrogen-bonding, etc.) can be modeled using a pairwise potential between two molecules due primarily to electrostatic effects. The hydrophobic effect has the unique property of being a solvent mediated interaction, which is problematic for modeling hydrophobic interactions from first principles. A significant amount of theoretical research has provided important insight into the interactions between hydrophobic molecules and their surroundings[3-7], but it remains challenging to examine this behavior experimentally[8].

Several experimental techniques have been used to study hydrophobic surfaces. For example, the surface force apparatus (SFA) has been used to measure the forces between two hydrophobic surfaces. The hydrophobic interaction between surfaces has been shown to be a long range interaction, whose strength decays exponentially with a characteristic length scale of ~1 nm [9]. In some cases, the hydrophobic interaction can be as much as an order of magnitude larger than van der Waals forces [9]. However, SFA measurements become increasingly challenging for surface separations less than ~1 nm [8]. Moreover, it is unclear how SFA measurements of hydrophobic interactions between two macroscopic surfaces can be applied to the hydrophobic interactions between individual molecules and a surface[8].

Another commonly used technique for measuring the hydrophobicity of surfaces is to measure the contact angle of water with the surface of interest. This technique provides a reliable, quantitative measure for macro-scale hydrophobicity. However, contact angles provide little molecular level, mechanistic insight into the hydrophobic interaction. For example, the roughness of many superhydrophobic surfaces[10, 11] is mechanistically as important as the surface chemistry in producing the high water contact angles. However, on the molecular length scales these surfaces may exhibit much lower effective hydrophobicity.

Scanning probe microscopy (SPM, such as chemical force microscopy[12, 13]) can give relative affinities of a functionalized probe for heterogeneous surfaces. However, this technique is qualitative in nature. SPM cannot be used to identify chemical species and results are often difficult to replicate[14]. Currently, scanning rates are insufficient to observe the fast dynamics of small molecules at the interface, which is essential to understanding the molecular interactions of single molecules with hydrophobic surfaces.

Single-molecule force spectroscopy (SMFS) is a versatile technique that has been used to study hydrophobic interaction phenomena including the dissociation energies and barrier widths of the hydrophobic interaction between two tethered hexadecane molecules[15] and the interaction between polymer molecules and hydrophobic surfaces[16]. However, SMFS relies on complex models to interpret data and has relatively large amounts of error associated with these both these models and the measurement itself[17, 18]. Furthermore, it remains challenging to separate the effects of the molecular tether and cantilever from the surface interaction of the probe molecule.

Single-molecule fluorescence has been used to study a wide variety of fundamental phenomena, from the structure of lipid membranes[19, 20] to the heterogeneity in hydrophobic chromatography beads[21]. However, it has seen limited use in the direct study of hydrophobic interactions. In previous work[22-27], we used single molecule total internal reflection fluorescence microscopy (smTIRFM) to investigate the dynamics of single fatty acids at the solid-liquid interface. We have found a surprising diversity of dynamic phenomena, including Arrhenius activated adsorption[24, 26] and diffusion[25, 27], multiple modes of diffusion[22, 25, 27], and the consequences of hydrophobic surface heterogeneity[23, 28, 29]. We have primarily investigated the hydrophobic interaction by observing fatty acid dynamics on hydrophobic (water contact angle ~85º) trimethylsilyl (TMS) surfaces. Modifying the solvent[24], temperature[27] and alkyl chain length of the fatty acid probe molecule[27] with this system has led to new insights into molecular-level hydrophobic interactions. These investigations have led us to hypothesize that the alkyl chain length of the modified surface itself may influence the hydrophobic interactions between an individual molecule and the surface.

Here we present results describing the surface diffusion and surface residence times of fluorescently-labeled dodecyl (fl-C12) fatty acid probe molecules interacting with alkylsilane self-assembled monolayers (SAMs) with alkyl chain lengths in the range of 4–18 carbons (C4–C18). Using smTIRFM, we determined that there are multiple modes of interaction between the fatty acid probe and all of the alkylsilane self-assembled monolayers; one mode is transient and fast-moving while the other is long-lived and slow-moving. A third mode, observed only on the C8-C18 monolayers, is intermediate between the two. Interestingly, although the macroscopic hydrophobicity (as determined by water contact angle) varies little between all of these SAM surfaces, there is a strong correlation between the probe-surface interactions and surface alkyl

chain length.

2.3 - Methods

2.3.1 – Materials

Surfaces were prepared by hydrophobic modification of 50 mm diameter fused silica (FS) wafers. The FS wafers were immersed in piranha solution (30% H_2O_2 / 70% H_2SO_4 by volume) heated to 90°C for ~60 min followed by UV-ozone treatment (Boekel UV Clean model 135500) for another ~60 min. The clean substrates were placed in a solution of toluene: alkyl triethoxysilane: n-propylamine in a 200:3:1 ratio by volume. The alkyl silanes used were butyl-, hexyl-, octyl-, decyl-, dodecyl-, hexadecyl-, and octadecyl- triethoxy silanes (Gelest), henceforth abbreviated as C4, C6, C8, C10, C12, C16, and C18 respectively. The deposition solution was maintained at a temperature of 25 ˚C for ~2h. The deposition yielded substrates coated with a SAM comprised of the appropriate chain length silane. Water contact angles were used to characterize the quality of the monolayers. The modified surfaces were then exposed to probe solutions of fluorescently-labeled dodecanoic acid (Invitrogen BODIPY ® 530/550, fl-C12) at concentrations of $2x10^{-15}$ M. fl-C12 was chosen as the hydrophobic probe molecule because both the long alkyl chain and the BODIPY fluorophore are strongly hydrophobic moieties, while still being sufficiently soluble in water due to the hydrogen bonding to the carboxyl group. Importantly, the concentration used is well below that required for any self-assembly to occur in solution or on the surface.

2.3.2 - Contact Angle Goniometery

Static water contact angle measurements were performed on a custom-built contact angle goniometer. The contact angle calculations were done by the Fta32 software (First Ten Ångstroms, Portsmouth, VA). Each measurement was done by placing a ~1μL drop of Millipore water (18.2 MΩ) on the surface and immediately acquiring an image. The contact angle of at least 5 water droplets was taken, each on a random position on the surface. The reported contact angles with error bars are the mean and standard deviation of these contact angle measurements, respectively.

2.3.3 - TIRF Microscopy and Trajectory Analysis

Time sequences of images were captured using a cooled EMCCD camera (Photometrics Cascade II-512) through a prism based total internal reflection fluorescence (TIRF) microscope (Nikon Eclipse TE2000-U) that has been described previously[25]. The excitation light source was a 532 nm diode pumped solid state laser (Cobolt Samba 50). Image frames were acquired continuously for 7 minutes with each frame having an exposure time of 400 ms. Image analysis was performed in Mathematica using algorithms described previously[23, 30]. Briefly, fl-C12 molecules appeared as diffraction limited spots on each image and localized using a center of intensity fit. These centers of intensity positions were linked together from frame-to-frame to form trajectories for each molecule. To account for surface and sample heterogeneity, time series of images were recorded for at least four sample positions on two independent sample surfaces for each alkyl chain length.

A molecule's surface residence time was calculated by determining the number of images that it appeared on the surface multiplied by the exposure time of the frame. Cumulative residence time

distributions were calculated as previously described [31]. Objects that had a total surface residence time of only one or two frames were omitted from this analysis, since these observations are heavily influenced by noise in the images. The function used to fit these cumulative residence time distributions is shown in Eq. 1. With *C(t)* being the cumulative probability of residence time (*t*). The adjustable parameters were the fraction of molecules exhibiting a particular residence time (f_i) and characteristic residence time for each fraction (τ_i). For these experiments two statistically different populations (n=2) were observed for the C4 and C6 monolayers and three distinct populations (n=3) were observed for C8-18 monolayers.

$$C(t) = \sum_{i=1}^{n} f_i e^{-t/\tau_i} \quad (1)$$

The cumulative squared displacement distributions were calculated as described previously[25]. Briefly, each squared molecular step size was ordered sequentially and the probability of a given step size or larger occurring was plotted Eq. 2 shows the function used to fit the cumulative residence time distributions. The fitting parameters were the fraction (f_i) and the diffusion coefficient (D_i) for each population. The time per frame (*t*), which is 0.4 s in this study, was determined by the experimental setup.

$$C(r^2,t) = \sum_{i=1}^{n} f_i e^{-r^2/4D_i t} \quad (2)$$

2.4 – Results

In order to provide context for a comparison between conventional macroscopic characterization of surface hydrophobicity and the hydrophobic interactions between single molecules and these surfaces, we measured the contact angle of water on all SAMs used in the single molecule experiments. The C4 SAM exhibited a significantly lower contact angle of ~80˚, while SAMs comprised of all other chain lengths exhibited contact angles of about 100˚. The deposition procedure described above produced disordered SAMs, and this disorder caused the C6–C18 surfaces to have virtually the same macroscopic hydrophobicity, despite a factor of three difference in alkyl chain length. Thus the single molecule results primarily addressed the effects of chain length (i.e. SAM thickness) in the absence of a discrete order-disorder transition.

To characterize molecular level hydrophobic interactions, we observed the dynamics of fl-C12 on C4–C18 SAMs. The analysis of molecular trajectories at the solid-liquid interface can be used to determine physical parameters associated with molecular-surface interactions. For example, the amount of time the molecule resides on the surface is related to the binding strength of the molecular-surface interaction. By examining cumulative probability distributions of large numbers of individual molecules, we can characterize these interactions with a high degree of statistical certainty [30]. Cumulative surface residence time distributions for the C4, C10, and C18 carbon chain surfaces are shown in Figure 1. The cumulative residence time distribution is analogous to a surface coverage versus time plot.

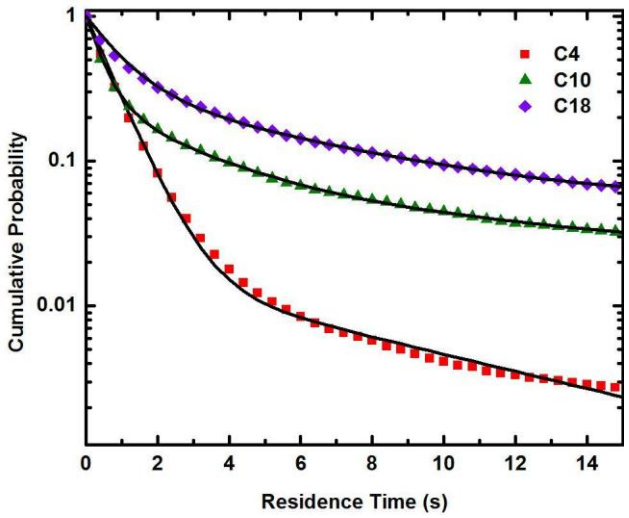

Figure 2.1 - Cumulative surface residence time distributions for fl-C12 on C4, C10, C18 SAMs. The black lines represent a bi-exponential fit to the C4 data and tri-exponential fits to the C10 and C16 data.

The systematic shift of the data in Figure 2.1 as a function of chain length indicates a tendency toward longer residence times for fl-C12 on alkyl monolayers of increasing chain length. This suggests that the probes are, on average, more strongly adsorbed to the longer alkylsilane surfaces. This was unexpected due to the negligible difference in macroscopic hydrophobicity (as determined by water contact angle measurements) of the monolayers. On the semi-logarithmic axes of Figure 2.1, a simple first-order desorption process would appear as a straight line with a slope related to the characteristic residence time. As described above, however, multiple exponentials were required to adequately describe the cumulative residence time distributions. To ensure the proper number of exponential terms in the fits, a Maximum Entropy analysis was performed on the data as described by Steinbach et. al.[32, 33]. This method calculates the probability distribution of exponential time constants for the data, with each peak in the distribution indicating a distinct population. The results of this analysis clearly indicated the presence of two exponential

terms for the C4 and C6 residence time distributions and three exponentials for the C8-C18 data (see Figure S1 in the Supporting Information below). These results suggested the presence of two distinct residence time populations for the shorter alkyl monolayers and three distinct populations for the longer monolayers. Notably, in previous work[22, 25, 34, 35], we also observed the presence of multiple characteristic residence times for different classes of probe molecules (including biomolecules) on surfaces displaying a variety of different chemistries.

For fl-C12 on C4–C18 SAMs, the short-lived populations exhibited characteristic residence times (τ_1) in the range 0.4–0.9 s; the long-lived populations had characteristic residence times (τ_3) of 7–20 s; and the intermediate populations observed on the C8-C18 SAMs had characteristic residence times (τ_2) of 1.3–2.4 s. Interestingly, there was no systematic variation in either τ_1, τ_2, or τ_3 (Figure 2.2.b) as a function of SAM chain length. The absence of a strong trend with chain length suggests that the strengths of these interactions have very little dependence on SAM chain length. Therefore, the significant changes in the mean residence time, and the residence time distributions shown in Figure 2.1, with increasing SAM chain length were not associated with changes in the actual characteristic residence times. Instead, the dramatic shift in the ensemble behavior was due to the fact that the relative fractions of the populations changed significantly, i.e. as the SAM chain length increased, the short-lived fraction (f_1) decreased and the longer-lived fractions (f_2, f_3) increased (by an order of magnitude), as shown in Figure 2.2.a. It should also be noted that photobleaching did not impact the observed residence times. With this experimental setup photobleaching lifetimes have been determined to be approximately 300 seconds, which is more than an order of magnitude larger than the longest observed residence time in these

experiments.

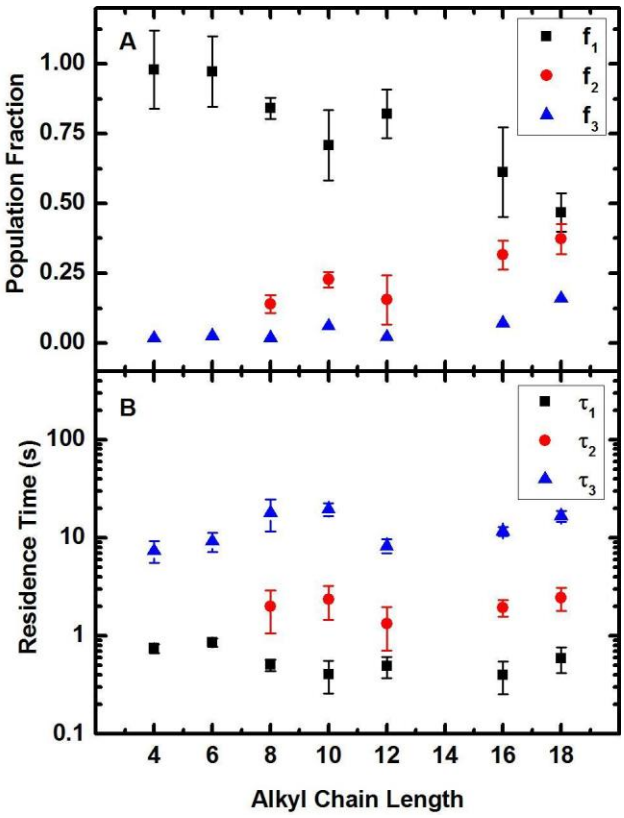

Figure 2.2 - Residence times of fl-C12 as a function of SAM chain length. (a) The population fractions of the short (f_1), intermediate (f_2, when present), and long lived (f_3) populations (black squares, red circles, and blue triangles respectively) and (b) the residence times corresponding to those populations (τ_1, τ_2, and τ_3). The error bars represent the combined error from the fit parameters and the standard deviation from replicate experiments.

The diffusion of the fatty acid molecules was also examined as a function of SAM chain length. Figure 2.3 shows the cumulative squared displacement distributions on C4, C10 and C18 surfaces. The systematic shift in the distributions with SAM chain length indicates that the mobility of fl-

C12 slowed systematically and significantly with increasing SAM chain length. Qualitatively, this trend suggested that an increased SAM chain length resulted in stronger hydrophobic interactions between the hydrophobic probe and the surface.

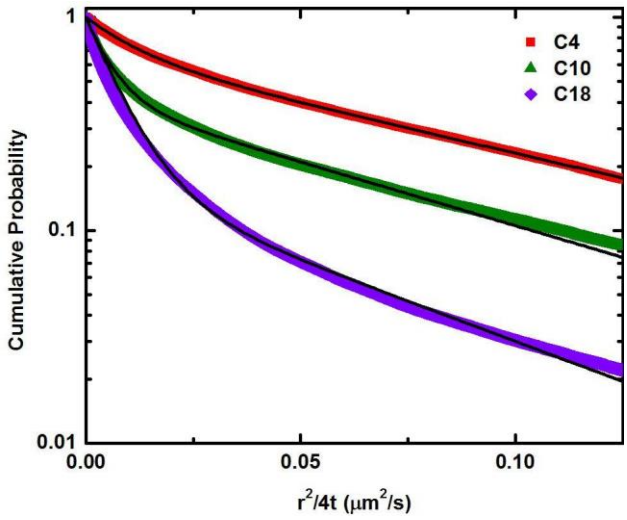

Figure 2.3 - Cumulative squared displacement distributions for fl-C12 on C4, C10, and C18 SAMs. The black lines represent double-Gaussian fits to the data.

On the semi-logarithmic plot of Figure 2.3, a distribution corresponding to a simple random walk (Gaussian diffusion) would be represented by a straight line, with a slope equal to $-1/D$ [36]. The non-linear appearance of the data measured here, however, indicates the presence of multiple diffusive modes, as was also observed in previous single-molecule tracking experiments[22, 25]. In particular, two diffusive modes were required to describe the squared displacement distributions for fl-C12 on each of the SAM surfaces studied. Fitting these distributions to more than two Gaussian terms did not improve the fit nor did it yield statistically distinct fitting parameters. As described above, a double Gaussian fit to each measured distribution allowed us to extract the magnitudes of the two-dimensional diffusion coefficients and the relative fraction of steps

associated with each diffusive mode.[22] The fast and slow modes exhibited effective diffusion coefficients of 0.05–0.10 $\mu m^2/s$ and 0.007–0.013 $\mu m^2/s$ respectively. These diffusion coefficient values are consistent with previous studies of the dynamics of fatty acids at the solid-liquid interface, where the two modes were shown to correspond to flying and crawling diffusive modes respectively[22, 25]. The flying mode is characterized by large, desorption mediated flights, while the crawling mode corresponds to local diffusion on molecular length scales [22, 25, 27]

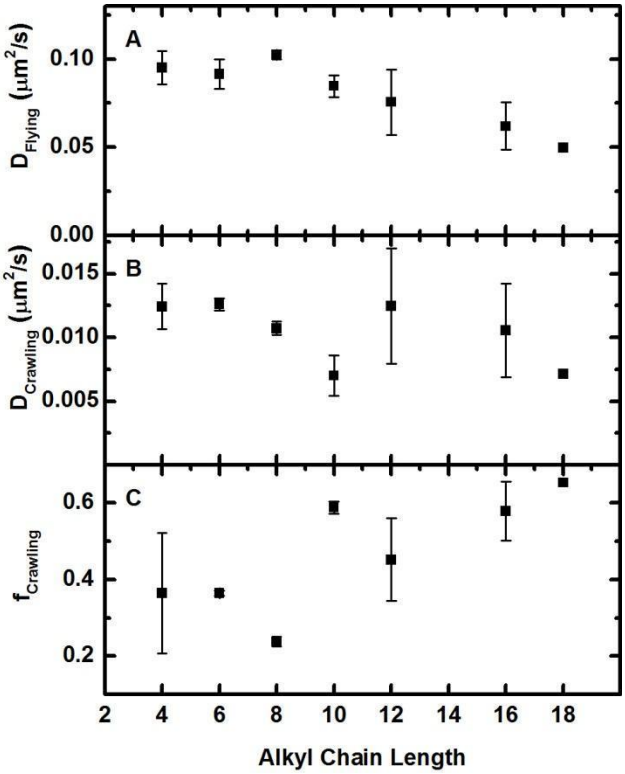

Figure 2.4 - Diffusion of fl-C12 acid versus SAM chain length. (a) Flying diffusion coefficient, (b) crawling diffusion coefficient, and (c) fraction of steps associated with the crawling mode. The error bars represent the standard deviation from replicate measurements.

Figure 2.4 shows the magnitudes of the respective diffusion coefficients and the fraction of steps

associated with the crawling mode $f_{Crawling}$ as a function of SAM chain length. While D_{Flying} decreased systematically by a factor of two with increasing SAM chain length (Figure 2.4.a), $D_{Crawling}$ exhibited only a modest overall decrease with significant scatter. In a finding reminiscent of the residence time results described above, the fraction of crawling mode steps increased significantly with increasing SAM chain length.

2.5 – Discussion

Historically, there have been relatively few reported molecular-level measurements of hydrophobic interactions due to a lack of appropriate experimental techniques. We have shown here that single molecule tracking allows one to use surface dynamics (e.g. desorption and surface diffusion) to probe the fundamental nature of hydrophobic interactions between an individual molecule and a hydrophobic surface. We have also demonstrated that these interactions are governed not only by the macroscopic hydrophobicity of the surface but also by the molecular structure of the surface itself. In general, the hydrophobicity of a surface is often characterized by measuring the water contact angle. However, the contact angle of the disordered alkylsilane SAMs we prepared varied little for alkyl chains longer than about 4 carbons. However, our single molecule results demonstrated that there was an increasingly strong interaction between a hydrophobic probe molecule and the hydrophobic SAM surfaces with increasing chain length, despite the fact that the macroscopic water contact angle did not change significantly. These increasing interactions were revealed by an overall increase in surface residence time and a decrease in the rate of surface diffusion.

Interestingly, the dynamic behavior of fl-C12 on the SAM surfaces was heterogeneous, indicating

the presence of up to three distinct populations on the basis of residence time, as well as two distinct diffusive modes. The increased residence time and decreased diffusivity with increasing SAM chain length was largely due to a dramatic shift in population/mode fractions, as opposed to a change in the characteristic residence times or diffusion coefficients of the populations/modes. In particular, for long-chain SAMs, a probe molecule was much more likely to adopt a configuration resulting in a long residence time and slow diffusion. This is consistent with our previous work showing that the flying diffusive mode is desorption-mediated[22, 25]. Thus a molecular configuration that results in a reduced probability of desorption will also reduce the frequency of "flights" and increase the relative number of crawling steps. The most plausible explanation for this behavior is that the long-lived slow-moving fl-C12 populations involve a molecular configuration where the fatty acid alkyl chain is intercalated to some degree within the SAM layer. Since the intermediate residence time modes are only visible on the longer chain silanes, it is possible that partial intercalation is more pronounced and thus distinguishable from the short lived population. Figure 2.5 is a cartoon schematic where short and long lived modes of interaction are represented. The superficial adsorption mode (Figure 2.5.a) is characterized by short residence times and fast diffusion. A hypothetical intercalated adsorption mode (Figure 2.5.b) exhibits longer residence times and slower diffusion. It is reasonable that fl-C12 will more readily intercalate into SAMs comprised of longer alkyl chains, resulting in a larger fraction of molecules exhibiting long residence times and slower diffusion.

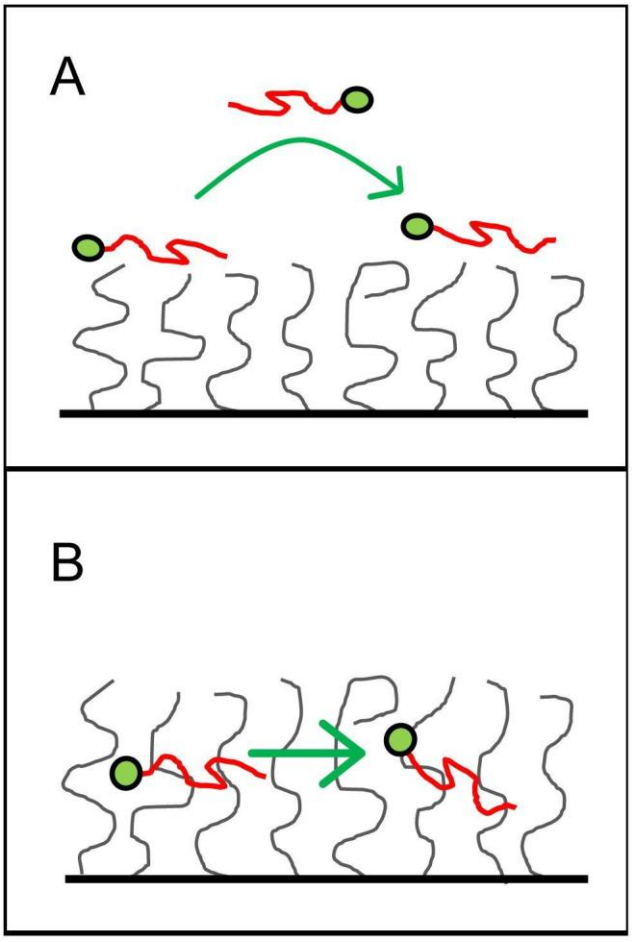

Figure 2.5 - Cartoon schematic of the proposed (a) superficial and (b) intercalated interaction mechanisms between the probe molecule and the SAM. Superficial adsorption is the dominant mode of interaction with short chain monolayers while intercalation is the preferred mechanism for interaction with long chain monolayers.

The dynamics of molecules on alkyl surfaces also has important implications for heterogeneous catalysis using self-assembled monolayers. Recent work by Marshall et al[37] has demonstrated that the presence of alkylthiol SAMs dramatically increased the selectivity of 1-epoxybutane formation from 1-epoxy-3-butene on supported palladium catalysts. Intriguingly, the reactivity of 1-epoxy-

3-butene also increased on catalytic surfaces with longer alkyl chain monolayers over shorter chain monolayers[37]. Our results here suggest an explanation for this finding, i.e. that the hydrophobic reactant molecule is more likely to exhibit long surface residence time on the long-chain SAMs, leading to a higher probability of reacting with the underlying substrate. While surface diffusion has been previously shown to be an important factor in reactivity of surfaces[38, 39], we would like to suggest that the surface residence time should also be considered as an important factor. The combination of slower diffusion and longer residence times is likely an important factor in the mechanism for the increased selectivity and activity of the reactions on SAM-coated heterogeneous catalysts. In particular, the intercalation of molecules into the SAM is likely a key factor in the observed enhancement of catalytic properties.

2.6 - Acknowledgements

NN acknowledges support from the U.S. Department of Energy Basic Energy Sciences, Chemical Science, Geosciences, and Biosciences Division (DE-SC0001854). RW also acknowledges support from the U.S. National Science Foundation (CHE 0841116).

2.7 – References

1. Dyson, H. J.; Wright, P. E.; Scheraga, H. A., The role of hydrophobic interactions in initiation and propagation of protein folding. *Proceedings of the National Academy of Sciences* **2006,** 103, (35), 13057-13061.

2. Israelachvili, J. N.; Mitchell, D. J.; Ninham, B. W., Theory of self-assembly of hydrocarbon amphiphiles into micelles and bilayers. *Journal of the Chemical Society, Faraday Transactions 2: Molecular and Chemical Physics* **1976,** 72, 1525-1568.

3. Chandler, D., Interfaces and the driving force of hydrophobic assembly. *Nature* **2005,** 437, (7059), 640-647.

4. Patel, A. J.; Varilly, P.; Jamadagni, S. N.; Acharya, H.; Garde, S.; Chandler, D., Extended surfaces modulate hydrophobic interactions of neighboring solutes. *Proceedings of the National Academy of Sciences* **2011,** 108, (43), 17678-17683.

5. Patel, A. J.; Varilly, P.; Jamadagni, S. N.; Hagan, M. F.; Chandler, D.; Garde, S., Sitting at the Edge: How Biomolecules use Hydrophobicity to Tune Their Interactions and Function. *The Journal of Physical Chemistry B* **2012,** 116, (8), 2498-2503.

6. Acharya, H.; Vembanur, S.; Jamadagni, S. N.; Garde, S., Mapping hydrophobicity at the nanoscale: Applications to heterogeneous surfaces and proteins. *Faraday Discuss.* **2010,** 146, 353-365.

7. Rajamani, S.; Truskett, T. M.; Garde, S., Hydrophobic hydration from small to large lengthscales: Understanding and manipulating the crossover. *Proc. Natl. Acad. Sci. U. S. A.* **2005,** 102, (27), 9475-9480.

8. Meyer, E. E.; Rosenberg, K. J.; Israelachvili, J., Recent progress in understanding hydrophobic interactions. *Proceedings of the National Academy of Sciences* **2006,** 103, (43), 15739-15746.

9. Israelachvili, J.; Pashley, R., The hydrophobic interaction is long range, decaying exponentially with distance. *Nature* **1982,** 300, (5890), 341-342.

10. Patankar, N. A., On the Modeling of Hydrophobic Contact Angles on Rough Surfaces. *Langmuir* **2003,** 19, (4), 1249-1253.

11. Yan, Y. Y.; Gao, N.; Barthlott, W., Mimicking natural superhydrophobic surfaces and grasping the wetting process: A review on recent progress in preparing superhydrophobic surfaces. *Advances in Colloid and Interface Science* **2011,** 169, (2), 80-105.

12. Noy, A., Chemical force microscopy of chemical and biological interactions. *Surface and Interface Analysis* **2006,** 38, (11), 1429-1441.

13. Vezenov, D. V.; Noy, A.; Ashby, P., Chemical force microscopy: probing chemical origin of interfacial forces and adhesion. *Journal of Adhesion Science and Technology* **2005,** 19, (3-5), 313-364.

14. Honciuc, A.; Baptiste, D. J.; Schwartz, D. K., Hydrophobic Interaction Microscopy: Mapping the Solid/Liquid Interface Using Amphiphilic Probe Molecules. *Langmuir* **2009,** 25, (8), 4339-4342.

15. Ray, C.; Brown, J. R.; Akhremitchev, B. B., Single-molecule Force Spectroscopy Measurements of "Hydrophobic Bond" between Tethered Hexadecane Molecules. *The Journal of Physical Chemistry B* **2006,** 110, (35), 17578-17583.

16. Friedsam, C.; Gaub, H.; Netz, R., Probing surfaces with single-polymer atomic force microscope experiments. *Biointerphases* **2006,** 1, (1), MR1-MR21.

17. Ray, C.; Brown, J. R.; Akhremitchev, B. B., Correction of Systematic Errors in Single-Molecule Force Spectroscopy with Polymeric Tethers by Atomic Force Microscopy. *The Journal of Physical Chemistry B* **2007,** 111, (8), 1963-1974.

18. Ray, C.; Brown, J. R.; Akhremitchev, B. B., Rupture Force Analysis and the Associated Systematic Errors in Force Spectroscopy by AFM. *Langmuir* **2007,** 23, (11), 6076-6083.

19. Livanec, P. W.; Dunn, R. C., Single-Molecule Probes of Lipid Membrane Structure. *Langmuir* **2008,** 24, (24), 14066-14073.

20. Huckabay, H. A.; Dunn, R. C., Hydration Effects on Membrane Structure Probed by Single Molecule Orientations. *Langmuir* 27, (6), 2658-2666.

21. Zhong, Z.; Lowry, M.; Wang, G.; Geng, L., Probing Strong Adsorption of Solute onto C18-Silica Gel by Fluorescence Correlation Imaging and Single-Molecule Spectroscopy under RPLC Conditions. *Analytical Chemistry* **2005,** 77, (8), 2303-2310.

22. Walder, R.; Nelson, N.; Schwartz, D. K., Single Molecule Observations of Desorption-Mediated Diffusion at the Solid-Liquid Interface. *Physical Review Letters* **2011,** 107, (15), 156102.

23. Walder, R.; Nelson, N.; Schwartz, D. K., Super-resolution surface mapping using the trajectories of molecular probes. *Nat Commun* **2011,** 2, 515.

24. Honciuc, A.; Baptiste, D. J.; Campbell, I. P.; Schwartz, D. K., Solvent Dependence of the Activation Energy of Attachment Determined by Single Molecule Observations of Surfactant Adsorption. *Langmuir* **2009,** 25, (13), 7389-7392.

25. Honciuc, A.; Harant, A. W.; Schwartz, D. K., Single-molecule observations of surfactant diffusion at the solution-solid interface. *Langmuir* **2008,** 24, (13), 6562-6566.

26. Honciuc, A.; Howard, A. L.; Schwartz, D. K., Single Molecule Observations of Fatty Acid

Adsorption at the Silica/Water Interface: Activation Energy of Attachment. *J. Phys. Chem. C* **2009,** 113, (6), 2078-2081.

27. Honciuc, A.; Schwartz, D. K., Probing Hydrophobic Interactions Using Trajectories of Amphiphilic Molecules at a Hydrophobic/Water Interface. *J. Am. Chem. Soc.* **2009,** 131, (16), 5973-5979.

28. Walder, R.; Honciuc, A.; Schwartz, D. K., Directed Nanoparticle Motion on an Interfacial Free Energy Gradient. *Langmuir* **2009,** 26, (3), 1501-1503.

29. Honciuc, A.; Baptiste, D. J.; Schwartz, D. K., Hydrophobic Interaction Microscopy: Mapping the Solid/ Liquid Interface Using Amphiphilic Probe Molecules. *Langmuir* **2009,** 25, (8), 4339-4342.

30. Walder, R.; Kastantin, M.; Schwartz, D. K., High throughput single molecule tracking for analysis of rare populations and events. *Analyst* **2012**.

31. Walder, R.; Schwartz, D. K., Single Molecule Observations of Multiple Protein Populations at the Oil-Water Interface. *Langmuir* **2010,** 26, (16), 13364-13367.

32. Steinbach, P. J., Filtering artifacts from lifetime distributions when maximizing entropy using a bootstrapped model. *Analytical Biochemistry* **2012,** 427, (1), 102-105.

33. Steinbach, P. J.; Ionescu, R.; Matthews, C. R., Analysis of Kinetics Using a Hybrid Maximum-Entropy/Nonlinear-Least-Squares Method: Application to Protein Folding. *Biophys. J.* **2002,** 82, (4), 2244-2255.

34. Kastantin, M.; Langdon, B. B.; Chang, E. L.; Schwartz, D. K., Single-Molecule Resolution of Interfacial Fibrinogen Behavior: Effects of Oligomer Populations and Surface Chemistry. *J. Am. Chem. Soc.* **2011,** 133, (13), 4975-4983.

35. Walder, R.; Honciuc, A.; Schwartz, D., Phospholipid Diffusion at the Oil-Water Interface.

Journal of Physical Chemistry B **2010,** 114, (35), 11484-11488.

36. Schütz, G. J.; Schindler, H.; Schmidt, T., Single-molecule microscopy on model membranes reveals anomalous diffusion. *Biophys. J.* **1997,** 73, (2), 1073-1080.

37. Marshall, S. T.; O'Brien, M.; Oetter, B.; Corpuz, A.; Richards, R. M.; Schwartz, D. K.; Medlin, J. W., Controlled selectivity for palladium catalysts using self-assembled monolayers. *Nat. Mater.* **2010,** 9, (10), 853-858.

38. Allen, C. E.; Seebauer, E. G., Surface diffusivities and reaction rate constants: Making a quantitative experimental connection. *J. Chem. Phys.* **1996,** 104, (7), 2557-2565.

39. Cukier, R. I., The effect of surface diffusion on surface reaction rates. *The Journal of Chemical Physics* **1983,** 79, (5), 2430-2435.

Chapter 3: Specific Ion (Hofmeister) Effects on Adsorption, Desorption, and Diffusion at the Solid-Aqueous Interface

3.1 - Abstract

Certain salts in aqueous solution are known to significantly increase the affinity of molecules with hydrophobic moieties for a hydrophobic interface, but the mechanism of this effect is poorly understood. We used single molecule total internal reflection fluorescence microscopy to directly observe the underlying dynamic interfacial phenomena for a fluorescent fatty acid probe molecule at a self-assembled monolayer surface. Both NaF and NaSCN increased the surface affinity of the probe from that observed in pure water, and consistent with expectations, the surface affinity was greater in the presence of NaF than NaSCN. Notably, the primary cause of the increase in surface affinity was specifically due to an increase in the absolute rate of adsorption from solution. In contrast, the surface residence time and the surface diffusion coefficient of the probe molecules did not depend significantly on the solution conditions.

3.2 – Introduction

The behavior of hydrophobic molecules in electrolyte solutions is significantly altered by the specific identity of the ions in solution. In 1888, Franz Hofmeister first noted that the solubility of proteins was altered in the presence of specific salts[1]. The effect of specific ions that Hofmeister first observed was later noted to affect the behavior of all molecules with a hydrophobic component. Anions are typically arranged in the empirically observed series, $F^- \approx SO_4^{2-} > HPO_4^{2-} > Cl^- > NO_3^- > Br^- > ClO_3^- > I^- > ClO_4^- > SCN^-$, where anions on the left decrease the solubility of hydrophobic molecules, known as having a "salting-out" effect, while anions on the right have a lesser effect and can even increase the solubility of said molecules ("salting-in").

Macroscopic (bulk) thermodynamic behavior of molecules in the presence of specific ions has been studied extensively. These studies show that the so-called "Hofmeister effect" alters a large number of parameters such as solubility, conformational stability of proteins, critical micelle concentrations (CMC) of surfactants, and adsorption isotherms of surfactants to interfaces[2-7]. The effect of specific ions on these behaviors depends strongly on the particular solute[8]. A number of studies have shown that surfactants partition more strongly to hydrophobic interfaces and have an increased tendency to form micelles in the presence of specific ions[4, 6, 7]. However, there remains much debate as to the exact mechanism that allows specific ions to have varying degrees of effect[8]. Current thought is that specific ions alter the structuring of water, which, in turn, alters the effective strength of the interaction between hydrophobic molecules, known as the hydrophobic effect[5, 9-11]. Molecular dynamics (MD) simulations have been used extensively to probe potential mechanisms behind these observed macroscopic behaviors[12-16]. Unfortunately, few molecular level experimental results are available to validate the findings of these simulations[9, 17].

In this work we use single molecule total internal reflection fluorescence (TIRF) microscopy to study the effects of ions taken from opposite ends of the Hofmeister series on the dynamics of a hydrophobic probe molecule at a hydrophobic self-assembled monolayer (SAM)/aqueous interface. By studying molecular level dynamic behavior one obtains mechanistic information on the impact of specific ions on the surface affinity, adsorption rate, surface residence time, and surface diffusion of the hydrophobic probe molecule. In particular, independent information about adsorption and desorption rates allows for greater understanding of the previously observed changes in the *net* surface affinity associated with the Hofmeister effect.

3.3 - Materials and Methods

For these experiments, 1.0 M NaF and 1.0 M NaSCN were chosen from opposite ends of the anion Hofmeister series, while all other factors, including counter-ion and valency, remained constant. A probe molecule, 4,4-Difluoro-5,7-Dimethyl-4-Bora-3a,4a-Diaza-*s*-Indacene-3-Dodecanoic Acid (BODIPY fl-C_{12}, Invitrogen Inc., USA), henceforth abbreviated "fl-C12", was selected because both the fluorophore and the fatty acid tail are strongly hydrophobic and uncharged at neutral pH. Unlike experiments with larger molecules, the BODIPY fluorophore represents a significant portion of the fl-C12 probe and was considered as a hydrophobic entity for the purposes of this discussion. The probe was dissolved in water or salt solutions at an extremely low concentration of ~$2x10^{-12}$ M; these solutions were then placed in contact with an octadecylsilane (ODS) SAM that had been deposited on a fused silica substrate[18]. More detail about the experimental procedures is provided in the Supporting Information below. The probe concentration was chosen to give sufficient surface coverage to acquire a statistically-significant data set, while also maintaining an average separation between molecules of at least 5 μm for the

purposes of object identification. This concentration is several orders of magnitude smaller than the concentration necessary for self-assembly in solution or on the surface (~mM concentrations are necessary for C-12 fatty acid self-assembly)[19]. The system was allowed to reach steady state at 30°C for a period of at least 15 minutes.

Sequences of images of the probe on the interface were captured using a prism based single molecule total internal reflection fluorescence (TIRF) microscope as detailed in the Supporting Information below. These sequences showed fluorescent molecules adsorbed at the solid-liquid interface as diffraction limited spots. The centers of intensity of these spots were localized in each image (frame), then linked together frame-to-frame to form trajectories where the surface residence time of a molecule was calculated as the number of frames in which a given molecule was observed (multiplied by the acquisition time), and diffusive step sizes were calculated by measuring how far a molecule moved between sequential frames[20]. By accumulating many thousands of trajectories it was possible to independently determine several molecular behaviors, including surface coverage, adsorption rate, residence time, and diffusive step size distributions. For the purposes of this work, objects that were present only for one or two consecutive frames were ignored, since such short trajectories are highly susceptible to tracking error due to noise in the images. Each solution condition was repeated five times and errors in measured values were calculated as the standard deviation between replicates. At least 10,000 molecules were observed and tracked in each replicate.

Through single molecule tracking, we first looked simply at the number of molecules on the surface (i.e. the steady-state surface coverage) under a given set of solution conditions. The surface

coverage of a probe molecule is directly related to its macroscopic affinity for the surface under low coverage conditions[18]. Beyond this steady-state measurement, dynamic single molecule tracking experiments uniquely allowed for the independent measurement of the opposing processes that determine surface coverage, i.e. adsorption and desorption. The surface mobility (diffusion) of the probe molecules was measured, providing an indication of the way in which a probe molecule interacts with the surface while it is adsorbed.

3.4 - Results

Figure 3.1 shows the normalized molecular surface coverage (Γ) where Γ is defined as the average number of observed molecules per unit area, normalized to the bulk concentration of probe in solution. Γ therefore has units of length, where the length is defined as the thickness of the solution layer that contains the same number of molecules as are present on the surface. Under low coverage conditions, where intermolecular interactions are negligible, Γ is a fundamental and well-defined quantity that is independent of solution concentration. That is, Γ is related to the bulk surface affinity for the probe molecule, but excludes any intermolecular interactions between probes due to the extremely dilute conditions of these experiments[21]. As indicated in Figure 3.1, both NaSCN and NaF were observed to increase the surface coverage of fl-C12 over that observed for pure water, with NaF resulting in a significantly higher surface coverage than NaSCN. In particular, pure water resulted in an fl-C12 surface coverage of 2.2 ± 0.4 μm. NaSCN and NaF had surface coverages of 3.0 ± 0.3 μm and 5.4 ± 0.8 μm respectively. These results are conceptually consistent with previously reported results where both of these Hofmeister salts have been shown to exhibit "salting-out" behavior (an increase in the strength of the hydrophobic interaction) in surfactant molecules. Furthermore, previous studies have shown that NaF induced a larger

increase than NaSCN in a number of systems ranging from the self-assembly of surfactants in solution to the solubility of various hydrophobic molecules in aqueous solution[3, 22].

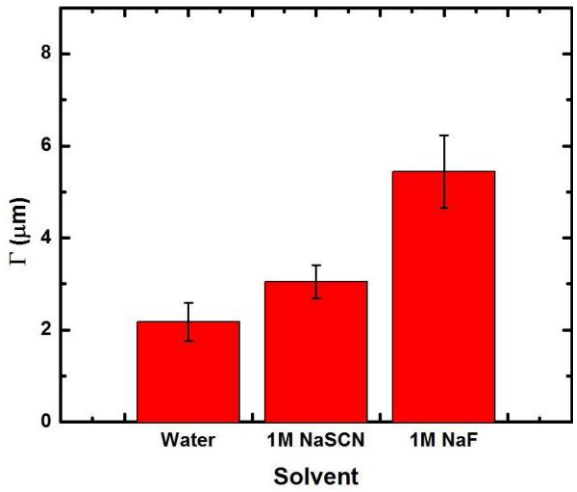

Figure 3.1 - Surface coverage (Γ) for fl-C12 adsorbed to an ODS monolayer normalized to the bulk concentration in solution. Error bars represent one standard deviation between replicates.

Since our experiments probe the interaction between hydrophobic molecules and a hydrophobic surface, it is appropriate to compare the magnitude of our measured surface affinity effects with bulk experiments that probe other measures of the hydrophobic interaction strength, such as micelle formation. For example, Miagishi et.al. observed that the critical micelle concentration (CMC) of Mega-8 (a nonionic surfactant) decreased from 70mM in water to 52.8 mM in 1.0 M NaSCN and to 30mM in 1.0 M NaF[4]. Thus, compared to that in pure water, the CMC decreased by a factor of ~1.3 in 1M NaSCN and a factor of ~2.3 in 1M NaF. In our experiments, the surface coverage increased by a factor of ~1.4 in NaSCN and by ~2.5 in NaF. The consistency of these results suggests that the adsorption of a hydrophobic solute on a hydrophobic surface is a valid

model for dynamic studies of Hofmeister effects.

The real strength of single-molecule tracking, however, involves the ability to separate the two opposing dynamic molecular processes that contribute to the steady-state surface coverage. In particular, by tracking large numbers of individual trajectories, it is possible to obtain careful measurements of the number of molecules adsorbing to the surface and the rate at which they leave (desorb). In terms of these quantities, the steady-state surface coverage (Γ) discussed earlier is given by the expression $\Gamma=k_a/k_d$, where k_a is the adsorption rate constant and k_d is the desorption rate constant. By analyzing these rates independently, one can tease apart molecular mechanisms that underlie the observed trends in macroscopic steady-state parameters such as surface coverage. Figure 3.2.a shows the probe molecule adsorption rate constants as a function of solution conditions, while Figure 3.2.b shows the average desorption rate constant, k_d. In the analysis presented here, the desorption rate constant is defined as the inverse of the average residence time.

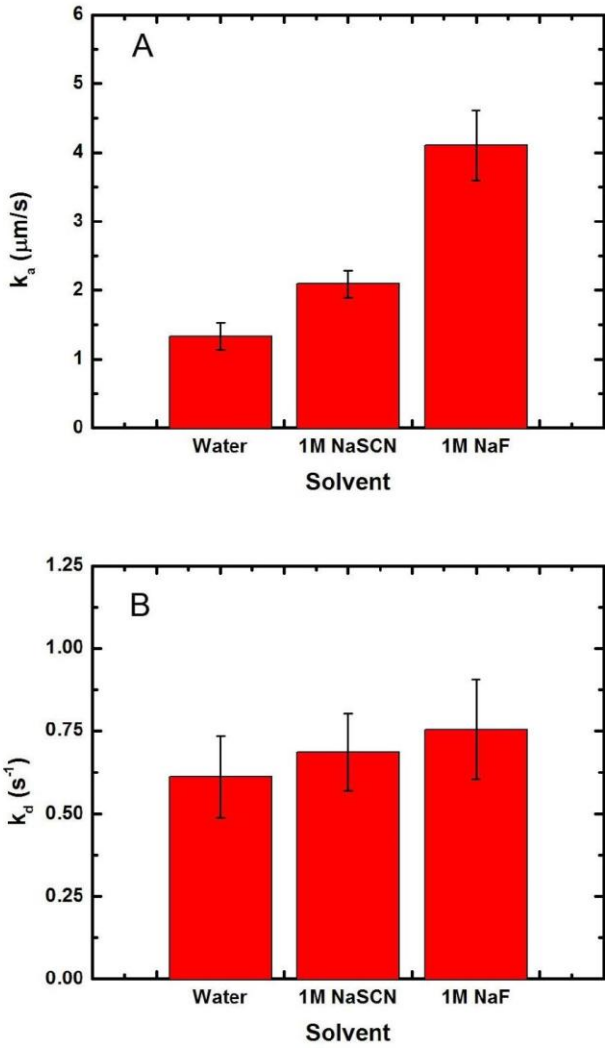

Figure 3.2 - (A) Adsorption rate constant (k_a) and (B) desorption rate constant (k_d) for each solution condition. Adsorption rates are normalized to the bulk concentration.

As shown in Figure 3.2.a, k_a in both NaF and NaSCN solution is significantly higher than in pure water, with NaF increasing the adsorption rate by approximately twice as much as NaSCN. However, k_d is unchanged (within statistical uncertainty) between the different conditions. The desorption rate constant corresponds to a mean surface residence time of approximately 1.4 seconds for any given molecule (see Supporting Information below for further discussion on

residence time calculations and the effects of artifacts, including photobleaching, on these calculations.). These experiments show conclusively that the observed increase in surface coverage shown in Figure 3.1 (which is directly connected to macroscopic observations such as surface affinity) is due entirely to an increase in the adsorption rate of fl-C12 onto the hydrophobic substrate rather than a change in the desorption rate of the probe from the surface.

We also measured the diffusion of the probe molecules adsorbed to the interface an effort to further understand the effects of specific ions on the interaction between the probe molecules and the surface. Molecules undergo significant two-dimensional diffusion while adsorbed to an interface, with the diffusion rate being directly related to the corrugation in the free energy of the surface[23]. A difference in surface diffusion between the solution conditions would indicate that the specific ions modify the free energy landscape experienced by adsorbed probe molecules. These experiments, however, showed no significant difference in the mean diffusion coefficients of adsorbed fl-C12 at the interface between the hydrophobic surface and water (0.027±0.002 $\mu m^2/s$), 1.0 M NaSCN (0.026±0.003 $\mu m^2/s$) and 1.0 M NaF (0.028±0.009 $\mu m^2/s$).

In previous work, we found that adsorbed molecules typically do not execute simple 2D Brownian motion on the surface[20], leaving open the possibility that a careful analysis of the diffusive step sizes could provide insight into ion-specific effects. Figure 3.3 shows the complementary cumulative probability distribution of squared displacements of fl-C12 under the various conditions. The construction of these plots is detailed in the Supporting Information. Briefly, these distributions represent the probability that a given squared displacement will be of size $r^2/4t$ or longer, where the lag time t is the time between

successive localizations of the molecule. A straight line on this plot would indicate a single Gaussian mode of diffusion with the slope of the line being directly proportional to the diffusion coefficient expected for 2-D Brownian motion. However, the actual data were clearly not consistent with a single mode of simple Brownian motion. Guided by previous work, the actual motion was interpreted as being due to two interspersed diffusive modes, dubbed flying and crawling modes respectively[18, 20]. These modes represent two distinct mechanisms for motion across the interface. Crawling refers to Brownian motion in two dimensions while flying diffusive steps are characterized by detachment from the interface, an interval of three-dimensional Brownian motion, followed by re-adsorption[20].

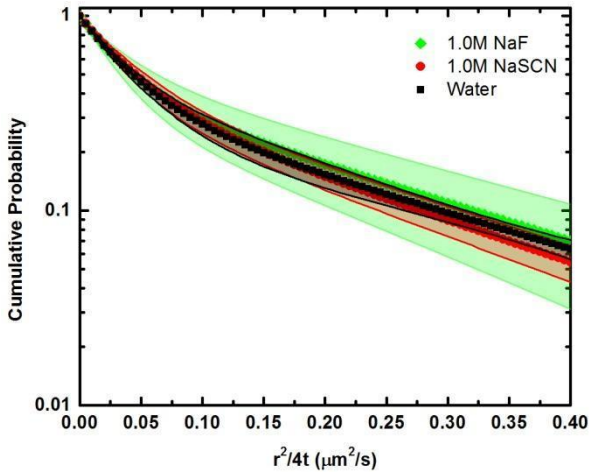

Figure 3.3 - Complementary cumulative probability distribution of the squared displacement divided by 4*t*, where *t* is the lag time between successive image acquisitions. Error bars represent the standard deviation between runs and are displayed as shaded regions for clarity.

The cumulative probability distribution was fitted to a sum of two Gaussians as detailed in the Supporting Information section[18, 20]. The diffusion coefficients, as well as the fraction of steps observed in each mode are detailed in Table 3.1, where the error is the standard deviation between

replicates. Interestingly, as with the desorption rate, no significant difference between the solution conditions was observed for the diffusion coefficients of either the crawling (D_{crawl}) or flying (D_{fly}) modes or the fraction of steps observed for each mode, f_{crawl} and 1-f_{crawl}, respectively. These results indicate that the presence of salt and the specific identity of the salts have no significant impact on the free energy landscape experienced by adsorbed hydrophobic probe molecules.

Table 3.1 - Summary of diffusion fractions and coefficients. Errors are one standard deviation between replicates.

Solvent	**f_{crawl}**	**D_{crawl} ($\mu m^2/s$)**	**D_{fly} ($\mu m^2/s$)**	**D_{avg} ($\mu m^2/s$)**
Water	0.64±0.12	0.0091±0.0011	0.059±0.012	0.027±0.002
1.0M NaSCN	0.61±0.04	0.0096±0.0014	0.050±0.0048	0.026±0.003
1.0M NaF	0.56±0.09	0.0084±0.0011	0.051±0.008	0.028±0.009

3.5 - Discussion

In this work, we have demonstrated that hydrophobic molecules exhibit a higher surface coverage on hydrophobic surfaces in salt solutions that have been shown to increase the surface affinity and CMC for various molecules[3, 4, 6]. Single molecule trajectory analysis allowed us to separately analyze surface coverage, adsorption and desorption, leading to the conclusion that the increase in surface coverage was entirely dominated by an increased adsorption rate.

In particular, the combined results presented above suggest that the ionic effects associated with interfacial phenomena are specific to the adsorption process itself, i.e. the adsorption rate increased systematically in the presence of ions that are expected to increase hydrophobic interactions. However, once a hydrophobic solute molecule has adsorbed to a hydrophobic surface, specific ion

effects were negligible, as indicated by the insensitivity of the desorption rate and statistical details of the surface diffusion to solution conditions. Qualitatively, this suggests that the effect of ions may be to weaken the effective free energy barrier associated with adsorption, while the strength of the actual hydrophobic interaction is not affected. One specific hypothesis, consistent with these observations, is that the ions may alter the free energy of the hydrophobic probe in the bulk liquid phase, but do not significantly impact the free energy or the magnitude of the barrier to desorption from the surface. The change of the liquid phase free energy is consistent with the notion that specific ions can impact the hydration shells around a hydrophobic molecule in solution. Recent work contends that some ions, such as fluoride, are expelled more strongly from the hydration shell around hydrophobic solutes than are other ions[24]. This expulsion would lower the entropy of hydrophobic molecules in solution without having an impact on the free energy of molecules interacting with the surface. Figure 3.4 provides a schematic picture for the free energy of a probe molecule as a function of distance from the solid surface. The general shape of this curve is consistent with that predicted by molecular dynamics simulations for pairwise interactions between hydrophobic solutes, where a free energy barrier is associated with bringing molecules together from infinity, and the free energy is minimized upon close approach[15].

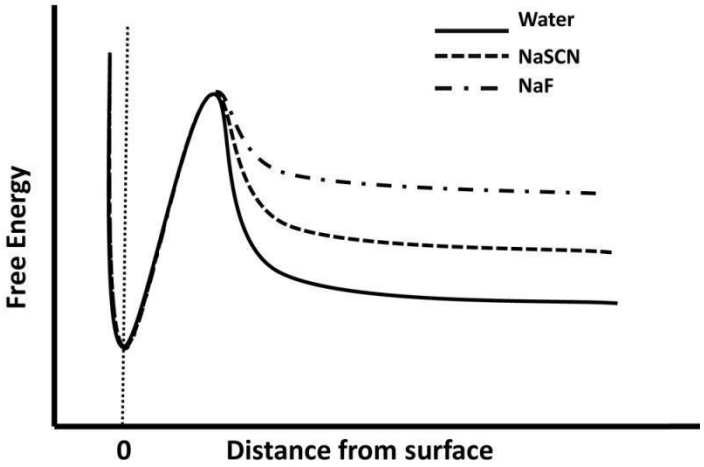

Figure 3.4 - Qualitative representation of the free energy of an fl-C12 molecule as a function of distance from the surface.

3.6 – Supporting information

3.6.1 - Sample preparation

Hydrophobic surfaces were prepared through chemical modification of 50 mm diameter fused silica (FS) wafers. The FS wafers were cleaned by immersion in hot (90 °C) piranha solution (30% H_2O_2/70% H_2SO_4 by volume) for ~60 min followed by UV-ozone treatment (Boekel UV Clean model 135500) for an additional ~60 min. Extra care should be used when handling piranha solution as it is strongly corrosive. Following the UV-ozone treatment, the wafers were immediately placed in a 25 °C solution of toluene/octadecyltriethoxysilane (OTES)/n-propylamine with a ratio of 200:3:1 by volume for ~12 hours[18]. This process yielded FS substrates coated with an octadecylsilane (OTS) self-assembled monolayer. Surfaces were characterized by contact angle goniometry, with all surfaces exhibiting a water contact angle of 105° ± 3°. Modified surfaces were then placed in a custom built TIRF microscopy flow cell and exposed to solutions of 1.0 M salt (NaF or NaSCN) containing fluorescently labeled dodecanoic acid 4,4-Difluoro-5,7-Dimethyl-4-Bora-3a,4a-Diaza-*s*-Indacene-3-Dodecanoic Acid (BODIPY FL-C_{12}, Invitrogen Inc., USA) at a concentration of $2x10^{-12}$M. The probe was chosen because both the dodecanoic acid and the BODIPY fluorophore moieties are strongly hydrophobic and uncharged at neutral pH.

3.6.2 - TIRF Microscopy and Trajectory Analysis

Time sequences of images were acquired using a cooled EMCCD camera (Andor iXon3) and a custom-built prism-based TIRF microscope (Nikon Eclipse TE2000-U) that has been described previously[25]. Excitation light with a wavelength of 491 nm was provided by a diode pumped solid

state laser (Cobalt Calypso 100). Images were collected continuously for 4 minutes with an exposure time of 200 ms per image. A sample image is shown in figure 3.5 where the bright spots are single probe molecules.

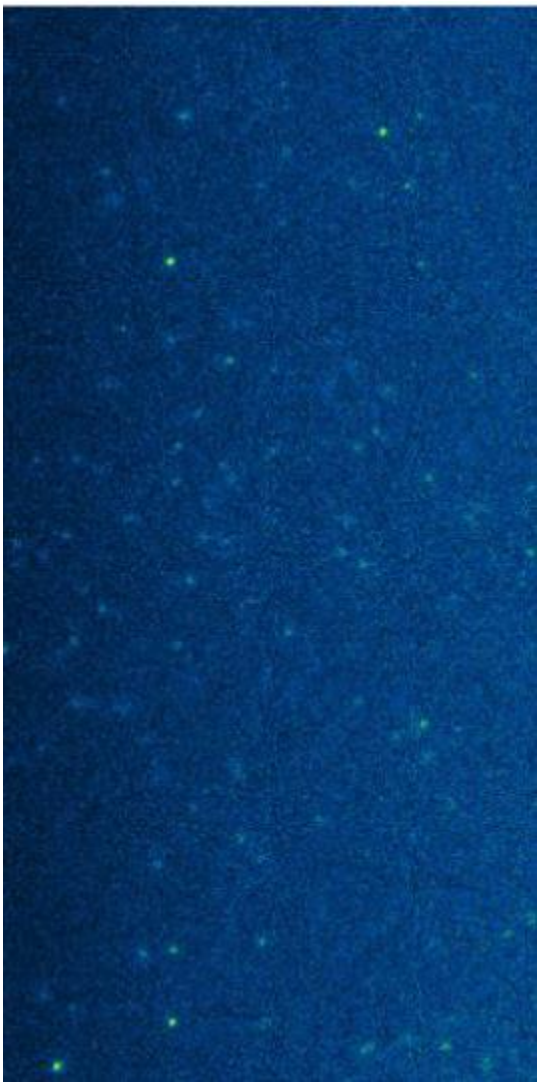

Figure 3.5 - A false-colored sample image of fl-C12 molecules on an OTS interface. Bright spots green are individual probe molecules.

Analysis was performed in Mathematica using algorithms previously described[26]. In short, fl-C12 probe molecules appeared as diffraction-limited spots. These spots were localized using center of

intensity fits and subsequently linked together, frame-to-frame, to form trajectories for each molecule. A diffraction-limited spot was determined to be the same molecule if the center of intensity was within 2 μm of a spot from the previous frame. An example of the image tracking is shown in figure 3.6. Molecules are outlined by the white circles and identified by a unique number. Diffusive steps are plotted as a yellow line between the locations of the probe molecule on sequential frames.

Figure 3.6 - An example of molecular tracking of fl-C12 molecules at the OTS-Aqueous interface. Yellow lines connect the location of the probe molecule on sequential frames.

Adsorption rates were calculated simply by counting the number of new molecules that appeared in the images over the course of each experiment and normalizing by the exposure time. Surface residence times were calculated by multiplying the number of frames an object was present on the surface by the exposure time per frame.

3.6.3 - Residence Time Calculations

Previous experiments have shown that there is a broad distribution in the residence times for molecules on the surface[18,27]. These experiments showed a similar trend, but the distributions for the various experimental conditions were not significantly different. The average residence time for each replicate experiment was calculated by averaging the number of frames each molecule resided on the surface multiplied by the time per frame (0.2 seconds per frame). The error given represented the standard deviation between replicates

As with any fluorescence experiment, photobleaching must be considered. For typical illumination conditions in our experiments, the characteristic photobleaching time of the probe molecule was determined to be ~300 seconds[28], which is two orders of magnitude longer than the mean residence time. This indicated that photobleaching has a negligible effect on these measurements.

3.6.4 - Cumulative Distributions

Complementary cumulative distributions are constructed counting the number of displacements that are of length $r^2/4t$ or longer and dividing by the total number of displacements observed.

$$C(r^2, t) = \frac{\sum_{r^* \geq r}^{\infty} \frac{r^{*2}}{4t}}{\sum_{r^2=0}^{\infty} \frac{r^{*2}}{4t}}$$

3.6.5 - Double Gaussian Fit

The double Gaussian function used to fit the cumulative squared step-size probability distribution is shown below. The free parameters are f_{crawl}, D_{crawl}, and D_{fly} as described in the text.

$$C(r^2, t) = f_{crawl} * e^{-\frac{r^2}{4tD_{crawl}}} + (1 - f_{crawl}) * e^{-\frac{r^2}{4tD_{fly}}}$$

3.7 - Acknowledgements

The authors acknowledge support from the U.S. Department of Energy Basic Energy Sciences, Chemical Science, Geosciences, and Biosciences Division (DE-SC0001854).

3.8 - References

1. Hofmeister, F., Zur Lehre Von Der Wirkung Der Salze. *Arch. Exp. Pathol. Pharmakol.* **1888,** *24*, 247-260.

2. Long, F. A.; McDevit, W. F., Activity Coefficients of Nonelectrolyte Solutes in Aqueous Salt Solutions. *Chem. Rev.* **1952,** *51*, 119-169.

3. Janado, M.; Yano, Y.; Doi, Y.; Sakamoto, H., Peculiar Effects of Alkali Thiocyanates on the Activity Coefficients of Aromatic Hydrocarbons in Water. *J. Solution Chem.* **1983,** *12*, 741-754.

4. Miyagishi, S.; Okada, K.; Asakawa, T., Salt Effect on Critical Micelle Concentrations of Nonionic Surfactants, N-Acyl-N-Methylglucamides (Mega-N). *J. Colloid Interf. Sci.* **2001,** *238*, 91-95.

5. Zhang, Y.; Cremer, P. S., Interactions between Macromolecules and Ions: The Hofmeister Series. *Curr. Opin. Chem. Biol.* **2006,** *10*, 658-663.

6. Para, G.; Jarek, E.; Warszynski, P., The Hofmeister Series Effect in Adsorption of Cationic Surfactants-Theoretical Description and Experimental Results. *Adv. Colloid Interface Sci.* **2006,** *122*, 39-55.

7. Para, G.; Warszynski, P., Cationic Surfactant Adsorption in the Presence of Divalent Ions. *Colloid Surface A* **2007,** *300*, 346-352.

8. Kunz, W.; Lo Nostro, P.; Ninham, B. W., The Present State of Affairs with Hofmeister Effects. *Curr. Opin. Colloid In.* **2004,** *9*, 1-18.

9. Cacace, M. G.; Landau, E. M.; Ramsden, J. J., The Hofmeister Series: Salt and Solvent Effects on Interfacial Phenomena. *Q. Rev. Biophys.* **1997,** *30*, 241-277.

10. Jungwirth, P.; Winter, B., Ions at Aqueous Interfaces: From Water Surface to Hydrated

Proteins. *Annu. Rev. Phys. Chem.* **2008,** *59*, 343-366.

11. Petersen, P. B.; Saykally, R. J., On the Nature of Ions at the Liquid Water Surface. *Annu. Rev. Phys. Chem.* **2006,** *57*, 333-364.

12. Schwierz, N.; Horinek, D.; Netz, R. R., Anionic and Cationic Hofmeister Effects on Hydrophobic and Hydrophilic Surfaces. *Langmuir* **2013,** *29*, 2602-2614.

13. Horinek, D.; Serr, A.; Bonthuis, D. J.; Bostrom, M.; Kunz, W.; Netz, R. R., Molecular Hydrophobic Attraction and Ion-Specific Effects Studied by Molecular Dynamics. *Langmuir* **2008,** *24*, 1271-1283.

14. Thomas, A. S.; Elcock, A. H., Direct Observation of Salt Effects on Molecular Interactions through Explicit-Solvent Molecular Dynamics Simulations: Differential Effects on Electrostatic and Hydrophobic Interactions and Comparisons to Poisson-Boltzmann Theory. *J. Am. Chem. Soc.* **2006,** *128*, 7796-7806.

15. Thomas, A. S.; Elcock, A. H., Molecular Dynamics Simulations of Hydrophobic Associations in Aqueous Salt Solutions Indicate a Connection between Water Hydrogen Bonding and the Hofmeister Effect. *J. Am. Chem. Soc.* **2007,** *129*, 14887-14898.

16. Baer, M. D.; Mundy, C. J., Toward an Understanding of the Specific Ion Effect Using Density Functional Theory. *J. Phys. Chem. Lett.* **2011,** *2*, 1088-1093.

17. Yang, Q.; Zhao, J., Hofmeister Effect on the Interfacial Dynamics of Single Polymer Molecules. *Langmuir* **2011,** *27*, 11757-11760.

18. Nelson, N.; Walder, R.; Schwartz, D. K., Single Molecule Dynamics on Hydrophobic Self-Assembled Monolayers. *Langmuir* **2013,** *28*, 12108-12113.

19. Kumar, A.; Bullard, R. L.; Patel, P.; Paslay, L. C.; Singh, D.; Bienkiewicz, E. A.; Morgan, S. E.; Rangachari, V., Non-Esterified Fatty Acids Generate Distinct Low-Molecular Weight

Amyloid-B (Aβ42) Oligomers Along Pathway Different from Fibril Formation. *PLOS ONE* **2011,** *6*, e18759.

20. Walder, R.; Nelson, N.; Schwartz, D. K., Single Molecule Observations of Desorption-Mediated Diffusion at the Solid-Liquid Interface. *Phys. Rev. Lett.* **2011,** *107*, 156102.

21. Langmuir, I., The Adsorption of Gases on Plane Surfaces of Glass, Mica and Platinum. *J. Am. Chem. Soc.* **1918,** *40*, 1361-1403.

22. Ray, A.; Nemethy, G., Effects of Ionic Protein Denaturants on Micelle Formation by Nonionic Detergents. *J. Am. Chem. Soc.* **1971,** *93*, 6787-6793.

23. Dobbs, K. D.; Doren, D. J., Dynamics of Molecular Surface Diffusion: Origins and Consequences of Long Jumps. *J. Chem. Phys.* **1992,** *97*, 3722-3735.

24. Rankin, B. M.; Ben-Amotz, D., Expulsion of Ions from Hydrophobic Hydration Shells. *J. Am. Chem. Soc.* **2013,** *135*, 8818-8821.

25. Honciuc, A.; Harant, A. W.; Schwartz, D. K., Single-Molecule Observations of Surfactant Diffusion at the Solution-Solid Interface. *Langmuir* **2008,** *24*, 6562-6566.

26. Walder, R.; Nelson, N.; Schwartz, D. K., Super-Resolution Surface Mapping Using the Trajectories of Molecular Probes. *Nat. Commun.* **2011,** *2*, 515.

27. Walder, R.; Schwartz, D. K., Single Molecule Observations of Multiple Protein Populations at the Oil-Water Interface. *Langmuir* **2010,** *26*, 13364-13367.

28. Monserud, J. H.; Schwartz, D. K., Effects of Molecular Size and Surface Hydrophobicity on Oligonucleotide Interfacial Dynamics. *Biomacromolecules* **2012,** *13*, 4002-4011.

Chapter 4: Super-Resolution Surface Mapping using the Trajectories of Molecular Probes

4.1 - Abstract

We have developed a new chemical imaging method, MAPT (Mapping using Accumulated Probe Trajectories) that generates maps of surface interactions based on the quantitative behavior of dynamic probe molecules. The approach is based on distributing different aspects of molecular trajectories (e.g. adsorption events, diffusive steps, and desorption events) into distinct locations and then combining many trajectories to generate spatial maps. The maps are super-resolution in nature, because they are accumulated from single molecule observations, each of which is highly localized. Unlike other super-resolution techniques, which report only photon or point counts, our analysis generates spatial maps of physical quantities (adsorption rate, desorption probability, local surface diffusion coefficient, surface coverage/occupancy) that are directly associated with the molecular interactions between the probe molecule and the surface. We demonstrate the feasibility of this characterization using a surface patterned with various degrees of hydrophobicity.

4.2 - Introduction

Surface modification has become a critical component of micro- and nanofabrication with applications in technologies ranging from biodetection[1,2] to catalysis[3,4] and many more[5-8]. Many of these applications exploit non-covalent interactions and molecular recognition. In contrast with the situation for "hard" materials *in vacuo*, where numerous analytical methods exist to detect and map atomic species, there is a dearth of appropriate characterization methods for "soft" molecular materials, where non-covalent molecular interactions are paramount, and applications often involve "wet" conditions. Methods based on scanning probe microscopy (SPM, e.g. chemical force microscopy[9-11]) can provide some local information about surface interactions. However, SPM has significant limitations in this regard, not the least of which is the need to understand the surface chemistry of the probe tip itself. In addition, the time resolution of SPM is poor and there are severe challenges with respect to the robustness and reproducibility of probe chemistry.

In recent years, super-resolution optical microscopy methods have been developed that compile accumulated observations of individual molecules to create images with resolution beyond the diffraction limit. STORM[12] (Stochastic Optical Reconstruction Microscopy) and PALM[13] (photoactivated localization microscopy) are perhaps the best-known examples. Similar approaches have recently been applied at surfaces (e.g. PAINT[14]), using randomly adsorbed molecules from solution to identify surface features with super-resolution precision[14-17]. This is a powerful concept; however, the methods developed to date provide images that are based purely upon "point counts" (a relative contrast mechanism) and lack the general ability to connect observed features with specific material properties and interactions. In addition, these techniques are thus far limited to special cases of complementary DNA[15] on surfaces, local surface

enhancement from hotspots[17] or where the surface selectively quenches fluorescence outside features of interest[14,16]. Our goal here is to develop a generally-applicable super-resolution surface mapping method, where features observed in images can be directly-related to specific surface functionalities.

In previous work, we demonstrated the ability of single molecule total internal reflection fluorescence microscopy (TIRFM) to quantify the adsorption[18,19] and diffusion[19-21] of surfactant probes at the solid-liquid interface in an effort to understand fundamental dynamic interfacial behavior. In this paper, we turn this approach upside-down, and use the trajectories of probe molecules (BODIPY labeled dodecanoic acid) to provide images based on the lateral heterogeneity of probe-surface interactions. Importantly, we use the absolute physical properties of these interactions to map a surface, rather than arbitrary photon or point counts. We call this new approach Mapping using Accumulated Probe Trajectories, or MAPT. In order to implement mapping based on the dynamic details of molecular trajectories, an enormous leap was required in terms of the number of trajectories analyzed, from ~10^2 in a typical single-molecule tracking experiment, to 10^5–10^6. This was achieved by developing efficient, high-throughput computational methods, which enabled us to extract quantitative information from massive data sets.

Recent molecular simulations have suggested that single molecule interactions can potentially identify nanoscale differences in hydrophobicity[22]. Here, we use a photo-patterned hydrophobically-modified surface[23] as a model system to prepare spatially well-defined areas of varying hydrophobicity, and a fluorescently-labeled fatty acid (BODIPY labeled dodecanoic acid)

as a probe molecule. Fatty acid surfactants are good model systems for studying hydrophobic interactions in aqueous interfacial systems – in part due to the carboxyl group which enhances water-solubility through hydrogen bonding, and to the alkyl tail that remains largely unsolvated in an aqueous phase, while retaining sufficient solubility. BODIPY is one of the most hydrophobic fluorophores available, so it is also particularly appropriate for these experiments. Consistent with these expectations, previous experiments that measured activation energies associated with the surface diffusion of BODIPY-labeled fatty acids [21], and images based on probe-surface affinity[23] suggested that this homologous series of probe molecules interacted with TMS-coated fused silica primarily via hydrophobic interactions. After obtaining maps of several dynamic probe properties (adsorption rate, interfacial mobility, occupancy, desorption probability), we directly relate these physical properties back to "calibration" data from uniform surfaces to identify the specific hydrophobicity associated with each region. This demonstration system (where hydrophobic interactions are the dominant interaction) allows us to make direct connections between standard macro scale measurements of hydrophobicity (contact angle) and small scale probe-surface interactions of the MAPT technique. We also demonstrate that spatial features can be identified at super-resolution length scales

4.3 - Results

In order to demonstrate the utility of MAPT, we created a patterned trimethylsilyl (TMS) surface using UV photodegradation. The sample surface was exposed to UV light for 180 s with a TEM grid as a contact mask. To put this into context, 180s of photodegradation reduced the water contact angle of a homogeneous TMS surface from ~94˚ to ~69˚. The surface was exposed to a solution of BODIPY-dodecanoic acid at concentrations of 10^{-12} M to 10^{-15} M. These

concentrations are sufficiently low that no significant self-assembly occurs on the surface. In fact, except for a tiny fraction of photobleached molecules, we can explicitly see each molecule adsorbed on the surface, and the average fractional surface coverage is typically on the order of 10^{-9}. Figure 4.1 shows MAPT images of the photo-patterned TMS surface that are based on the (a) adsorption rate, (b) average diffusion coefficient, (c) desorption probability, and (d) occupancy (i.e. mean surface coverage) of the surface. The bin (i.e. pixel) size for these images was 270 nm x 270 nm. All four images were extracted simultaneously from the same ~330,000 probe trajectories. The pattern associated with the photomask is clearly visible in all four MAPT images. In particular, square regions associated with the less hydrophobic photodegraded areas are visible, surrounded by more hydrophobic un-degraded regions. In Figure 4.1.a, the adsorption rate is greater (red, yellow, green) in the hydrophobic areas, while the adsorption rate is lower (blue, green) in the degraded regions. In Figure 4.1.b, one sees slower probe diffusion (green, blue) in the un-degraded regions and faster diffusion (red, yellow) within the degraded regions. There is also a significant amount of black (i.e. empty pixels corresponding to no displacements), which is a consequence of the lower overall adsorption rate and the high probability of desorption seen in Figure 4.1.c. In Figure 4.1.c, the hydrophobic areas have a lower probability of desorption (blue, green, yellow), whereas in the less hydrophobic regions mostly red pixels are observed, which correspond to a high probability of desorption. Figure 4.1.d shows that the surface coverage in the hydrophobic areas is significantly higher (red, yellow, green) than in the hydrophilic regions (blue, black).

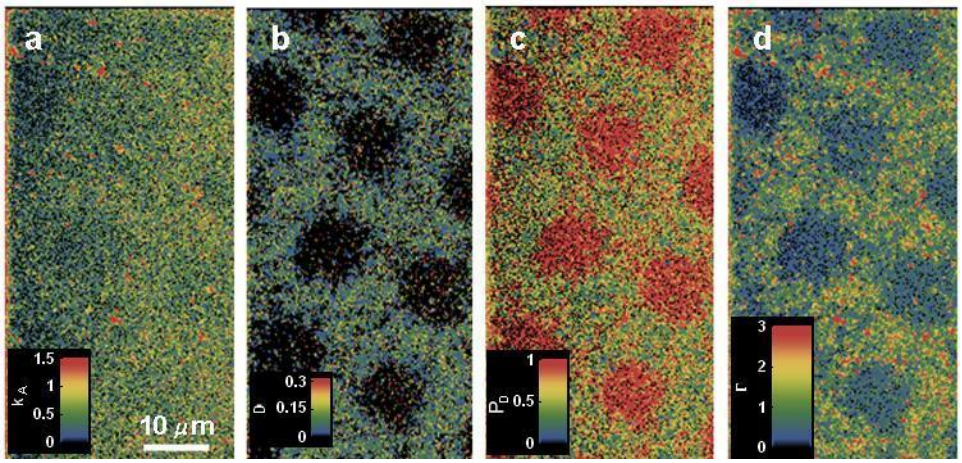

Figure 4.1 - MAPT images of the photopatterned TMS surface. MAPT images of (**a**) adsorption rate (10^{13} $\mu m^{-2}s^{-1}M^{-1}$) (**b**) average diffusion coefficient ($\mu m^2/s$) (**c**) desorption probability per 400 ms and (**d**) surface coverage/occupancy (10^{13} $\mu m^{-2}s^{-1}M^{-1}$) on a photo-patterned TMS surface.

In addition to the overall trend observed in the various dynamic probe behaviors, local variation is also clearly observed on μm length scales within both the degraded and un-degraded regions. The cross-correlation of various properties provides strong evidence that this spatial variation is representative of actual material properties. For example, in the un-degraded TMS regions, we see many small (sub-micron) regions of high adsorption (bright red regions in Figure 4.1.a) that also correspond to areas of high occupancy (co-localized red spots in Figure 4.1.d), lower desorption probability (blue spots in Figure 4.1.c), and slower interfacial diffusion (green or blue in Figure 4.1.b). These features persist across independent measurements of the surface, indicating that they are not merely statistical artifacts, but real surface features. The "hot spots" have not been seen in AFM images[23] of TMS or photodegraded TMS surfaces. Many of these small features on these maps also contain interesting substructure, which can be accessed by decreasing the size of the bins. The resolution limits of such substructures will be explored later in the letter.

An important experimental consideration is the effect of photobleaching on the MAPT desorption probability image. We can place a lower limit on the characteristic time-scale for photobleaching using the longest-lived molecular population. On TMS, this is measured to be 14.5 s +/- 1.4 s, which corresponds to a desorption probability of 0.028 +/- 0.003. In the context of MAPT imaging, this represents a background level in the desorption probability channel, and it is an order of magnitude lower than any desorption probability seen in the maps.

Surface roughness from the photodegradation might be expected to contribute to both the overall trends in dynamics, as well as the "hotspots". However, in previous work[24] the primary source of surface roughness was determined to be from the fused silica substrate, not the photodegredation of the TMS layer. Therefore, the surface chemistry would appear to be the dominant factor for the trends in overall dynamics, as well as the "hotspots".

The fact that the details of the contrast in the images in Figure 4.1 can be directly related to actual physical phenomena provides deep insight into the local probe-surface interactions. However, the ultimate goal of MAPT is to go beyond this, and to directly identify regions of an image with a particular surface chemistry. This is possible because the numerical values comprising the MAPT images are not arbitrary, but rather represent absolute values of measureable physical properties. Therefore, one can separately perform calibration experiments on un-patterned surfaces of known surface chemistry, and compare the corresponding values of dynamic parameters to local values in MAPT images.

Figure 4.2 shows an overview of the values obtained in such calibration experiments, where parameters of mean adsorption rate, surface diffusion coefficient, etc. were measured on un-patterned TMS surfaces that had been photodegraded for various lengths of time. In addition, Figure 4.2.a shows the contact angle on these surfaces, specifically the increase in $\cos(\theta_c)$ with degradation time, where θ_c is the static contact angle of water on the surface under ambient conditions. In previous work[24], we have shown that the static, receding and advancing contact angle for undegraded and photodegraded TMS surfaces are equivalent within experimental uncertainty. This trend shows a transition from a hydrophobic surface for pure TMS, to a hydrophilic surface at long degradation times, with the contact angle at 480 s matching the expected contact angle for water on an FS surface. While some of the properties vary in a smooth and intuitive way with increased degradation time, others exhibit unexpected non-monotonic behavior, which we hypothesize may be related to nanoscale heterogeneity introduced by the photodegradation process. We emphasize that the main purpose of these data in the context of this manuscript is to obtain a characteristic "fingerprint" of a given type of surface in terms of dynamic probe properties.

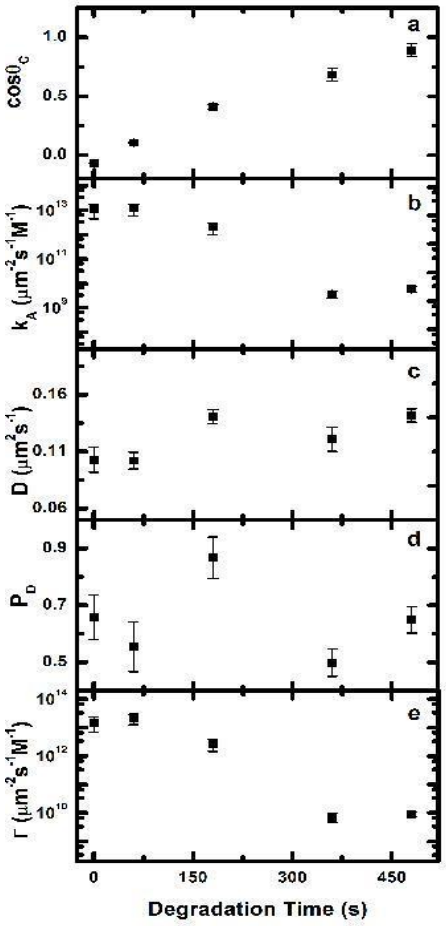

Figure 4.2 - Characterization data from homogenous TMS surfaces vs. UV degradation exposure. (**a**) Cosine of the contact angle, (**b**) adsorption rate, (**c**) average diffusion coefficient, (**d**) desorption probability per 400 ms, (**e**) surface coverage (i.e. occupancy).

In Figure 4.2.b the average adsorption rate k_A is observed to decrease rapidly by nearly three orders of magnitude over the range of the degradation times measured. It is important to note that this is the rate of individual molecules adsorbing to the surface, not the macroscopic *net* absorption rate that is measured using ensemble-averaging methods. The average diffusion coefficient, *D*,

increases gradually with decreasing hydrophobicity (Figure 4.2.c), but varies in an irregular way in intermediate ranges. The average desorption probability, P_D, also exhibits non-monotonic behavior with a clear maximum at 180s degradation time (Figure 4.2.d). Figure 4.2.e shows the average surface coverage, Γ, which is conceptually related to the competition between adsorption rate and desorption probability; this quantity decreases rapidly with degradation time (Figure 4.2.e). These data collectively show how fatty acid probe interactions (Figure 4.2.b-e) change with increasing photodegradation of TMS surfaces, and form a basis for correlating the local quantities obtained from MAPT image sets with macroscopic properties such as hydrophobicity.

In order to make direct connections between MAPT images in Figure 4.1 and the calibration data in Figure 4.2, we chose several regions of interest that are marked in Figure 4.3.a as numbered yellow squares. Regions 1-3 are in photodegraded areas, while regions 4 and 5 are in areas that were protected by the photomask. Figure 4.3.b compares the mean values of surface coverage/occupancy and adsorption rate from both the homogenous surface measurements (plotted with symbols) and the regions of interest (plotted with numbers corresponding to the region of interest in Figure 4.3.a).

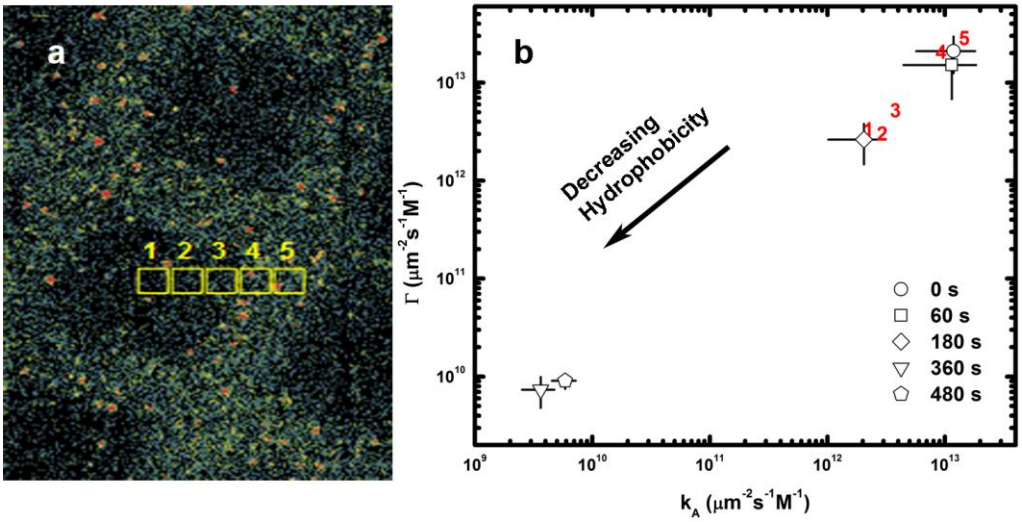

Figure 4.3 - MAPT image regions compared to data for homogenous TMS surfaces. (**a**) Spatial map of adsorption on a TMS surface patterned by UV light for 180s with the regions of interest marked by yellow squares and labeled with corresponding identification numbers. (**b**) Surface coverage versus adsorption rate from the homogenous surface measurements (plotted with symbols) and the regions of interest (plotted with numbers corresponding to the region of interest in Fig. 4.3.**a**).

In Figure 4.3.b, the values of both adsorption rate and occupancy for regions 1 and 2 are within experimental uncertainty of the values associated with the homogenous surface degraded for 180s (diamond). Similarly, the values of both parameters for regions 4 and 5 are within experimental uncertainty of the values associated with the un-degraded TMS surface (circle). Interestingly, region 3 exhibits values of the adsorption rate and surface occupancy that are intermediate between the values associated with homogeneous surfaces degraded for 60s (square) and 180s (diamond), suggesting that region 3 corresponds to a location with an intermediate hydrophobicity. This is expected given its location near the edge of the degraded region. Such hydrophobicity gradients

have been previously observed[24] and correlated with novel nanoparticle dynamics. This analysis demonstrates that we can make calibration measurements of absolute physical quantities on homogenous surfaces and then match these quantities to the measured properties of regions on heterogeneous surfaces. In effect, single molecule interactions can be used to probe local hydrophobicity quantitatively on an absolute scale.

Thus far, we have demonstrated that MAPT can be used to identify heterogeneity of surface chemical functionality on length scales of ~0.5–20 μm. However, because the MAPT approach involves the accumulation of single-molecule trajectories, it is inherently capable of resolving features that are smaller than the diffraction-limit. Figure 4.4.a and 4.4.c demonstrate the super-resolution capabilities of MAPT using two representative surface maps of surface coverage, which are on TMS surfaces that had been degraded for 360s and 210s respectively. Figure 4.4.b and 4.4.d show corresponding line scans associated with the arrows in Figure 4.4.a and 4.4.c respectively. In these examples, we use the full-width at half-maximum (FWHM) of the indicated features to estimate the width of the surface feature. The apparent width of the feature in Figure 4.4.b is 175 nm and in Figure 4.4.d 125 nm, which are significantly below the diffraction limit (~300 nm).

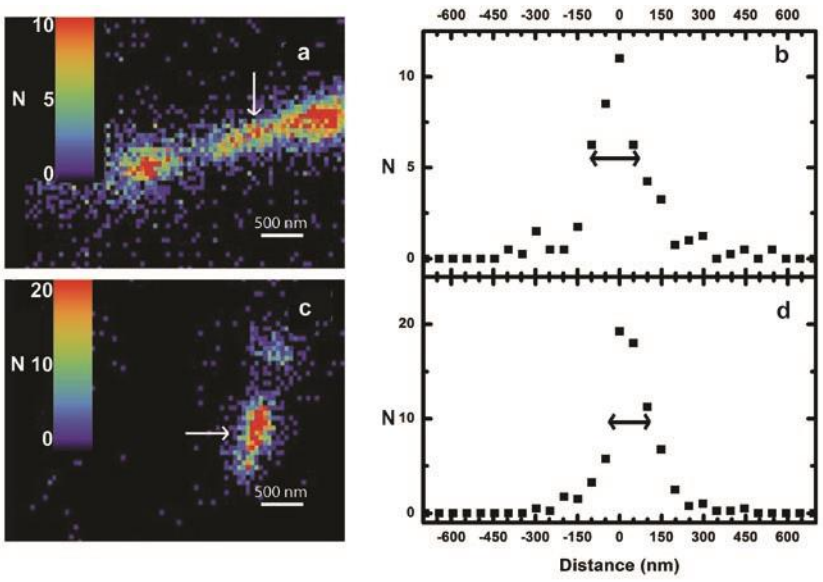

Figure 4.4 - MAPT images with line scan graphs demonstrating super-resolution. Surface coverage maps of small features on a TMS surface degraded for 360 seconds (**a**) and a TMS surface degraded for 210 seconds (**c**) with corresponding cross sections showing the full width, half maximum (indicated by the double arrows) of (**b**) 175 nm and (**d**) 125 nm.

The ultimate resolution limits for super resolution techniques depend on many factors[25], including the interfacial mobility of the molecules, the frame acquisition time, the signal to background ratio of the fluorescent emission from single molecules, the number of molecules, compensation for mechanical drift, and the details of the calculation of the center of intensity. Using the PAINT technique, resolution limits of 18 nm have been reported[16] and MAPT is fundamentally capable of producing similar results under the same experimental conditions. In our experiment, the long acquisition time (400 ms), lack of compensation for mechanical drift, and mobility of the molecules are the primary sources of the relatively large resolution limit (125 nm), in comparison to similar experiments (18 nm). While faster acquisition time and mechanical drift can be corrected for by modification of the experimental setup, the mobility of the molecules likely

represents a fundamental limitation of spatial resolution (from point spread function broadening) of the MAPT technique. The probe mobility also provides advantages, however, because mobile probe molecules "explore" large areas of the surface, which enhances the molecular targeting of any rare, small scale surface features. Here we demonstrate that even using mobile single surfactant molecules on a general hydrophobic surface (without quenching to enhance contrast), it is possible to map features with super resolution.

4.4 - Discussion

The MAPT technique provides spatial maps, based on unique *in-situ* molecular-probe dynamics, that are distinct from and complementary to images obtained using pre-existing methods, e.g. scanning probe microscopy. In principle, the MAPT technique could reach the same probe densities as AFM/STM measurements, given enough molecules on the surface, which is mainly a matter of increasing the total time of trajectory accumulation. In practice, however, to reach such high densities would require a number of single molecule localizations that is not currently computationally feasible. Thus the practical resolution limit for the MAPT technique is likely similar to other techniques that rely on random adsorbing molecules, which is an order of magnitude greater than typical AFM experiments. The contrasting nature of length scales and measurement versatility show that the MAPT technique is not a replacement for AFM/STM, but rather a complementary technique.

Interestingly, the actual contrast precision and resolution of MAPT images are not purely a function of the total number of accumulated trajectories. For example, even with a large overall density of molecular trajectories in Figure 4.1, the diffusion coefficient map (Figure 4.1.b) exhibits

low density within the photodegraded areas. This is due to the very short residence times in those surface regions, which results in short local trajectories. This demonstrates an interesting feature of this method: because we are exploiting intrinsic dynamic interfacial phenomena of the adsorbate molecules to prepare these maps, for a given probe-surface combination, certain contrast mechanisms will typically provide greater contrast and/or resolution than others. By exploiting a wide range of different combinations of probe chemistry, solvent and surface, our expectation is that the MAPT technique will be able to visualize and identify many varied surface chemistries.

It is interesting to speculate on possible applications of MAPT to other examples of surface chemistry heterogeneity. For example, single molecule imaging was recently used to show a lack of spatial correlations for chemical reactions on a surface[26]. Using MAPT for a similar system, one could quantify absolute chemical reaction rates on surfaces. Furthermore, using single molecule FRET, conformation changes in large molecules (such as polymers or proteins) could be linked to spatial heterogeneities in surface chemistry. Lipid bilayers would also be a useful system for surface mapping, where heterogeneities in mobility could be used to both probe the structure of the bilayer and correlate novel dynamics of membrane proteins with these features.

In conclusion, we have developed a new chemical imaging method based on accumulating single molecule trajectories to generate molecular interaction maps of surfaces. We demonstrated that this mapping technique could be used to quantify spatially heterogeneous average physical quantities associated with hydrophobicity and then identify the specific contact angles associated with those regions using calibration data from uniform surfaces. We also showed that these maps are capable of identifying spatial heterogeneities on super-resolution length scales.

4.5 - Methods

4.5.1 - Sample Preparation

Surfaces were prepared by photodegradation of hydrophobically-modified fused silica (FS) surfaces[23]. A 50 mm-diameter FS wafer (MTI Corp.) was cleaned in hot piranha solution for ~1 h followed by UV−ozone treatment for another ~60 min. The clean hydrophilic substrate was placed in a sealed glass container containing hexamethyldisilazane (HMDS, 99.8% purity, Acros Organics) and positioned ~5 cm above the liquid to expose its surface to HDMS vapor for ~48 h. In contrast with solution deposition of SAMs, this vapor-deposition process ensured that the trimethylsilyl (TMS) layer contained no fluorescent impurities as confirmed by control TIRFM experiments carried out with pure deionized water (Millipore, Milli-Q UV, 18.3 MΩ·cm). These TMS-modified surfaces were then exposed for the desired degradation time to UV illumination from a Hg pen lamp (UVP 254 nm) held ~5 mm from the surface. The intensity was ~0.3 mW/cm^2 at this distance. Patterning was accomplished by photodegradation using 1500 fine grid mesh (Structure Probe, Inc.) as a contact photomask. The patterned surfaces were then exposed to solutions containing fluorescently-labeled dodecanoic acid (Invitrogen Bodipy® FL-C_{12}) at concentrations of 10^{-12} M to 10^{-15} M (significantly below the concentration required for self-assembly) and a time series of TIRFM images was obtained. Images for the time series were sampled continuously for 7 minutes, with each frame having an exposure time of 300-500 ms.

4.5.2 - Surface Mapping Data Analysis

The basis of our surface mapping method is to divide the microscope viewing area into a spatial

grid divided into *bins* of a user-determined size (each bin serves as a pixel in the final image). The positions of all events of interest are determined for each probe molecule trajectory. These data are then sorted into the appropriate spatial bins and finally the accumulated value of each physical quantity is calculated for every bin. For example, the first position of every trajectory is defined as the adsorption location of that probe. The average local adsorption rate is therefore related to the number of molecules that adsorb within a particular bin. For consistency between experiments, the adsorption count is divided by the bin area, the total time for the experiment, and the concentration of probe molecules in solution. The scaling of the adsorption rate by the number of available probes in solution is an appropriate normalization factor for direct comparison of multiple experiments. While the near-surface concentration would be the ideal absolute quantity to use for normalization, we cannot directly know this concentration. However, in our probe-surface system the hydrophobic interaction is dominant, and from first principles one does not expect a significant difference between the near-surface concentration and the bulk solution concentration. A similar approach is used to prepare surface maps of the mean interfacial diffusion coefficient, the desorption probability, and the mean surface occupancy. Details of the algorithms for converting each component of molecular trajectories into surface maps of physical quantities will be described in detail below. Figure 4.5 is a schematic diagram showing several overlaid trajectories; this diagram will be used to illustrate the calculations described in the following sections.

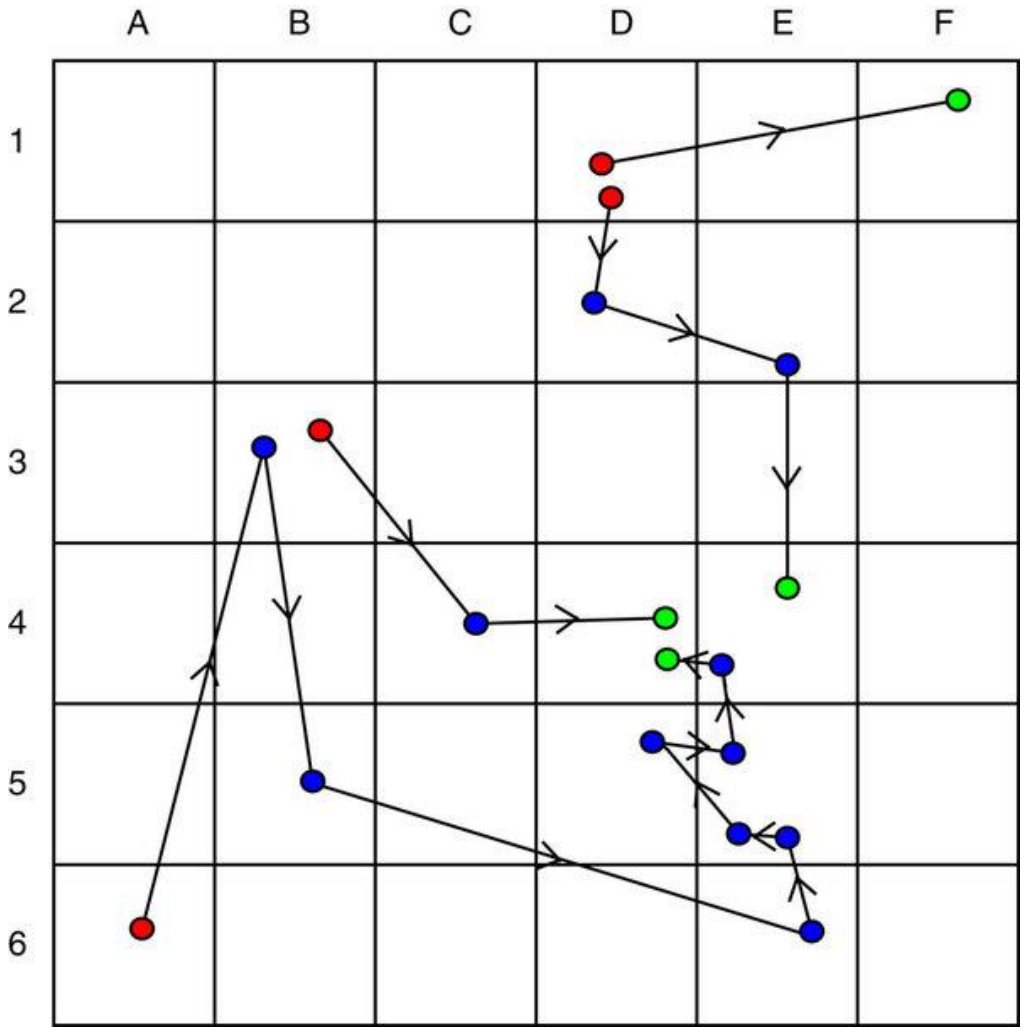

Figure 4.5 - Schematic diagram of single-molecule trajectories within a grid. First position (red), intermediate position (blue) and last position (green).

4.5.3 - Adsorption rate

Adsorption rate refers to the average number of molecules attaching to the surface per area, per time; it is also normalized by bulk concentration. This is different from the net macroscale adsorption rate, which measures the difference between the adsorption and desorption rate. The

adsorption position is defined as the first position of a trajectory. The number of adsorption events for each bin is then counted. For example, in Figure 4.5, bin D1 has two adsorptions, bin B3 and A6 have one adsorption each and all other bins have no adsorptions. These raw numbers are then turned into an adsorption rate by the following formula.

$$K_A = \frac{N_A}{T * A_{Bin} * C_{Probe}} \qquad (1)$$

Where N_A is the number of adsorbed molecules, T is the total time, A_{Bin} is the area per bin and C_{probe} is the bulk solution concentration of probe.

4.5.4 - Desorption Rate

Desorption rate refers to the average number of molecules detaching from the surface per area, per time and bulk concentration. The desorption position is the last position of a trajectory. The number of last positions for each grid area is then counted. In Figure 5, bin D4 has two desorption events, and bins E4 and F1 have one desorption event each. These raw numbers are then turned into desorption rate by the following formula.

$$K_D = \frac{N_D}{T * A_{Bin}} \qquad (2)$$

Where N_D is the number of desorbed molecules, T is the total time and A_{Bin} is the area per bin.

4.5.5 - Surface coverage

Surface coverage (or occupancy) refers to the average number of molecules on the surface per area, per time and bulk concentration. Every recorded position of the trajectory is used to map surface coverage. The number of positions for each grid area is then counted. In Figure 4.5, bin E5 has a raw occupancy of 3, bins B3, D1, D4 and E4 have raw occupancies of 2 and so on. These raw numbers are then turned into surface coverage by the following formula.

$$\Gamma = \frac{N_{MP}}{T * A_{Bin} * C_{Probe}} \quad (3)$$

Where N_{MP} is the number of molecule positions, T is the total time, A_{Bin} is the area per bin and C_{probe} is the bulk solution concentration of probe.

4.5.6 - Desorption Probability

The desorption probability is the probability that a molecule in a given area will desorb in the next time step of the movie. For example, in Figure 4.5 grid E4, there is one desorption event and one molecule position from another trajectory. The desorption probability would be 0.5 because there is one desorption event divided by two molecule positions (one of which is the desorption position). The formula for this calculation is as follows.

$$P_D = \frac{N_D}{N_{MP}} \quad (4)$$

Where N_{MP} is the number of molecule positions and N_D is the number of desorbed molecules.

4.5.7 - Mean Diffusion Coefficient

The mean diffusion is the local mean diffusion within a bin. To create a scalar map of this value, we must designate a location for the displacement vector, which is actually defined by its start and end locations. We have chosen to define the average between the start and end positions (the midpoint) as the position of the displacement. For example, a displacement occurs in Figure 4.5 between bins D1 and F1. Although the displacement starts in D1 and ends at F1, the displacement event will be mapped to bin E1, as this is where the midpoint of the displacement takes place. To determine an effective local diffusion coefficient, we then calculate the square of all displacements for a grid area and divide this average by four times the time per frame as described in the following formula.

$$D = \frac{\langle \Delta x^2 \rangle}{4t} \qquad (5)$$

Where $\langle \Delta x^2 \rangle$ is the mean squared displacement and t is the time per frame.

The uncertainty associated with the average value of an individual bin for diffusion requires an extra term, due to the uncertainty in localizing the vector into a bin of finite size. The uncertainty for a MAPT diffusion pixel is

$$\sigma_{\text{DiffusionBin}} = \frac{\sigma_{x^2}}{4t}\sqrt{\frac{1}{N} + \frac{4Dt}{w^2}} \qquad (6)$$

Where σ_x^2 is the uncertainty of the squared displacements, N is the number of displacements, D is the average diffusion coefficient, t is the time per frame and w is the width of the bin. The first term in the radical is for the standard error portion of the uncertainty. The second term is a ratio of average displacement to bin width, which accounts for the uncertainty in localizing the vector into a bin of finite size.

4.5.8 - Mean direction

The mean direction is the local mean direction of the displacement vectors. This quantity uses the same position (midpoint of the displacement) as the mean diffusion. However, here we take the average displacement vector in a grid area and then calculate the direction of this vector.

4.6 - Acknowledgements

This work was supported by the US National Science Foundation (CHE 0841116) and the US Department of Energy (DE-0001854).

4.7 – References

1. Gupta, N. *et al.* A versatile approach to high-throughput microarrays using thiol-ene chemistry. *Nat. Chem.* **2**, 138-145, doi:10.1038/nchem.478 (2010).
2. Barone, P. W., Baik, S., Heller, D. A. & Strano, M. S. Near-infrared optical sensors based on single-walled carbon nanotubes. *Nat. Mater.* **4**, 86-U16, doi:10.1038/nmat1276 (2005).
3. Marshall, S. T. *et al.* Controlled selectivity for palladium catalysts using self-assembled monolayers. *Nat. Mater.* **9**, 853-858, doi:10.1038/nmat2849 (2010).
4. Krogman, K. C., Lowery, J. L., Zacharia, N. S., Rutledge, G. C. & Hammond, P. T. Spraying asymmetry into functional membranes layer-by-layer. *Nat. Mater.* **8**, 512-518, doi:10.1038/nmat2430 (2009).
5. Yamamoto, M. *et al.* Patterning Reactive Microdomains inside Polydimethylsiloxane Microchannels by Trapping and Melting Functional Polymer Particles. *Journal of the American Chemical Society* **130**, 14044-14045, doi:10.1021/ja804803s (2008).
6. Xu, H. *et al.* Microcontact Printing of Dendrimers, Proteins, and Nanoparticles by Porous Stamps. *Journal of the American Chemical Society* **131**, 797-803, doi:10.1021/ja807611n (2008).
7. Calhoun, M. F., Sanchez, J., Olaya, D., Gershenson, M. E. & Podzorov, V. Electronic functionalization of the surface of organic semiconductors with self-assembled monolayers. *Nat. Mater.* **7**, 84-89, doi:10.1038/nmat2059 (2008).
8. Sanghvi, A. B., Miller, K. P. H., Belcher, A. M. & Schmidt, C. E. Biomaterials functionalization using a novel peptide that selectively binds to a conducting polymer. *Nat. Mater.* **4**, 496-502, doi:10.1038/nmat1397 (2005).
9. Vezenov, D. V., Noy, A. & Ashby, P. Chemical force microscopy: probing chemical origin

of interfacial forces and adhesion. *J. Adhes. Sci. Technol.* **19**, 313-364 (2005).

10. Yebra, D. M., Kiil, S. & Dam-Johansen, K. Antifouling technology - past, present and future steps towards efficient and environmentally friendly antifouling coatings. *Prog. Org. Coat.* **50**, 75-104, doi:10.1016/j.porgcoat.2003.06.001 (2004).
11. Zhang, S. G. Fabrication of novel biomaterials through molecular self-assembly. *Nat. Biotechnol.* **21**, 1171-1178, doi:10.1038/nbt874 (2003).
12. Rust, M. J., Bates, M. & Zhuang, X. W. Sub-diffraction-limit imaging by stochastic optical reconstruction microscopy (STORM). *Nat. Methods* **3**, 793-795, doi:10.1038/nmeth929 (2006).
13. Betzig, E. *et al.* Imaging Intracellular Fluorescent Proteins at Nanometer Resolution. *Science* **313**, 1642-1645, doi:10.1126/science.1127344 (2006).
14. Sharonov, A. & Hochstrasser, R. M. Wide-field subdiffraction imaging by accumulated binding of diffusing probes. *Proc. Natl. Acad. Sci. U. S. A.* **103**, 18911-18916, doi:10.1073/pnas.0609643104 (2006).
15. Jungmann, R. *et al.* Single-Molecule Kinetics and Super-Resolution Microscopy by Fluorescence Imaging of Transient Binding on DNA Origami. *Nano Lett.* **10**, 4756-4761, doi:10.1021/nl103427w (2010).
16. Wu, D. M., Liu, Z. W., Sun, C. & Zhang, X. Super-resolution imaging by random adsorbed molecule probes. *Nano Lett.* **8**, 1159-1162, doi:10.1021/nl0733280 (2008).
17. Cang, H. *et al.* Probing the electromagnetic field of a 15-nanometre hotspot by single molecule imaging. *Nature* **469**, 385-+, doi:10.1038/nature09698 (2011).
18. Honciuc, A., Howard, A. L. & Schwartz, D. K. Single Molecule Observations of Fatty

Acid Adsorption at the Silica/Water Interface: Activation Energy of Attachment. *Journal of Physical Chemistry C* **113**, 2078-2081, doi:10.1021/jp8051856 (2009).

19. Honciuc, A., Baptiste, D. J., Campbell, I. P. & Schwartz, D. K. Solvent Dependence of the Activation Energy of Attachment Determined by Single Molecule Observations of Surfactant Adsorption. *Langmuir* **25**, 7389-7392, doi:10.1021/la900307f (2009).
20. Honciuc, A., Harant, A. W. & Schwartz, D. K. Single-molecule observations of surfactant diffusion at the solution-solid interface. *Langmuir* **24**, 6562-6566, doi:10.1021/la8007365 (2008).
21. Honciuc, A. & Schwartz, D. K. Probing Hydrophobic Interactions Using Trajectories of Amphiphilic Molecules at a Hydrophobic/Water Interface. *Journal of the American Chemical Society* **131**, 5973-5979, doi:10.1021/ja900607g (2009).
22. Acharya, H., Vembanur, S., Jamadagni, S. N. & Garde, S. Mapping hydrophobicity at the nanoscale: Applications to heterogeneous surfaces and proteins. *Faraday Discuss.* **146**, 353-365, doi:10.1039/b927019a (2010).
23. Honciuc, A., Baptiste, D. J. & Schwartz, D. K. Hydrophobic Interaction Microscopy: Mapping the Solid/Liquid Interface Using Amphiphilic Probe Molecules. *Langmuir* **25**, 4339-4342, doi:10.1021/la9004246 (2009).
24. Walder, R., Honciuc, A. & Schwartz, D. K. Directed Nanoparticle Motion on an Interfacial Free Energy Gradient. *Langmuir* **26**, 1501-1503, doi:10.1021/la903753z (2010).

25. Huang, B., Bates, M. & Zhuang, X. W. Super-Resolution Fluorescence Microscopy. *Annu. Rev. Biochem.* **78**, 993-1016, doi:10.1146/annurev.biochem.77.061906.092014 (2009).

26. Esfandiari, N. M. *et al.* Single-Molecule Imaging of Platinum Ligand Exchange Reaction Reveals Reactivity Distribution. *Journal of the American Chemical Society* **132**, 15167-15169, doi:10.1021/ja105517d (2010).

Chapter 5: Single Molecule Observations of Desorption-Mediated Diffusion at the Solid-Liquid Interface

5.1 - Abstract

By directly observing molecular trajectories on a chemically heterogeneous surface, we have identified two distinct modes of diffusion involving: (1) displacements within isolated surface "islands" ("crawling" mode), and (2) displacements where a molecule desorbs from an island, diffuses through the adjacent liquid phase, and re-adsorbs on another island ("flying" mode). The diffusion coefficients corresponding to these two modes differ by an order of magnitude, and both modes are also observed on chemically homogeneous surfaces. Comparison with previous results suggested that desorption-mediated diffusion is the primary transport mechanism in self-assembled monolayer formation.

5.2 – Introduction

The mobility of molecules at the solid-liquid interface is of critical importance to several applications of surface science, including self-assembled monolayer growth[1, 2], surface reactivity[3, 4], and molecular recognition associated with both biomembranes and biosensors[5-7]. In these applications, a fundamental issue involves the way in which a molecule identifies a target on a surface. If molecular surface transport is slow, then direct adsorption from solution onto the target is, by default, the dominant mechanism for molecular targeting. As surface mobility increases, both the magnitude and mechanism of diffusion becomes important for molecular targeting. For example, heterogeneous surfaces can have spatial barriers to purely surface bound diffusion[8]. However, if adsorbate molecules can undergo desorption-mediated surface diffusion[9], then molecules can "fly" over these barriers.

The "flying" diffusion mechanism is particularly important for molecular targeting with low solution concentrations (and consequentially low adsorption rates), since the magnitude of diffusion is significantly larger than purely surface-bound diffusion. The larger diffusion coefficient allows the molecules to "explore" larger areas of the surface to find a target. With increasing solute concentrations, adsorption/desorption rates will become increasingly important; however, previous theoretical work suggests that surface diffusion still remains a critically-important factor in determining the efficiency of targeting under relevant conditions[6, 7]. Also, even at arbitrarily high solute concentrations, the flying mode will still increase the rate of any kinetic process in which surface diffusion is important, such as in the formation of self-assembled monolayers[1, 2].

While some phenomena associated with the solid-liquid interface (e.g. adsorption and desorption) share many commonalities with those of other interfaces, the immobile nature of the solid phase creates a unique situation with respect to molecular mobility. In particular, the dominant qualitative mechanism of molecular diffusion at a gas-liquid[10-16] or liquid-liquid[10, 17-22] interface is directly analogous to diffusion within a homogeneous fluid medium, involving Brownian motion amidst mobile solvent molecules. On a solid surface, however, an adsorbate molecule must "detach" to some degree in order to relocate. In general, two competing pictures have been used to describe this process. In the dominant paradigm, molecular mobility is considered an activated process consisting of a series of "hops" between localized binding sites that are separated by small energy barriers[8, 23, 24]. In this picture, the binding sites are spatially separated by atomic/molecular length scales. O'Shaughnessy and coworkers considered an alternative model, called desorption-mediated diffusion, where adsorbate molecules are imagined to detach completely from the interface, diffuse through the liquid phase, and re-adsorb at the interface[9]. They suggested that under some conditions, this mechanism of interfacial diffusion may be dominant, and theoretically described the statistical details of such a hypothetical mode, showing that it would lead to anomalous diffusion, including long flights. To date, it has proven difficult to directly test this prediction. In principle, of course, both types of diffusion may be operative simultaneously.

It is challenging to study surface diffusion under conditions where other surface processes are occurring simultaneously. Under special conditions, fluorescence recovery after photobleaching (FRAP) can be used to study the surface diffusion[25] of adsorbates in contact with aqueous solution. In general, however, it is impossible to unambiguously separate the fluorescence recovery associated with lateral diffusion from that due to adsorption and desorption[26]. Similarly, fluorescence correlation spectroscopy can be used to measure surface diffusion[27], but is susceptible

to the same issues involving adsorption and desorption from the surface. On the other hand, total internal reflectance fluorescence microscopy (TIRFM), when used to track individual molecular trajectories, can explicitly identify and distinguish surface adsorption, diffusion, and desorption processes for every individual molecule that adsorbs to the surface. Our group has exploited single-molecule TIRFM to determine mechanisms of surfactant behavior at the solid-liquid interface, including activation energies of adsorption[28, 29] and interfacial diffusion[8], consequences of surface heterogeneity[30], and multiple diffusive modes related to molecular conformation[24].

In this Letter, we present the results of single molecule TIRFM measurements of the dynamics of a fluorescently-labeled surfactant on both homogenous and heterogeneous hydrophobic surfaces. By exploiting surface features of the heterogeneous (i.e. "patchy") trimethylsilyl surface, we show directly that adsorbate molecules exhibit both a slow surface diffusion mode (crawling) and a desorption-mediated fast mode of diffusion (flying), and describe these modes quantitatively.

5.3 – Methods

Surfaces were prepared by photodegradation of hydrophobically-modified fused silica (FS) surfaces[30]. A 50 mm-diameter FS wafer (MTI Corp) was cleaned in hot piranha solution for ~1 h followed by UV−ozone treatment for another ~60 min. The clean hydrophilic substrate was placed in a sealed glass container containing hexamethyldisilazane (HMDS, 99.8% purity, Acros Organics) and positioned ~5 cm above the liquid to expose its surface to HDMS vapor for ~48 h. In contrast with solution deposition of SAMs, this vapor-deposition process ensured that the trimethylsilyl (TMS) layer contained no fluorescent impurities as confirmed by control TIRFM experiments carried out with pure deionized water (Millipore, Milli-Q UV, 18.3 MΩ·cm). These

TMS-modified surfaces were then exposed for the desired degradation time to UV illumination from a Hg pen lamp (UVP 254 nm) held ~5 mm from the surface. The intensity was ~0.3 mW/cm^2 at this distance. The surfaces were then exposed to solutions fluorescently-labeled dodecanoic acid (Invitrogen Bodipy® FL-C_{12}) at concentrations of 2 x10^{-13} M for photodegraded TMS surfaces and 2 x10^{-15} M for TMS surfaces. A time series of TIRFM images was obtained were sampled continuously for 7 minutes, with each frame having an exposure time of 400 ms.

5.4 - Results

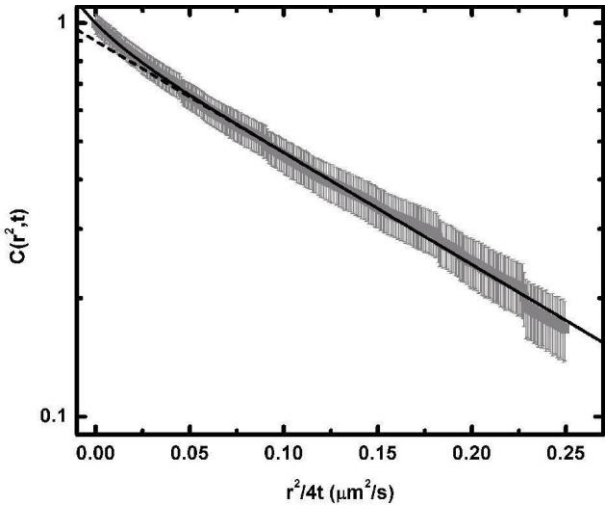

Figure 5.1 - Cumulative squared displacement distribution for dodecanoic acid on a trimethylsilyl surface. The dashed and solid lines correspond to single-exponential and double-exponential fits as described in the text.

Figure 5.1 shows the cumulative (i.e. integrated) squared-displacement distribution, $C(r^2,t)$, of the dodecanoic acid molecules on a uniform TMS surface. On this semi-log plot, a straight line would indicate a single Gaussian mode of diffusion. However, the systematic deviation from the best fit

to a single exponential (dashed line in Figure 5.1) indicates that multiple modes of diffusion are needed to describe the trajectories. The overall surface diffusion is a weighted average of these different modes of diffusion, where the weights are the fraction of steps in each mode. A double exponential (solid line in Figure 5.1) provides satisfactory agreement with the data. This analysis suggests that there is a fast mode (D_{fast} = 0.153 ± 0.001 μm^2/s) that corresponds to 90% of the displacements, and a slow mode (D_{slow} = 0.019 ± 0.003 μm^2/s) representing the remaining 10% of displacements.

Multiple modes of diffusion are common for interfacial diffusion[8, 20, 24, 31], and can be due to a number of factors including multiple binding modes, molecular conformations, lateral heterogeneity, etc. For the gas-liquid and liquid-liquid interfaces, theoretical models involving modifications of Stokes-Einstein diffusion for 2D systems[32, 33] provide a direct connection between a diffusion coefficient and the apparent hydrodynamic radius. This connection has been exploited to determine molecular conformations associated with interfacial diffusion coefficients at the oil-water interface[21]. However, the solid-liquid interface has no such theoretical model directly linking a particular diffusive mode to a specific molecular mechanism. Such a connection requires additional information beyond the diffusion coefficient itself. For example, in previous work studying interfacial diffusion of proteins at the solid-liquid[31] and liquid-liquid[21] interfaces, the fluorescence intensity and surface residence times of protein objects were correlated with diffusion to determine that diffusion modes were primarily associated with the oligomer state of the protein. In another study with fatty acids diffusing at the solid-liquid interface[24], the temperature dependence of diffusion showed that one mode of diffusion was an Arrhenius activated process. In the current work, the heterogeneity of the surface itself was used to determine the mechanism of the fast diffusion mode.

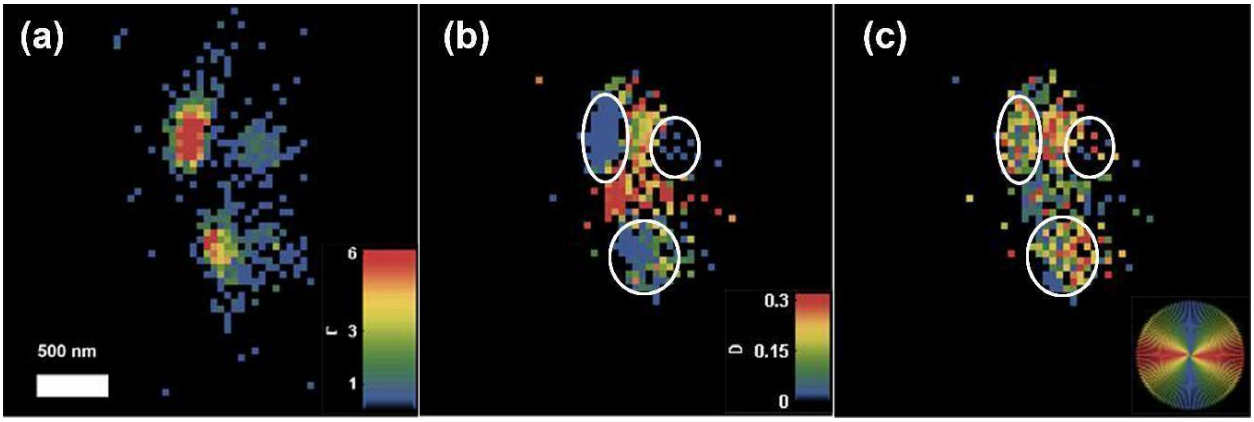

Figure 5.2 - MAPT images of (a) surface coverage (10^{-12} $\mu m^{-2}s^{-1}M^{-1}$) (b) diffusion magnitude ($\mu m^2/s$) and (c) diffusion direction for a selected region of the degraded TMS surface.

As shown in Figure 5.2, MAPT (Mapping Accumulated Probe Trajectories) was used to characterize the spatial heterogeneity of partially degraded hydrophobic surfaces. MAPT is a super resolution imaging technique[34] based on distributing the various accumulated properties of many single molecule trajectories (adsorption, diffusion, desorption, etc) into spatial areas and then computing spatial maps of these properties. In Figure 5.2.a, a MAPT image of surface coverage shows the spatial density of accumulated molecular positions on a small region of the surface. In this image, we see three local regions where the molecules reside, with gaps in between where the molecules are never present on the surface. The white outlines in Figures 5.2.b and 5.2.c provide guides to the eye to represent these areas of high coverage. The high coverage regions on the degraded TMS surface represent areas of higher residual hydrophobicity, as previously predicted by simulation[35], while the regions of low coverage represent hydrophilic "bare" fused silica regions from which the TMS monolayer has been removed[34]. In Figure 5.2.b, a MAPT image shows the magnitude of the local diffusion coefficient. It is important to note that, by convention,

the diffusion coefficient is mapped at the midpoint of displacements, not at recorded molecular locations. In Figure 5.2.b, six distinct regions are present, with slow diffusion (blue and green) on the regions corresponding to high surface coverage (from Figure 5.2.a, marked by white outlines) and fast diffusion (yellow and orange) directly between the high-coverage regions, in areas with little or no surface coverage. In Figure 5.2.c, a MAPT image of direction shows the average direction of the local diffusion coefficient, using a color coded "compass" showing whether the displacements are in the vertical direction (blue and green) or horizontal direction (red and yellow). In Figure 5.2.c, the displacements within the high-coverage regions (marked by white outlines) have random directions. However, the displacements in-between the high-coverage regions are horizontal (between the two regions on top) or vertical (between the lower region and both of the regions above) direction. The combined evidence from the magnitude and direction of these diffusive steps associated with regions of no surface coverage indicates that they are due to displacements that started in one region of high surface coverage and ended in another region of high surface coverage. By definition, these displacements are desorption-mediated displacements (flying mode), because molecular positions are never recorded for most of the region where the flying mode of diffusion occurs.

An important experimental consideration involves the question of whether the apparent flying mode displacements are, in fact, an artifact due to coincidental desorption of one molecule and adsorption of another molecule in consecutive movie frames. We have addressed this question statistically by calculating the expected number of such "coincidental events" based on independent measurements of adsorption and desorption rates. In Figure 5.3.a, a lower magnification MAPT image of the surface shows many areas of high surface coverage (orange in color), similar to the areas magnified in Figure 5.2.a, present throughout the surface. The mean

adsorption rate (0.5 ± 0.3 molecules sec^{-1} μm^{-2}) and desorption rate (0.65 ± 0.47 molecules sec^{-1}) was measured for 28 of these regions. Using these adsorption and desorption rates for two independent adsorption sites, 100 stochastic simulations were performed to determine the number of coincidental desorption and adsorption events in consecutive frames. In our simulations, we allowed for multiple molecules to exist on one adsorption site at the same time, with independent desorption. We calculated 1.0 ± 1.0 coincidental events per experiment in the simulations, compared to the 98 observed flying displacements between the two regions on the left in Figure 5.2.a. Therefore, apparent flying mode displacements due to coincidental events represent a negligible fraction of the total number of observed events.

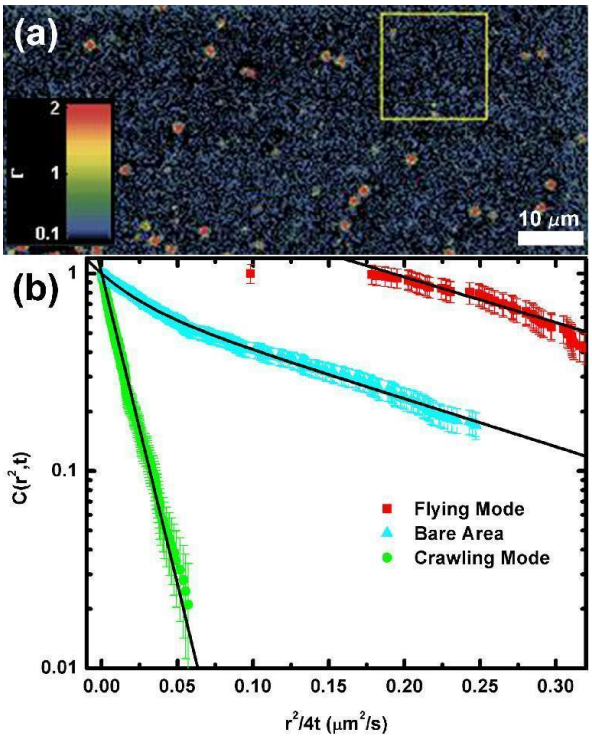

Figure 5.3 - (a) MAPT image of surface coverage (10^{-12} $\mu m^{-2}s^{-1}M^{-1}$) with a relatively uniform area denoted by the yellow box. (b) Cumulative squared displacement distribution for flying mode, crawling mode from Fig. 2 and bare area

denoted by the yellow box in Fig. 3(a).

It is interesting to compare the magnitudes of the crawling and flying modes found in Figure 5.2.a (that are characterized on a local region of extremely high surface coverage) to diffusion within uniform areas of the degraded TMS surface, representative of the majority of the surface area. Figure 5.3.b shows the cumulative squared displacement distributions for the steps between regions of high coverage (flying mode), the steps within regions of high coverage (crawling mode), and all steps within a large area of uniform surface coverage that is denoted by the yellow box in Figure 5.3.a. The uniform area exhibits both slow (D_{slow} = 0.026 ± 0.001 μm^2/s) and fast (D_{fast} = 0.179 ± 0.002 μm^2/s) diffusive modes that are similar in magnitude to those observed on the un-degraded TMS surface (Figure 5.1). The degraded TMS surface, however, exhibits a larger fraction (30%) of slow-mode displacements than does the un-degraded TMS surface (10%). Interestingly, D_{slow} and D_{fast} correspond closely to the apparent diffusion coefficients of the crawling and flying modes respectively. In particular, the apparent crawling mode diffusion coefficient within high coverage areas (0.0138 ± 0.0001 μm^2/s) was within a factor of two of D_{slow}, and the flying mode diffusion coefficient (0.18 ± 0.03 μm^2/s) was equal to D_{fast} within experimental uncertainty. We note that the flying mode apparent diffusion coefficient was calculated from the slope of the cumulative step size distribution in the range of 0.175 to 0.300 μm^2/s to avoid artifacts due to the depletion of small step sizes from the geometrical constraints of the system in Figure 5.2.

Table 5.1 summarizes the values of all diffusion coefficients described in this manuscript. We see that for all the surfaces and features, there are two distinct diffusion regimes that differ by an order of magnitude. The slow regime consists of the slow mode of the un-degraded TMS, the slow mode

of the degraded TMS uniform area, and the crawling mode diffusion within confined regions of high coverage. The fast regime consists of the fast mode of un-degraded TMS, the fast mode of the degraded TMS uniform area, and the flying mode diffusion between regions of high coverage. Based on these values, we infer a mechanistic connection between the diffusive modes corresponding to these two widely-separated regimes of mobility, in particular that the modes on uniform surfaces represented by D_{slow} are in fact crawling modes and that the modes on uniform surfaces represented by D_{fast} are flying modes (desorption-mediated surface diffusion). The large fractions corresponding to the fast diffusive mode on both the uniform TMS surface (90%) and the degraded TMS surface (71%) suggest that desorption-mediated diffusion is the dominant form of surface transport for fatty acids on these surfaces.

Table 5.1 - Summary of diffusion results for TMS surfaces and regions of interest.

Surface/Feature	**Fraction of Displacements**	***D* (μm^2/s)**
TMS	0.90 ± 0.01	0.153 ± 0.001
	0.10 ± 0.01	0.019 ± 0.003
Degraded TMS Uniform Area	0.71 ± 0.01	0.179 ± 0.002
	0.29 ± 0.01	0.026 ± 0.001
Degraded TMS Crawling Mode	1.0	0.0138 ± 0.0001
Degraded TMS Flying Mode	1.0	0.18 ± 0.03

5.5 – Discussion

While we have primarily looked at low concentration solutions, this flying mode should be relevant over a wide range of bulk solution concentrations. The surface concentration of surfactant (which

is dependent on bulk concentration) is the most important parameter in determining the relative importance of the two modes of diffusion. At low surface concentrations, the flying mode is clearly the dominant mode of surface transport. However, at high surface concentrations the situation is less clear. For example, we hypothesize that at high surface concentrations, desorption from the surface may be significantly impeded by lateral interactions with other surfactants. The crawling mode is also likely to be slowed due to increased crowding/drag by neighboring surfactant molecules. The effects of surface crowding on the dynamics (adsorption, desorption, and diffusion will all be affected) of molecular-surface interactions cannot be inferred from the data presented in this letter and should be the focus of future experiments.

As mentioned previously, desorption-mediated surface diffusion has been theoretically described for both solid-liquid and liquid-liquid interfaces[9]. This theoretical model predicts a deviation from typical Gaussian distributions of step sizes due to the apparent Levy flights performed by the molecules when projected onto the surface plane. Specifically, the probability distribution of displacements was predicted to be a Cauchy distribution characterized by an effective "speed" $c=D/h$, where c is the speed, D is the diffusion coefficient in the liquid phase, and h is the surface displacement length. Our experimental data are in better agreement with a Gaussian model; however, using a fit to the Cauchy distribution, we estimate the effective speed to be c=0.47 μm/s in the context of this theory. It is possible that the deviation of our experimental data from the Cauchy distribution may be due to acquisition time effects, i.e. that observed flying displacements actually represent a time-weighted average of desorption-mediated and crawling displacements.

The dominance of desorption mediated diffusion has important implications for many surface processes, but the example of self-assembled monolayer growth kinetics provides a unique opportunity to make connections between the current findings and previous experimental estimates

of surface diffusion. Kinetic "population-balance" models are widely-used to describe cluster nucleation and growth in epitaxial films[36-39] or self-assembled monolayers[1, 2]. Using these models, the surface diffusion coefficient can be estimated from the nucleation and growth rate of small patches of self-assembled surfactants during the growth of a self-assembled surfactant monolayer. The surface diffusion coefficient for octadecylphosphonic acid on mica[2] was estimated to be 0.29 ± 0.03 $\mu m^2/s$, which is larger but still within a factor of two of the flying mode of diffusion measured in our system. Given the similarity of these systems, the crawling mode (which is an order of magnitude lower diffusion coefficient) would be an unlikely mechanism for a diffusion coefficient that is faster than the flying mode in our system. The similarity of the diffusion coefficients suggests that the flying mode is the main mechanism of diffusion associated with the formation of self-assembled monolayers.

5.6 - Acknowledgements

This work was supported by the US National Science Foundation (CHE 0841116) and the US Department of Energy (DE-0001854).

5.7 - References

1. Doudevski, I.; Hayes, W. A.; Schwartz, D. K., Submonolayer island nucleation and growth kinetics during self-assembled monolayer formation. *Physical Review Letters* **1998,** 81, (22), 4927.

2. Doudevski, I.; Schwartz, D. K., Concentration dependence of self-assembled monolayer island nucleation and growth. *J. Am. Chem. Soc.* **2001,** 123, (28), 6867-6872.

3. Allen, C.; Seebauer, E., Surface diffusivities and reaction rate constants: Making a quantitative experimental connection. *The Journal of Chemical Physics* **1996,** 104, (7), 2557-2565.

4. Cukier, R., The effect of surface diffusion on surface reaction rates. *The Journal of Chemical Physics* **1983,** 79, (5), 2430-2435.

5. Axelrod, D.; Wang, M., Reduction-of-dimensionality kinetics at reaction-limited cell surface receptors. *Biophys. J.* **1994,** 66, (3), 588-600.

6. Chan, V.; Graves, D. J.; McKenzie, S. E., The biophysics of DNA hybridization with immobilized oligonucleotide probes. *Biophys. J.* **1995,** 69, (6), 2243-2255.

7. Lieto, A. M.; Lagerholm, B. C.; Thompson, N. L., Lateral diffusion from ligand dissociation and rebinding at surfaces. *Langmuir* **2003,** 19, (5), 1782-1787.

8. Honciuc, A.; Harant, A. W.; Schwartz, D. K., Single-Molecule Observations of Surfactant Diffusion at the Solution-Solid Interface. *Langmuir* **2008,** 24, (13), 6562-6566.

9. Bychuk, O. V.; O'Shaughnessy, B., Anomalous diffusion at liquid surfaces. *Physical Review Letters* **1995,** 74, (10), 1795.

10. Adalsteinsson, T.; Yu, H., Lipid lateral diffusion in multi-bilayers, and in monolayers at the air/water and heptane/water interfaces. *Langmuir* **2000,** 16, (24), 9410-9413.

11. Ke, P. C.; Naumann, C. A., Hindered diffusion in polymer-tethered phospholipid monolayers at the air-water interface: a single molecule fluorescence imaging study. *Langmuir* **2001,** 17, (16), 5076-5081.

12. Malec, A. D.; Wu, D. G.; Louie, M.; Skolimowski, J. J.; Majda, M., Gibbs monolayers at the air/water interface: Surface partitioning and lateral mobility of an electrochemically active surfactant. *Langmuir* **2004,** 20, (4), 1305-1310.

13. Selle, C.; RÃ¼ckerl, F.; Martin, D. S.; Forstner, M. B.; KÃ¤s, J. A., Measurement of diffusion in Langmuir monolayers by single-particle tracking. *Physical Chemistry Chemical Physics* **2004,** 6, (24), 5535-5542.

14. Tamada, K.; Kim, S.; Yu, H., Lateral diffusion of a probe lipid in biphasic phospholipid monolayers: liquid/gas coexistence films. *Langmuir* **1993,** 9, (6), 1545-1550.

15. Tanaka, K.; Manning, P. A.; Lau, V. K.; Yu, H., Lipid lateral diffusion in Dilauroylphosphatidylcholine/Cholesterol mixed monolayers at the air/water interface. *Langmuir* **1999,** 15, (2), 600-606.

16. Tanaka, K.; Yu, H., Lipase activity on lipid/polymer binary monolayers: lateral diffusion-controlled enzyme kinetics. *Langmuir* **2002,** 18, (3), 797-804.

17. Hashimoto, F.; Tsukahara, S.; Watarai, H., Lateral diffusion dynamics for single molecules of fluorescent cyanine dye at the free and surfactant-modified dodecane-water interface. *Langmuir* **2003,** 19, (10), 4197-4204.

18. Negishi, M.; Seto, H.; Hase, M.; Yoshikawa, K., How does the mobility of phospholipid molecules at a water/oil interface reflect the viscosity of the surrounding oil? *Langmuir* **2008,** 24, (16), 8431-8434.

19. Schütz, G.; Schindler, H.; Schmidt, T., Single-molecule microscopy on model membranes reveals anomalous diffusion. *Biophys. J.* **1997,** 73, (2), 1073-1080.

20. Walder, R.; Honciuc, A.; Schwartz, D., Phospholipid Diffusion at the Oil-Water Interface. *Journal of Physical Chemistry B* **2010,** 114, (35), 11484-11488.

21. Walder, R.; Schwartz, D. K., Single Molecule Observations of Multiple Protein Populations at the Oil-Water Interface. *Langmuir* **2010,** 26, (16), 13364-13367.

22. Walder, R.; Schwartz, D. K., Dynamics of protein aggregation at the oil-water interface characterized by single molecule TIRF microscopy. *Soft Matter* **2011**.

23. Dobbs, K.; Doren, D., Dynamics of molecular surface diffusion: Origins and consequences of long jumps. *The Journal of Chemical Physics* **1992,** 97, (5), 3722-3735.

24. Honciuc, A.; Schwartz, D. K., Probing Hydrophobic Interactions Using Trajectories of Amphiphilic Molecules at a Hydrophobic/Water Interface. *J. Am. Chem. Soc.* **2009,** 131, (16), 5973-5979.

25. Heitzman, C. E.; Tu, H.; Braun, P. V., Two-dimensional diffusion of prodan on self-assembled monolayers studied by fluorescence recovery after photobleaching. *The Journal of Physical Chemistry B* **2004,** 108, (36), 13764-13770.

26. Schmidt, C.; Zimmermann, R.; Gaub, H., Multilayer adsorption of lysozyme on a hydrophobic substrate. *Biophys. J.* **1990,** 57, (3), 577-588.

27. Burgos, P.; Zhang, Z.; Golestanian, R.; Leggett, G. J.; Geoghegan, M., Directed single molecule diffusion triggered by surface energy gradients. *ACS Nano* **2009,** 3, (10), 3235-3243.

28. Honciuc, A.; Baptiste, D. J.; Campbell, I. P.; Schwartz, D. K., Solvent Dependence of the Activation Energy of Attachment Determined by Single Molecule Observations of Surfactant Adsorption. *Langmuir* **2009,** 25, (13), 7389-7392.

29. Honciuc, A.; Howard, A. L.; Schwartz, D. K., Single Molecule Observations of Fatty Acid Adsorption at the Silica/Water Interface: Activation Energy of Attachment. *J. Phys. Chem. C* **2009,** 113, (6), 2078-2081.

30. Honciuc, A.; Baptiste, D. J.; Schwartz, D. K., Hydrophobic Interaction Microscopy: Mapping the Solid/Liquid Interface Using Amphiphilic Probe Molecules. *Langmuir* **2009,** 25, (8), 4339-4342.

31. Kastantin, M.; Langdon, B. B.; Chang, E. L.; Schwartz, D. K., Single-Molecule Resolution of Interfacial Fibrinogen Behavior: Effects of Oligomer Populations and Surface Chemistry. *J. Am. Chem. Soc.* **2011,** 133, (13), 4975-4983.

32. Hughes, B.; Pailthorpe, B.; White, L., The translational and rotational drag on a cylinder moving in a membrane. *J. Fluid Mech.* **1981,** 110, 349-372.

33. Saffman, P.; DelbrÃ¼ck, M., Brownian motion in biological membranes. *Proceedings of the National Academy of Sciences* **1975,** 72, (8), 3111-3113.

34. Walder, R.; Nelson, N.; Schwartz, D. K., Super-Resolution Surface Mapping using the Trajectories of Molecular Probes. *Nat. Commun.* **2011,** 2, 515.

35. Acharya, H.; Vembanur, S.; Jamadagni, S. N.; Garde, S., Mapping hydrophobicity at the nanoscale: Applications to heterogeneous surfaces and proteins. *Faraday Discuss.* **2010,** 146, 353-365.

36. Amar, J. G.; Family, F., Critical cluster size: Island morphology and size distribution in submonolayer epitaxial growth. *Physical Review Letters* **1995,** 74, (11), 2066.

37. Amar, J. G.; Family, F., Kinetics of submonolayer and multilayer epitaxial growth. *Thin Solid Films* **1996,** 272, (2), 208-222.

38. Venables, J., Rate equation approaches to thin film nucleation kinetics. *Philosophical Magazine* **1973,** 27, (3), 697-738.

39. Venables, J.; Spiller, G.; Hanbucken, M., Nucleation and growth of thin films. *Reports on Progress in Physics* **1984,** 47, (4), 399.

Chapter 6 - Unbiased Clustering of Molecular Dynamics for Spatially-Resolved Analysis of Chemically Heterogeneous Surfaces

6.1- Abstract

A technique is described for resolving and interpreting molecular interactions with a chemically heterogeneous surface. Using total internal reflection fluorescence microscopy, dynamic single molecule trajectories were accumulated simultaneously for fluorescently labeled fatty acid (interacting primarily via hydrophobic interactions) and dextran (interacting via hydrogen-bonding interactions) probe molecules at the interface between an aqueous solvent and a photopatterned solid surface with distinct regions of amine-terminated and poly(ethylene glycol) self-assembled monolayers. Using dynamic properties of the probe molecules (adsorption rate, surface diffusion coefficient, residence time), an unsupervised Gaussian mixture model algorithm was used to identify areas of the surface that were chemically related to each other, and the dynamic behaviors of the probe molecules were studied statistically on these distinct regions. The dynamic data were compared to data from homogeneous surfaces of known chemistry to provide a chemical identification of each location on the surface. Spatial maps were also constructed, allowing for spatial visualization of surface chemistry on a hydrophilic substrate. This work enables the direct study of interactions between single-molecule probes and distinct surface chemistries, even in the presence of spatial heterogeneity, without human bias, assumptions about surface structure, or model-dependent analysis.

6.2 - Introduction

Spatially heterogeneous surfaces are ubiquitous throughout many areas of science and technology, including biology, nanofabrication, and even chromatography. Either by nature or design, these interfaces do not always have well defined variations that are easily detected through conventional microscopy techniques. Multi-phase lipid bilayers, for example, are fluid systems that have heterogeneous chemistry where there is great interest in how molecules interact with each domain in the system[1, 2]. Also of interest are chromatography stationary phase media which have been found to contain defects that significantly impact their performance[3-5]. Understanding how probe molecules interact with heterogeneous surfaces will prove invaluable to the activity and performance on these and other systems.

While significant attention has been paid to the need to obtain spatial images, or maps, that define regions of distinct surface chemistry, in many cases it is equally important to understand and distinguish how molecules of interest interact cumulatively with chemically-distinct regions. For example, cell culture surfaces can be created with distinct regions of hydrophilic and hydrophobic surface chemistry to impact the cell adhesion.[6] In addition to intentionally patterned substrates, phase separated polymer blends are being studied for their use as drug delivery media[7]. It would be desirable to study how molecules interact with distinct spatial regions on these materials without relying on methods that involve human bias, such as mathematical models (involving arbitrary pre-determined assumptions) to separate distinct populations from a spatially averaged measurement, or manual selection of spatial regions of interest.

Other surfaces are designed to be homogeneous in nature, but in practice may contain defects and

other heterogeneities that can affect performance; examples include biomaterials, stationary phase media for chromatography[3-5], and polymeric media for separations. A method that is capable of identifying these defects, and the areas without defects, and studying them individually and simultaneously would improve our understanding of how these materials perform, the roles that imperfections can play, and how materials can be designed for improved performance.

There are several techniques that can identify and visualize heterogeneities in surface chemistry under ambient conditions, such as SPM (Scanning Probe Microscopy).[8, 9] SPM provides excellent spatial resolution on chemically heterogeneous surfaces using the relative affinity of the chemically-functionalized probe for each location on the surface as a contrast mechanism. However, it is typically challenging to replicate quantitative measurements and temporal resolution is poor.[10] Moreover, many analytical methods exist to identify chemical species on the surface. These include x-ray photoelectron spectroscopy, mass spectrometry, infrared spectrometry and many others. While these approaches can provide a detailed analysis of the surface composition averaged over a region of interest, they have limited spatial resolution, are not always applicable under relevant *in situ* conditions, and do not provide insight into how individual molecules will interact with a particular chemistry.

Single-molecule force spectroscopy (SMFS) can provide detailed information about the ways in which probe molecules interact with surfaces. This technique uses a single molecule attached to a cantilever to assess the interaction between that molecule and the surface of interest.[11] SMFS has been used to study the hydrophobic effect in great detail and provides excellent thermodynamic data for this interaction. However, this is a serial method, and it is difficult to obtain statistically meaningful information using many molecules, under *in situ* conditions. For the same reason,

SMFS cannot easily assess spatially-dependent interactions on a heterogeneous surface, particularly when the heterogeneities are sparse (such as on chromatography adsorption media). Furthermore SMFS does not provide information on spontaneous dynamic molecular behavior since the probe is tethered to the cantilever and mechanically brought into and out of contact with the surface.[12, 13]

Previous work has shown that the dynamic behavior of fluorescent probe molecules, when visualized using single molecule microscopy, has a very strong dependence on the underlying surface properties[10, 14]. These interactions were used to create images of laterally heterogeneous surfaces using accumulated probe trajectories (MAPT)[15]. This method plotted a heat map, in two dimensions, of the local numerical value associated with a particular dynamic molecular activity on the surface (e.g. local surface residence time or local diffusion coefficient) to create an image. MAPT images have the advantage of being super-resolution in nature due to the use of dynamically adsorbing and desorbing molecules as probes and are based on absolute quantitative values as opposed to arbitrary qualitative contrast mechanisms. These images, however, do not directly identify regions on a heterogeneous surface that share the same chemistry. Such identification would require subsequent .analysis of MAPT images (like any other image), using standard methods such as thresholding.

In this work we seek to exploit the variation in molecular dynamics such as adsorption rate and surface diffusion in order to identify distinct regions on a heterogeneous surface and subsequently obtain detailed distributions of single-molecule data from each region independently. Unlike standard imaging methods, the technique presented here does not rely on human input to identify regions of interest or to study molecular behavior on chemically-similar regions of the surface.

This region-specific identification also allowed us to correlate molecular behavior on the regions of a heterogeneous surface to known homogeneous surfaces, assigning a chemical identity to each class of surface region. These identifications were further used to create a map of the underlying surface chemistry with micron-scale resolution.

6.3 - Methods

6.3.1 - Surface Preparation

Surfaces were prepared using liquid phase deposition of triethoxy silanes onto 2" fused silica wafers. Wafers were first cleaned with hot piranha solution (30% H_2O_2/70% H_2SO_4 by volume at 70 °C) for one hour. The wafers were then treated with UV-ozone (Boekel UV-clean model 135500) for an additional hour. The cleaned fused silica wafers were then placed in a 200:3 (by volume) solution of toluene:aminohexylaminopropyl triethoxysilane at room temperature for 45 min. This deposition yielded an aminohexylaminopropyl triethoxysilane (AHAPTES) monolayer. Micron scale patterns in surface chemistry were created using 1500 line-per-inch nickel grid meshes (Structure Probe, Inc.) as contact photomasks under a UV-Pen lamp (UVP 254 nm). The incident UV radiation on the surface was ~0.3 mW/cm^2 and surfaces were exposed for 60 min. A magnet was placed under the fused silica wafer to hold the nickel grid contact mask flat against the surface. The 60 min UV exposure time ensured near complete removal of the AHAPTES monolayer on the unmasked areas of the surface. Following photopatterning, the wafer was immersed in a 200:3:1 by volume solution of toluene:1-methyl(polyethoxy) triethoxysilane:n-butylamine deposition solution for 12 hours to back-fill the photodegraded regions with a 1-methyl(polyethoxy) triethoxysilane (PEG) monolayer. The n-butylamine serves as a catalyst for

the reaction with the surface and is unnecessary when depositing silanes that contain a primary amine[16]. A schematic of this deposition and photopatterning procedure (Figure S1) as well as the SAM structures (Figure S2) are included in the supplementary information. Homogeneous PEG monolayers were prepared using the same deposition procedure with a freshly piranha cleaned fused silica wafer instead of a photopatterned surface. For these experiments, AHAPTES and PEG were selected as challenging test surfaces due to the fact that both were relatively hydrophilic, but exhibited different hydrogen bonding mechanisms. AHAPTES can both donate and accept hydrogen bonds while PEG surfaces acts only as an h-bond acceptor. During the course of the experiments, it was determined that depositing AHAPTES first, then using PEG as the backfill produced the best results. Inverting the order yielded surfaces with less distinct surfaces, perhaps due to intercalation of AHAPTES into voids in the PEG layer, or perhaps to multilayer formation by AHAPTES on top of the PEG regions.

6.3.2 - Imaging

Solutions of fluorescent probes were prepared using $1x10^{-8}$ M Alexa-647 labeled dextran (10,000 MW) and $1x10^{-10}$ M BODIPY C-12 fatty acid (4,4-difluoro-5,7-dimethyl-4-bora-3a,4a-diaza-s-indacene-3-dodecanoic acid, Invitrogen Inc., U.S.A) in milli-Q water. Dextran and the C12 fatty acid (Figure S3) were selected because they have fundamentally different interactions with the surface; dextran undergoes hydrogen bonding while the fatty acid experiences mostly hydrophobic attractions[10, 17]. The photopatterned fused silica substrates were exposed to the fluorophore solution in a custom-built flow-cell held at 30 °C for imaging using a custom built, prism-based, total internal reflection fluorescence (TIRF) microscope (Nikon Eclipse TE2000-U)[18]. Fluorophore excitation was accomplished through simultaneous exposure to laser light at 491 nm

(Cobalt Calypso 100) and 647 nm wavelengths (CrystaLaser DL 640-100-0). Images were acquired through a 60x objective using a cooled EMCCD camera (Andor iXon3). The emission light from each fluorophore was directed onto separate regions of the camera detector using an Optosplit III image splitter (Cairn Research, UK). A schematic for this optical setup is included in Figure S4. Time-series of images were captured with an acquisition time of 200 ms per frame for 1,000 seconds (5000 frames), with individual fluorescently-labeled molecules appearing as diffraction-limited spots. Photobleaching occurred over the total period of image acquisition, but did not significantly impact residence time calculations because the residence times were several orders of magnitude shorter (~1-10 seconds) than the characteristic photobleaching time (>100 seconds)[19]. These experiments required the incident laser excitation intensity to be homogeneous across the field of view in order to not change the apparent adsorption rate across the surface. An inhomogeneous field resulted in lower apparent adsorption rates on the lower intensity areas, negatively impacting the ability to compare one region on the surface to another.

6.3.3 - Molecular tracking

Molecules were identified using a disk matrix thresholding algorithm described previously.[15, 20] Using this approach, each molecule was localized with ~50 nm confidence. Molecules were tracked from frame to frame with a maximum single displacement (i.e. tracking radius) of 1μm. The likelihood that a long step was, in fact, two separate molecules coincidentally desorbing then adsorbing in subsequent frames was very small for distances less than 1μm ($p<0.0005$), but increased with the displacement threshold squared. Therefore, molecules that moved more than 1μm from one frame to the next were considered new molecules in these experiments.

6.3.4 - Clustering

Accumulated molecular trajectories were locally-averaged to yield mean adsorption rates, diffusive squared displacements, and residence times for each probe within each 1.3 μm^2 bin (5x5 pixels), yielding six independent experimental values for each bin. The bin size was selected so that each contained a sufficient number of trajectories to give statistically meaningful molecular averages, but was still smaller than the characteristic length scale of heterogeneity on the surface, in this case ~10um. These bins were then grouped together into clusters on the basis of the 6-dimensional numerical values (with no regard for spatial location) by applying a Gaussian mixture model (*mclust V4 for R*[21]). In particular, a normal mixture model algorithm was used to assign each six-dimensional data point (corresponding to a bin) to a cluster that shared similar values for each of the 6 dimensions (6D) of dynamic probe behavior. Each cluster was described by a 6D Gaussian probability distribution with the entire data set being described by the superposition of these 6D Gaussian distributions. Using a predefined number of Gaussian distributions (clusters) the method takes an iterative approach to determine the maximum likelihood values for the mean and covariance matrix of each cluster as well as calculating the optimal mixing proportions in order to best describe the data. Since the adsorption rate varied over orders of magnitude, the log of the adsorption rate was used in the clustering process, in order to prevent it from dominating the cluster identification by the algorithm.

The number of variables used for parameterization of the covariance matrices was determined using Bayesian information criteria (BIC). This process selected the type of covariance matrix (e.g. diagonal or unstructured) as well as whether the separate clusters had independent orientation, shape and size by penalizing over-parameterization while still fitting the data appropriately. The *mclust* package is also capable of determining the number of clusters present in the data through

the use of BIC. However, this method did not provide definitive results for the relatively small number of clusters present in our system (compared, e.g. with genomic data), i.e. the maximum of the BIC as a function of cluster number was very broad and weak. Instead, we developed an alternative subgroup-based method that allowed us to select an appropriate number of clusters for each surface. First, we randomly divided the bins into two different data subsets. Then, we systematically varied the number of clusters (N) between 2 and 6. The N for the combined data set was selected as the N where the clusters identified in the subsets were self-consistent. This allowed us to determine the minimal number of clusters required to identify true clusters corresponding to distinct regions of surface chemistry. The addition of extra clusters generally identified highly-variable regions based on isolated defects or anomalous rare populations. In the case of the photopatterned surfaces, 4 clusters were identified while on homogeneous surfaces only 2 clusters were detected using this approach; BIC identified more than 7 clusters in both cases.

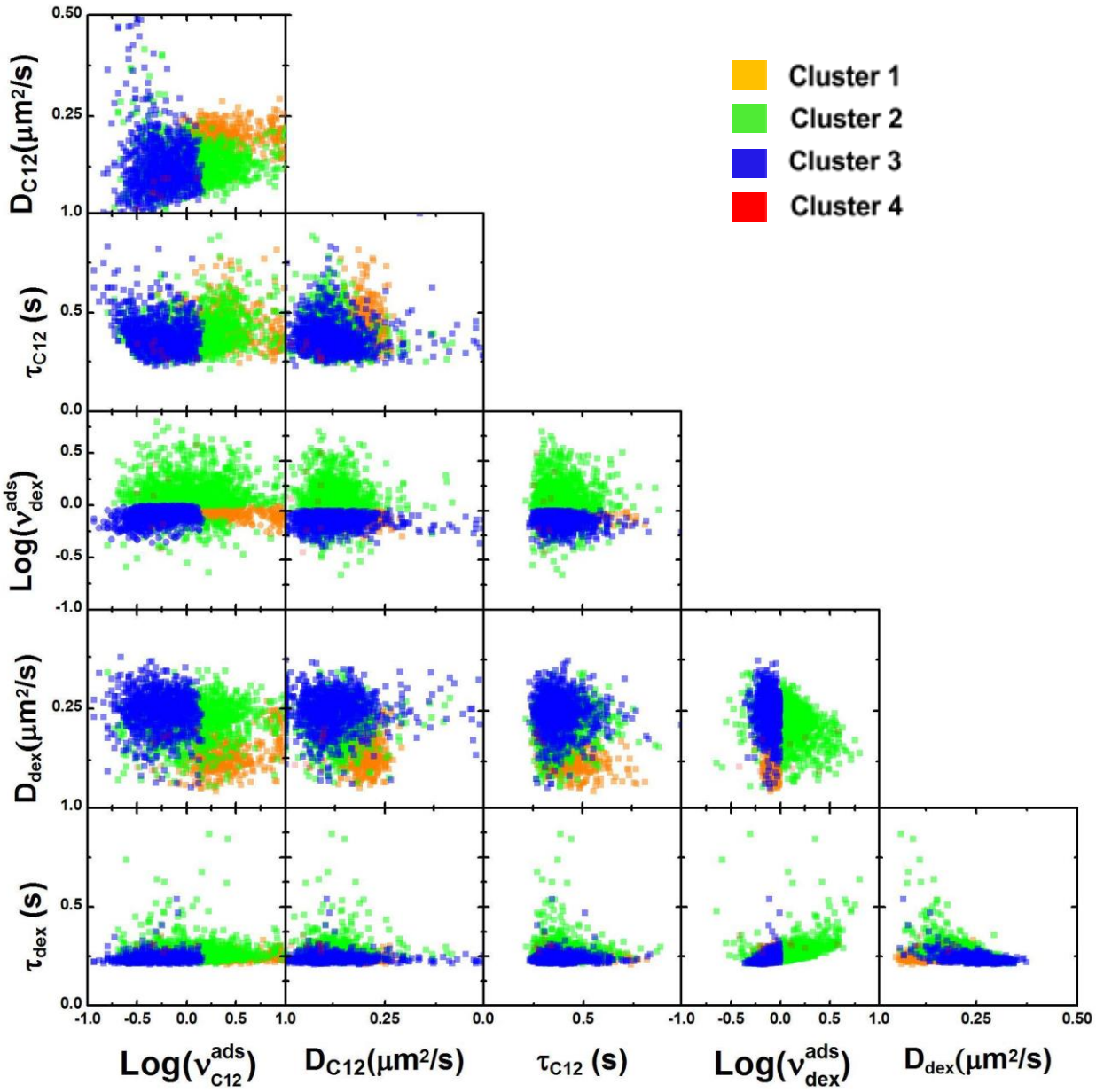

Figure 6.1 – Two dimensional cross sections of scatter plots where values associated with individual bins are shaded to represent their assigned cluster.

6.4 - Results

In principle, the raw data from a given experiment can be represented as a six-dimensional scatter plot, where each data point represents the mean values of each dynamic behavior within a given

bin. To give a visual sense of these data, two-dimensional cross sections are presented in Figure 6.1 for data obtained in dual-probe experiments on a AHAPTES/PEG photopatterned surface in which four robust data clusters were identified. The three observable dynamic behaviors for each probe are the local adsorption rate (v^{ads}), apparent diffusion coefficient (D), and the surface residence time (τ). For these experiments the relative adsorption rate

$$\bar{v}^{ads} = (local\ adsorption\ rate)/(mean\ adsorption\ rate)$$

was used rather than the absolute adsorption rate to mitigate variations caused by day-to-day changes in excitation intensity. The apparent diffusion coefficients were calculated as:

$$D = \frac{< r^2 >}{4t}$$

Where r is the average step length for each bin and *t* is the acquisition time (in this case 0.2 s).

In Figure 6.1, 2-dimensional cross sections of the 6-dimensional distribution of values for $log(\bar{v}^{ads})$, diffusion (D), and residence time (τ) for each probe are presented in scatter plots with a color corresponding to each bin's cluster assignment. The identification of each bin is shown in Figure 1 with orange bins belonging to cluster 1, green bins in cluster 2, blue bins in cluster 3 and a very small number of bins in cluster 4 (red). Each cluster is comprised of bins that share similar residence times, step sizes and adsorption rates for both probes. For example, cluster 1 indicates a group of bins on which dextran adsorbed more rapidly, moved more quickly, and resided longer than C12. Conversely, cluster 2 describes a group of bins where C12 adsorbed more frequently, diffused faster, and remained on the surface for longer than dextran. Cluster 3 represents regions of the surface on which the mobilities and residence times of the two probes were similar to those in cluster 2; however, compared to cluster 2, C12 adsorbed more slowly. As discussed further below, cluster 4 represents isolated surface regions that exhibited anomalously slow diffusion

and/or long residence times. These "hotspots" were routinely observed on virtually every surface, and one advantage of the clustering approach involves the ability to isolate these regions (which, although small, can have an anomalously large effect on mean values) from a careful analysis of the regions that are representative of particular chemistries.

The center and standard deviation for each cluster in the six dimensions is shown in Table 6.1. The fraction of bins belonging to each cluster (*f*) is also included. As suggested qualitatively from the scatter plots above, cluster 1 was distinguished by its unique diffusive behavior. Clusters 2 and 3 exhibited diffusive coefficients and residence times that were equal within experimental uncertainty, with significantly smaller adsorption rates for cluster 3. The bins included in cluster 4 were highly variable and represented areas of the surface that were dissimilar to the three primary regions, exhibiting anomalously low diffusion rates and/or residence times for C12 probe molecules. It is interesting to note that many of the clusters overlap significantly in each of the 6 dimensions, but these same clusters were detected even when running the clustering algorithm on only half of the bins.

Table 6.1 – Position and standard deviation for each cluster on the AHAPTES/PEG surface

Cluster	$log(\bar{v}_{dex}^{ads})$	$log(\bar{v}_{C12}^{ads})$	D_{dex}(μm^2/s)	D_{C12}(μm^2/s)	τ_{dex} (s)	τ_{C12} (s)	f
1 (green)	-0.07±0.05	0.43±0.30	0.14±0.04	0.20±0.03	0.24±0.02	0.43±0.10	0.37
2 (red)	0.12±0.18	0.06±0.34	0.24±0.04	0.12±0.07	0.27±0.05	0.39±0.09	0.35
3 (black)	-0.11±0.06	-0.27±0.22	0.22±0.05	0.13±0.05	0.24±0.02	0.38±0.09	0.25
4 (purple)	0.08±0.33	-0.26±0.17	0.14±0.04	0.07±0.02	0.42±0.33	0.31±0.04	0.03

Unsupervised clustering represents a robust and unbiased method to identify regions on a surface that share common probe behaviors. The accumulated data extracted from these regions therefore allows one to examine how probes interact with distinct chemical moieties on the surface without relying on assumptions about the nature or locations of specific chemistries that might be present, or a model-dependent analysis of ensemble-averaged measurements. As representative examples, the diffusive step size and residence time data from two clusters on an AHAPTES/PEG photopatterned surface are shown in Figure 6.2. Molecules exhibit distinctive dynamic behavior on each region of the surface, where a region represents the sum of the pixels associated with a given cluster. The diffusion coefficient for fatty acid probe molecules on the region of the surface characterized by cluster 1 (region 1) was distinctly slower than that of the fatty acid probe molecules on the region associated with cluster 2 (Figure 6.2.a). The opposite was true for the dextran probe molecules which moved markedly more quickly on region 1 than on region 2 (Figure 6.2.b). Furthermore, fatty acid probes exhibited much longer residence times on region 2 than on region 1 (Figure 6.2.c). The residence time distributions of dextran molecules were indistinguishable between chemically-distinct regions on the surface (Figure 6.2.d).

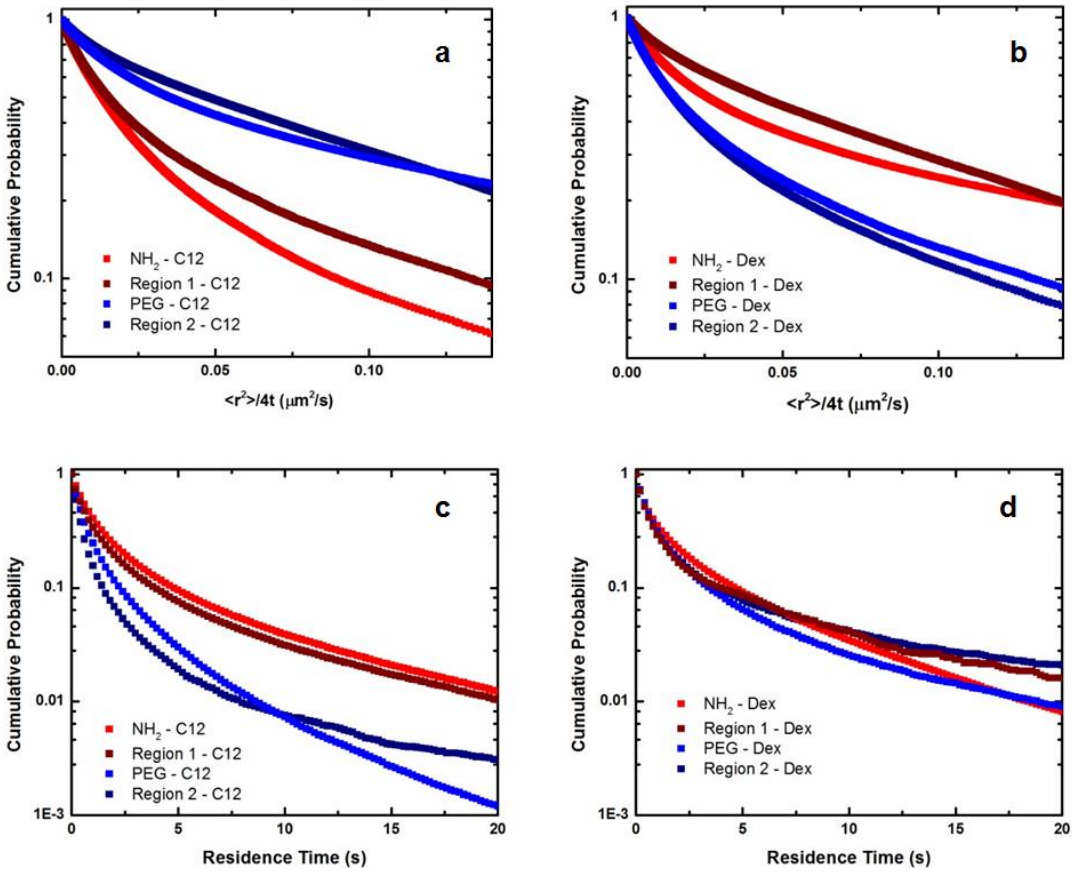

Figure 6.2 – Cumulative squared displacement distributions for fatty acid (a) and dextran (b) on regions 1 and 2 as well as distributions from homogeneous AHAPTES and PEG surfaces. Region 1 and AHAPTES displacements are indicated in red while region 2 and PEG squared displacements are indicated in blue. Residence time distributions for fatty acid (c) and dextran (d) on both clusters and homogeneous PEG (blue) and AHAPTES (red)

The statistical distributions associated with molecular dynamic behavior drawn from the clusters identified on heterogeneous surfaces were compared to data acquired from control homogeneous surfaces. The diffusive squared displacements and residence times of both the dextran and fatty

acid probes from region 1 closely matched those measured from a homogeneous AHAPTES (NH_2) surface. Similarly, both probes on region 2 had behavior that resembled the dynamics of the molecules on a homogeneous PEG surface (Figure 6.2). Moreover, due to the similar desorption and diffusion behavior on regions 2 and 3, we also identified region 3 with the back-filled PEG surface. The area fraction represented by the AHAPTES-like cluster (37%) was slightly less than expected based on the grid size (56%) but this was most likely due to imperfect photopatterning and backfilling. While the agreement between statistical distributions was fairly good in these cases, we note that the behavior of probes on the various regions of the photopatterned surface is not necessarily expected to be exactly the same as on homogeneous surfaces, primarily due to the differences in deposition procedures. For example, during the patterning process, there is potential for PEG silanes to react with the sparse, but still present, reactive groups remaining in an AHAPTES coated region, creating regions of mixed surface chemistry. Furthermore, the removal and backfilling process may yield lower quality monolayers than the freshly deposited PEG on pristine surfaces. The ability of the unsupervised clustering approach to identify two types of PEG regions (presumably observed because of subtle variations in imaging conditions across the field of view) highlights the robustness of this method and the fact that it is unnecessary to make assumptions about the spatial locations of the various clusters.

In general, the characterization approach described here can provide information that allows one to compare, in a functional way, the local surface chemistry of heterogeneous surfaces to the chemistry on separate homogeneous surfaces. Combined, these data shows that the unsupervised clustering approach permits one to accurately measure the distinctive dynamic behaviors of multiple types of probe molecule on specific surface chemistries, without any knowledge of the

locations of the particular chemical regions.

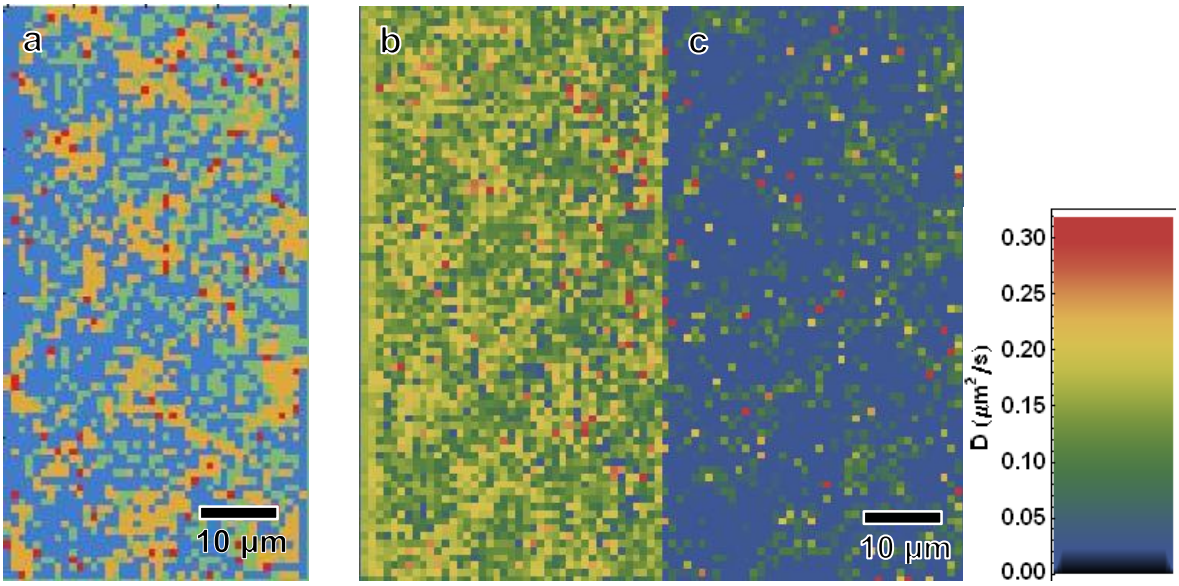

Figure 6.3 – (a) Cluster map of AHAPTES (grid lines) and PEG (squares) photopatterned surface. Orange is cluster 1, green is cluster 2, blue is cluster 3, and red is cluster 4. MAPT images of average diffusion coefficient for (b) dextran probe and (c) fatty acid probe with the values for diffusion coefficients indicated by the color table to the right.

A natural extension of this clustering approach was to indicate the identification of each bin on a two-dimensional array as shown in Figure 6.3. After comparing the data from the clusters to those obtained from homogeneous surfaces, a most probable surface chemistry was determined for each region on the surface with the two PEG-like clusters (clusters 2 and 3) plotted as green and blue while the AHAPTES-like cluster (cluster 1) was indicated in yellow (Figure 6.3.a). The red pixels (cluster 4) were locations associated with very high adsorption rates and long surface residence times. These pixels did not correspond to any surface chemistry studied thus far, which suggests that they were potentially defect sites (i.e. strong binding sites) in the monolayer.

To demonstrate the utility of the clustering analysis, MAPT images of the diffusion coefficient for C12 (Figure 6.3.b) and dextran (Figure 6.3.c) are shown for comparison. In these "maps", each bin is assigned a color corresponding to the local value of the mean diffusion coefficient that was extracted from the accumulated trajectories. These images show that each bin has a subtly varying diffusion coefficient from those around it making a determination of the chemistry on each region ambiguous. Furthermore, the cluster map provides much greater contrast between regions than the MAPT images allowing for easier visualization. These differences are most readily explained by the use of multiple dimensions for identification in the cluster map method, while MAPT images display data for one variable at a time.

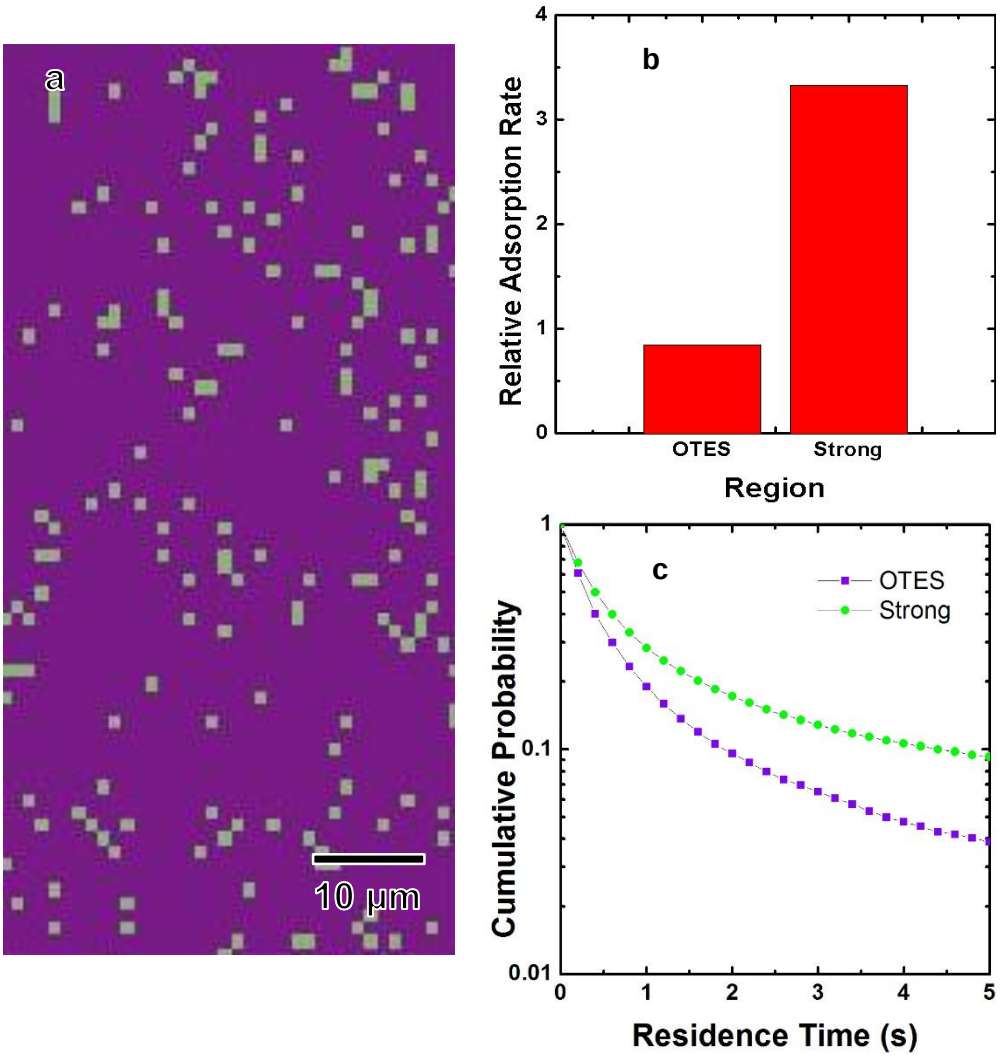

Figure 6.4 – (a) Cluster map of a homogeneous OTES surface, green pixels represent locations of anomalously strong adsorption and the purple represents the remaining OTES matrix, (b) Relative adsorption rates for the purple regions compared to the green regions, normalized to the average adsorption rate across the entire surface (c) Cumulative residence time distributions for strong adsorption sites (green) and the rest of the surface (purple).

In addition to mapping intentionally heterogeneous surfaces, the clustering technique can add another dimension to studying nominally homogeneous surface chemistry. Figure 6.4.a shows a

cluster map of a macroscopically-homogeneous OTES surface. Despite the fact that the surface was not deliberately patterned, two clusters of pixels were identified on this surface; one cluster corresponded to regions of anomalously high molecular adsorption and longer C12 residence times. These anomalous regions represented only 6% of the surface area but contained 20% of the molecules observed throughout the experiment. The relative adsorption rates for each region of the surface are shown in figure 6.4.b normalized to the average adsorption rate across the entire area. The strong adsorption sites had an adsorption rate more than three times greater than that of the rest of the surface. Cumulative residence time distributions for both the strong adsorption sites and the rest of the surface are shown in figure 6.4.c showing that the C12 residence times on the strong adsorption sites were significantly longer than on the rest of the surface. An ensemble averaged approach would detect an average residence time of 1.25±0.01 while the OTES regions of the surface only had an average residence time of 1.21±0.02. There was also a significant difference in average adsorption rate, where the OTES regions exhibited an adsorption rate 15% lower than the ensemble average adsorption rate. This discrepancy highlights the usefulness of this clustering technique in analyzing even homogeneous surfaces where small heterogeneities can have a significant impact on the data obtained from the surface.

6.5 - Discussion

Using these techniques it was possible to extract single-molecule data from distinct regions on a laterally heterogeneous surface without the need for arbitrary selection of regions of interest. These data were compared to data obtained from nominally homogenous surfaces and found to be consistent with their anticipated surface chemistry. This allowed us to construct maps of the surface with each area identified as a particular surface chemistry.

An intriguing application of this work is to identify anomalous regions on the surface that can have a large impact on the results from ensemble-averaging techniques[3]. These regions are observed on almost every surface, including nominally homogeneous ones[3, 15, 22]. By independently identifying these regions and eliminating them from analysis or studying them in greater detail one can develop a greater understanding of the molecular processes in play.

Cluster maps, for the first time, assigned each pixel the most likely surface chemistry for that region using an unbiased machine-learning approach. Previous imaging techniques, such as MAPT, have relied on plotting values for a single variable making the simultaneous analysis of many variables very difficult. Instead of relying on an individual contrast mechanism and human-based selection of regions for surface identification one can use statistical analysis to generate "images" of surface chemistry. Unfortunately the resolution of these images is coarser than MAPT due to the requirement for greater statistical certainty (more trajectories per pixel). This limitation can potentially be improved by gathering larger numbers of trajectories, at the computational cost of longer image processing times.

Clustering performs better when the contrast in behaviors of the probes is large. This contrast lowers the likelihood that a given bin will be misidentified. An additional consideration for this technique is that molecular probes have widely varying affinities for differing surface chemistries. Therefore, probes must be selected to have relatively high affinity for the surfaces being analyzed. Otherwise, there will be large areas with insufficient data points for statistical comparison. For these experiments, we selected dextran and the C12 fatty acid because both had similar affinities for both PEG and AHAPTES monolayers. Furthermore, the probes exhibited diffusive behavior that was distinctly different for the two surface chemistries. The primary advantage of using two probes is the increased number of dimensions available for clustering analysis. A greater number of dimensions allows the algorithm to distinguish clusters even when the differences in a single dimension are modest.

Comparing absolute adsorption rate data on patterned surfaces to those obtained from homogeneous surfaces was not feasible due to subtle variations in experimental conditions, which can vastly alter the apparent adsorption rate. Laser intensity per area and bulk fluorescent probe concentrations are the primary causes of these fluctuations meaning that the relative adsorption rates on an individual surface are consistent and reproducible. However, diffusion and residence time were suitable for comparison between experiments because they did not depend significantly on variation in these parameters.

6.6 – Acknowledgements

The authors acknowledge support from the U.S. Department of Energy Basic Energy Sciences, Chemical Science, Geosciences, and Biosciences Division (DE-SC0001854).

6.7 - References

1. Lin, Q.; London, E., Altering hydrophobic sequence lengths shows that hydrophobic mismatch controls affinity for ordered lipid domains (rafts) in the multitransmembrane strand protein perfringolysin O. *Journal of Biological Chemistry* **2013,** 288, (2), 1340-1352.

2. Lingwood, D.; Simons, K., Lipid rafts as a membrane-organizing principle. *science* **2010,** 327, (5961), 46-50.

3. Mabry, J. N.; Skaug, M. J.; Schwartz, D. K., Single-Molecule Insights into Retention at a Reversed-Phase Chromatographic Interface. *Analytical Chemistry* **2014,** 86, (19), 9451-9458.

4. Kisley, L.; Chen, J.; Mansur, A. P.; Shuang, B.; Kourentzi, K.; Poongavanam, M.-V.; Chen, W.-H.; Dhamane, S.; Willson, R. C.; Landes, C. F., Unified superresolution experiments and stochastic theory provide mechanistic insight into protein ion-exchange adsorptive separations. *Proceedings of the National Academy of Sciences* **2014,** 111, (6), 2075-2080.

5. Cooper, J. T.; Peterson, E. M.; Harris, J. M., Fluorescence Imaging of Single-Molecule Retention Trajectories in Reversed-Phase Chromatographic Particles. *Analytical Chemistry* **2013,** 85, (19), 9363-9370.

6. Yamato, M.; Konno, C.; Utsumi, M.; Kikuchi, A.; Okano, T., Thermally responsive polymer-grafted surfaces facilitate patterned cell seeding and co-culture. *Biomaterials* **2002,** 23, (2), 561-567.

7. Mi, F.-L.; Lin, Y.-M.; Wu, Y.-B.; Shyu, S.-S.; Tsai, Y.-H., Chitin/PLGA blend microspheres as a biodegradable drug-delivery system: phase-separation, degradation and release behavior. *Biomaterials* **2002,** 23, (15), 3257-3267.

8. Noy, A., Chemical force microscopy of chemical and biological interactions. *Surface and Interface Analysis* **2006,** 38, (11), 1429-1441.

9. Vezenov, D. V.; Noy, A.; Ashby, P., Chemical force microscopy: probing chemical origin of interfacial forces and adhesion. *Journal of Adhesion Science and Technology* **2005,** 19, (3-5), 313-364.

10. Honciuc, A.; Baptiste, D. J.; Schwartz, D. K., Hydrophobic Interaction Microscopy: Mapping the Solid/Liquid Interface Using Amphiphilic Probe Molecules. *Langmuir* **2009,** 25, (8), 4339-4342.

11. Friedsam, C.; Gaub, H.; Netz, R., Probing surfaces with single-polymer atomic force microscope experiments. *Biointerphases* **2006,** 1, (1), MR1-MR21.

12. Ray, C.; Brown, J. R.; Akhremitchev, B. B., Rupture Force Analysis and the Associated Systematic Errors in Force Spectroscopy by AFM. *Langmuir* **2007,** 23, (11), 6076-6083.

13. Ray, C.; Brown, J. R.; Akhremitchev, B. B., Correction of Systematic Errors in Single-Molecule Force Spectroscopy with Polymeric Tethers by Atomic Force Microscopy. *The Journal of Physical Chemistry B* **2007,** 111, (8), 1963-1974.

14. Nelson, N.; Walder, R.; Schwartz, D. K., Single Molecule Dynamics on Hydrophobic Self-Assembled Monolayers. *Langmuir* **2013,** 28, (33), 12108-12113.

15. Walder, R.; Nelson, N.; Schwartz, D. K., Super-Resolution Surface Mapping using the Trajectories of Molecular Probes. *Nat. Commun.* **2011,** 2, 515.

16. Walba, D. M.; Liberko, C. A.; Korblova, E.; Farrow, M.; Furtak, T. E.; Chow, B. C.; Schwartz, D. K.; Freeman, A. S.; Douglas, K.; Williams, S. D., Self-assembled monolayers for liquid crystal alignment: simple preparation on glass using alkyltrialkoxysilanes. *Liquid crystals* **2004,** 31, (4), 481-489.

17. Honciuc, A.; Schwartz, D. K., Probing Hydrophobic Interactions Using Trajectories of Amphiphilic Molecules at a Hydrophobic/Water Interface. *J. Am. Chem. Soc.* **2009,** 131, (16),

5973-5979.

18. Honciuc, A.; Harant, A. W.; Schwartz, D. K., Single-Molecule Observations of Surfactant Diffusion at the Solution-Solid Interface. *Langmuir* **2008,** 24, (13), 6562-6566.

19. Monserud, J. H.; Schwartz, D. K., Effects of Molecular Size and Surface Hydrophobicity on Oligonucleotide Interfacial Dynamics. *Biomacromolecules* **2012,** 13, (12), 4002-4011.

20. Walder, R.; Kastantin, M.; Schwartz, D. K., High throughput single molecule tracking for analysis of rare populations and events. *Analyst* **2012,** 137, (13), 2987-2996.

21. Fraley, C.; Raftery, A. E. *MCLUST version 3: an R package for normal mixture modeling and model-based clustering*; DTIC Document: 2006.

22. Walder, R.; Nelson, N.; Schwartz, D. K., Single Molecule Observations of Desorption-Mediated Diffusion at the Solid-Liquid Interface. *Phys. Rev. Lett.* **2011,** 107, (15), 156102.

Bibliography

Acharya, H.; Vembanur, S.; Jamadagni, S. N.; Garde, S., Mapping hydrophobicity at the nanoscale: Applications to heterogeneous surfaces and proteins. *Faraday Discuss.* **2010,** 146, 353-365.

Adalsteinsson, T.; Yu, H., Lipid lateral diffusion in multi-bilayers, and in monolayers at the air/water and heptane/water interfaces. *Langmuir* **2000,** 16, (24), 9410-9413.

Allen, C. E.; Seebauer, E. G., Surface diffusivities and reaction rate constants: Making a quantitative experimental connection. *J. Chem. Phys.* **1996,** 104, (7), 2557-2565.

Amar, J. G.; Family, F., Critical cluster size: Island morphology and size distribution in submonolayer epitaxial growth. *Physical Review Letters* **1995,** 74, (11), 2066.

Amar, J. G.; Family, F., Kinetics of submonolayer and multilayer epitaxial growth. *Thin Solid Films* **1996,** 272, (2), 208-222.

Axelrod, D., Total internal reflection fluorescence microscopy in cell biology. *Traffic* **2001,** 2, (11), 764-774.

Axelrod, D.; Burghardt, T. P.; Thompson, N. L., Total internal reflection fluorescence. *Annual review of biophysics and bioengineering* **1984,** 13, (1), 247-268.

Axelrod, D.; Koppel, D.; Schlessinger, J.; Elson, E.; Webb, W., Mobility measurement by analysis of fluorescence photobleaching recovery kinetics. *Biophys. J.* **1976,** 16, (9), 1055-1069.

Axelrod, D.; Wang, M., Reduction-of-dimensionality kinetics at reaction-limited cell surface receptors. *Biophys. J.* **1994,** 66, (3), 588-600.

Baer, M. D.; Mundy, C. J., Toward an Understanding of the Specific Ion Effect Using Density Functional Theory. *J. Phys. Chem. Lett.* **2011,** *2*, 1088-1093.

Barone, P. W., Baik, S., Heller, D. A. & Strano, M. S. Near-infrared optical sensors based on single-walled carbon nanotubes. *Nat. Mater.* **4**, 86-U16, doi:10.1038/nmat1276 (2005).

Betzig, E. *et al.* Imaging Intracellular Fluorescent Proteins at Nanometer Resolution. *Science* **313**, 1642-1645, doi:10.1126/science.1127344 (2006).

Burgos, P.; Zhang, Z.; Golestanian, R.; Leggett, G. J.; Geoghegan, M., Directed single molecule diffusion triggered by surface energy gradients. *ACS Nano* **2009,** 3, (10), 3235-3243.

Bychuk, O. V.; O'Shaughnessy, B., Anomalous diffusion at liquid surfaces. *Physical Review Letters* **1995,** 74, (10), 1795.

Cacace, M. G.; Landau, E. M.; Ramsden, J. J., The Hofmeister Series: Salt and Solvent Effects on Interfacial Phenomena. *Q. Rev. Biophys.* **1997,** *30*, 241-277.

Calhoun, M. F., Sanchez, J., Olaya, D., Gershenson, M. E. & Podzorov, V. Electronic functionalization of the surface of organic semiconductors with self-assembled monolayers. *Nat. Mater.* **7**, 84-89, doi:10.1038/nmat2059 (2008).

Cang, H. *et al.* Probing the electromagnetic field of a 15-nanometre hotspot by single molecule imaging. *Nature* **469**, 385-+, doi:10.1038/nature09698 (2011).

Chan, V.; Graves, D. J.; McKenzie, S. E., The biophysics of DNA hybridization with immobilized oligonucleotide probes. *Biophys. J.* **1995,** 69, (6), 2243-2255.

Chandler, D., Interfaces and the driving force of hydrophobic assembly. *Nature* **2005,** 437, (7059), 640-647.

Cukier, R. I., The effect of surface diffusion on surface reaction rates. *The Journal of Chemical Physics* **1983,** 79, (5), 2430-2435.

Dobbs, K. D.; Doren, D. J., Dynamics of Molecular Surface Diffusion: Origins and Consequences of Long Jumps. *J. Chem. Phys.* **1992,** *97*, 3722-3735.

Doudevski, I.; Hayes, W. A.; Schwartz, D. K., Submonolayer island nucleation and growth kinetics during self-assembled monolayer formation. *Physical Review Letters* **1998,** 81, (22), 4927.

Doudevski, I.; Schwartz, D. K., Concentration dependence of self-assembled monolayer island nucleation and growth. *J. Am. Chem. Soc.* **2001,** 123, (28), 6867-6872.

Dudko, O. K.; Hummer, G.; Szabo, A., Theory, analysis, and interpretation of single-molecule force spectroscopy experiments. *Proceedings of the National Academy of Sciences* **2008,** 105, (41), 15755-15760.

Dyson, H. J.; Wright, P. E.; Scheraga, H. A., The role of hydrophobic interactions in initiation and propagation of protein folding. *Proceedings of the National Academy of Sciences* **2006,** 103, (35), 13057-13061.

Esfandiari, N. M. *et al.* Single-Molecule Imaging of Platinum Ligand Exchange Reaction Reveals Reactivity Distribution. *Journal of the American Chemical Society* **132**, 15167-15169, doi:10.1021/ja105517d (2010).

Fraley, C.; Raftery, A. E. MCLUST version 3: an R package for normal mixture modeling and model-based clustering; DTIC Document: **2006**.

Friedsam, C.; Gaub, H.; Netz, R., Probing surfaces with single-polymer atomic force microscope experiments. *Biointerphases* **2006,** 1, (1), MR1-MR21.

Gupta, N. *et al.* A versatile approach to high-throughput microarrays using thiol-ene chemistry. *Nat. Chem.* **2**, 138-145, doi:10.1038/nchem.478 (2010).

Hashimoto, F.; Tsukahara, S.; Watarai, H., Lateral diffusion dynamics for single molecules of fluorescent cyanine dye at the free and surfactant-modified dodecane-water interface. *Langmuir* **2003,** 19, (10), 4197-4204.

Heitzman, C. E.; Tu, H.; Braun, P. V., Two-dimensional diffusion of prodan on self-assembled monolayers studied by fluorescence recovery after photobleaching. *The Journal of Physical Chemistry B* **2004,** 108, (36), 13764-13770.

Hofmeister, F., Zur Lehre Von Der Wirkung Der Salze. *Arch. Exp. Pathol. Pharmakol.* **1888,** *24*, 247-260.

Honciuc, A.; Baptiste, D. J.; Schwartz, D. K., Hydrophobic Interaction Microscopy: Mapping the Solid/Liquid Interface Using Amphiphilic Probe Molecules. *Langmuir* **2009,** 25, (8), 4339-4342.

Honciuc, A.; Baptiste, D. J.; Campbell, I. P.; Schwartz, D. K., Solvent Dependence of the Activation Energy of Attachment Determined by Single Molecule Observations of Surfactant Adsorption. *Langmuir* **2009,** 25, (13), 7389-7392.

Honciuc, A.; Harant, A. W.; Schwartz, D. K., Single-Molecule Observations of Surfactant Diffusion at the Solution-Solid Interface. *Langmuir* **2008,** 24, (13), 6562-6566.

Honciuc, A.; Howard, A. L.; Schwartz, D. K., Single Molecule Observations of Fatty Acid Adsorption at the Silica/Water Interface: Activation Energy of Attachment. *J. Phys. Chem. C* **2009,** 113, (6), 2078-2081.

Honciuc, A.; Schwartz, D. K., Probing Hydrophobic Interactions Using Trajectories of Amphiphilic Molecules at a Hydrophobic/Water Interface. *J. Am. Chem. Soc.* **2009,** 131, (16), 5973-5979.

Höök, F.; Rodahl, M.; Brzezinski, P.; Kasemo, B., Energy dissipation kinetics for protein and antibody-antigen adsorption under shear oscillation on a quartz crystal microbalance. *Langmuir* **1998,** 14, (4), 729-734.

Horinek, D.; Serr, A.; Bonthuis, D. J.; Bostrom, M.; Kunz, W.; Netz, R. R., Molecular Hydrophobic Attraction and Ion-Specific Effects Studied by Molecular Dynamics. *Langmuir* **2008,** *24*, 1271-1283.

Huang, B., Bates, M. & Zhuang, X. W. Super-Resolution Fluorescence Microscopy. *Annu. Rev. Biochem.* **78**, 993-1016, doi:10.1146/annurev.biochem.77.061906.092014 (2009).

Huckabay, H. A.; Dunn, R. C., Hydration Effects on Membrane Structure Probed by Single Molecule Orientations. *Langmuir* 27, (6), 2658-2666.

Hughes, B.; Pailthorpe, B.; White, L., The translational and rotational drag on a cylinder moving in a membrane. *J. Fluid Mech.* **1981,** 110, 349-372.

Israelachvili, J. N.; Mitchell, D. J.; Ninham, B. W., Theory of self-assembly of hydrocarbon amphiphiles into micelles and bilayers. *Journal of the Chemical Society, Faraday Transactions 2: Molecular and Chemical Physics* **1976,** 72, 1525-1568.

Israelachvili, J.; Pashley, R., The hydrophobic interaction is long range, decaying exponentially with distance. *Nature* **1982,** 300, (5890), 341-342.

Janado, M.; Yano, Y.; Doi, Y.; Sakamoto, H., Peculiar Effects of Alkali Thiocyanates on the Activity Coefficients of Aromatic Hydrocarbons in Water. *J. Solution Chem.* **1983,** *12*, 741-754.

Jungmann, R. *et al.* Single-Molecule Kinetics and Super-Resolution Microscopy by Fluorescence Imaging of Transient Binding on DNA Origami. *Nano Lett.* **10**, 4756-4761, doi:10.1021/nl103427w (2010).

Jungwirth, P.; Winter, B., Ions at Aqueous Interfaces: From Water Surface to Hydrated Proteins. *Annu. Rev. Phys. Chem.* **2008,** *59*, 343-366.

Kastantin, M.; Langdon, B. B.; Chang, E. L.; Schwartz, D. K., Single-Molecule Resolution of Interfacial Fibrinogen Behavior: Effects of Oligomer Populations and Surface Chemistry. *J. Am. Chem. Soc.* **2011,** 133, (13), 4975-4983.

Ke, P. C.; Naumann, C. A., Hindered diffusion in polymer-tethered phospholipid monolayers at the air-water interface: a single molecule fluorescence imaging study. *Langmuir* **2001,** 17, (16), 5076-5081.

Kisley, L.; Chen, J.; Mansur, A. P.; Shuang, B.; Kourentzi, K.; Poongavanam, M.-V.; Chen, W.-H.; Dhamane, S.; Willson, R. C.; Landes, C. F., Unified superresolution experiments and stochastic theory provide mechanistic insight into protein ion-exchange adsorptive separations. *Proceedings of the National Academy of Sciences* **2014,** 111, (6), 2075-2080.

Krieger, J.; Tóth, K.; Langowski, J., Fluorescence correlation spectroscopy. **2001**.

Krogman, K. C., Lowery, J. L., Zacharia, N. S., Rutledge, G. C. & Hammond, P. T. Spraying asymmetry into functional membranes layer-by-layer. *Nat. Mater.* **8**, 512-518, doi:10.1038/nmat2430 (2009).

Kumar, A.; Bullard, R. L.; Patel, P.; Paslay, L. C.; Singh, D.; Bienkiewicz, E. A.; Morgan, S. E.; Rangachari, V., Non-Esterified Fatty Acids Generate Distinct Low-Molecular Weight Amyloid-B (Aβ42) Oligomers Along Pathway Different from Fibril Formation. *PLOS ONE* **2011,** *6*, e18759.

Kunz, W.; Lo Nostro, P.; Ninham, B. W., The Present State of Affairs with Hofmeister Effects. *Curr. Opin. Colloid In.* **2004,** *9*, 1-18.

Langdon, B. B.; Kastantin, M.; Schwartz, D. K., Apparent activation energies associated with

protein dynamics on hydrophobic and hydrophilic surfaces. *Biophys. J.* **2012,** 102, (11), 2625-2633.

Langdon, B. B.; Kastantin, M.; Walder, R.; Schwartz, D. K., Interfacial Protein-Protein Associations. *Biomacromolecules* **2013,** 15, (1), 66-74.

Langmuir, I., The Adsorption of Gases on Plane Surfaces of Glass, Mica and Platinum. *J. Am. Chem. Soc.* **1918,** *40*, 1361-1403.

Lieto, A. M.; Lagerholm, B. C.; Thompson, N. L., Lateral diffusion from ligand dissociation and rebinding at surfaces. *Langmuir* **2003,** 19, (5), 1782-1787.

Lin, Q.; London, E., Altering hydrophobic sequence lengths shows that hydrophobic mismatch controls affinity for ordered lipid domains (rafts) in the multitransmembrane strand protein perfringolysin O. *Journal of Biological Chemistry* **2013**, 288, (2), 1340-1352

Lingwood, D.; Simons, K., Lipid rafts as a membrane-organizing principle. *science* **2010**, 327, (5961), 46-50

Livanec, P. W.; Dunn, R. C., Single-Molecule Probes of Lipid Membrane Structure. *Langmuir* **2008,** 24, (24), 14066-14073.

Long, F. A.; McDevit, W. F., Activity Coefficients of Nonelectrolyte Solutes in Aqueous Salt

Solutions. *Chem. Rev.* **1952,** *51*, 119-169.

Mabry, J. N.; Skaug, M. J.; Schwartz, D. K., Single-Molecule Insights into Retention at a Reversed-Phase Chromatographic Interface. Analytical Chemistry **2014**, 86, (19), 9451-9458

Malec, A. D.; Wu, D. G.; Louie, M.; Skolimowski, J. J.; Majda, M., Gibbs monolayers at the air/water interface: Surface partitioning and lateral mobility of an electrochemically active surfactant. *Langmuir* **2004,** 20, (4), 1305-1310.

Malone, S. M.; Schwartz, D. K., Polar and azimuthal alignment of a nematic liquid crystal by alkylsilane self-assembled monolayers: Effects of chain-length and mechanical rubbing. *Langmuir* **2008,** 24, (17), 9790-9794.

Marshall, S. T.; O'Brien, M.; Oetter, B.; Corpuz, A.; Richards, R. M.; Schwartz, D. K.; Medlin, J. W., Controlled selectivity for palladium catalysts using self-assembled monolayers. *Nat. Mater.* **2010,** 9, (10), 853-858.

Meyer, E. E.; Rosenberg, K. J.; Israelachvili, J., Recent progress in understanding hydrophobic interactions. *Proceedings of the National Academy of Sciences* **2006,** 103, (43), 15739-15746.

Mi, F.-L.; Lin, Y.-M.; Wu, Y.-B.; Shyu, S.-S.; Tsai, Y.-H., Chitin/PLGA blend microspheres as a biodegradable drug-delivery system: phase-separation, degradation and release behavior. Biomaterials **2002**, 23, (15), 3257-3267.

Miyagishi, S.; Okada, K.; Asakawa, T., Salt Effect on Critical Micelle Concentrations of Nonionic Surfactants, N-Acyl-N-Methylglucamides (Mega-N). *J. Colloid Interf. Sci.* **2001,** *238*, 91-95.

Monserud, J. H.; Schwartz, D. K., Effects of Molecular Size and Surface Hydrophobicity on Oligonucleotide Interfacial Dynamics. *Biomacromolecules* **2012,** *13*, 4002-4011.

Negishi, M.; Seto, H.; Hase, M.; Yoshikawa, K., How does the mobility of phospholipid molecules at a water/oil interface reflect the viscosity of the surrounding oil? *Langmuir* **2008,** 24, (16), 8431-8434.

Nelson, N.; Schwartz, D. K., Specific Ion (Hofmeister) Effects on Adsorption, Desorption, and Interfacial Diffusion. *J. Phys. Chem. Lett.* **2013,** 4, 4064.

Nelson, N.; Walder, R.; Schwartz, D. K., Single Molecule Dynamics on Hydrophobic Self-Assembled Monolayers. *Langmuir* **2013,** *28*, 12108-12113.

Noy, A., Chemical force microscopy of chemical and biological interactions. *Surface and Interface Analysis* **2006,** 38, (11), 1429-1441.

Para, G.; Jarek, E.; Warszynski, P., The Hofmeister Series Effect in Adsorption of Cationic Surfactants-Theoretical Description and Experimental Results. *Adv. Colloid Interface Sci.* **2006,** *122*, 39-55.

Patankar, N. A., On the Modeling of Hydrophobic Contact Angles on Rough Surfaces. *Langmuir* **2003,** 19, (4), 1249-1253.

Para, G.; Warszynski, P., Cationic Surfactant Adsorption in the Presence of Divalent Ions. *Colloid Surface A* **2007,** *300*, 346-352.

Patel, A. J.; Varilly, P.; Jamadagni, S. N.; Acharya, H.; Garde, S.; Chandler, D., Extended surfaces modulate hydrophobic interactions of neighboring solutes. *Proceedings of the National Academy of Sciences* **2011,** 108, (43), 17678-17683

Patel, A. J.; Varilly, P.; Jamadagni, S. N.; Hagan, M. F.; Chandler, D.; Garde, S., Sitting at the Edge: How Biomolecules use Hydrophobicity to Tune Their Interactions and Function. *The Journal of Physical Chemistry B* **2012,** 116, (8), 2498-2503.

Petersen, P. B.; Saykally, R. J., On the Nature of Ions at the Liquid Water Surface. *Annu. Rev. Phys. Chem.* **2006,** *57*, 333-364.

Rajamani, S.; Truskett, T. M.; Garde, S., Hydrophobic hydration from small to large lengthscales: Understanding and manipulating the crossover. *Proc. Natl. Acad. Sci. U. S. A.* **2005,** 102, (27), 9475-9480.

Rankin, B. M.; Ben-Amotz, D., Expulsion of Ions from Hydrophobic Hydration Shells. *J. Am. Chem. Soc.* **2013,** *135*, 8818-8821.

Ray, A.; Nemethy, G., Effects of Ionic Protein Denaturants on Micelle Formation by Nonionic Detergents. *J. Am. Chem. Soc.* **1971,** *93*, 6787-6793.

Ray, C.; Brown, J. R.; Akhremitchev, B. B., Correction of Systematic Errors in Single-Molecule Force Spectroscopy with Polymeric Tethers by Atomic Force Microscopy. *The Journal of Physical Chemistry B* **2007,** 111, (8), 1963-1974.

Ray, C.; Brown, J. R.; Akhremitchev, B. B., Rupture Force Analysis and the Associated Systematic Errors in Force Spectroscopy by AFM. *Langmuir* **2007,** 23, (11), 6076-6083.

Ray, C.; Brown, J. R.; Akhremitchev, B. B., Single-molecule Force Spectroscopy Measurements of "Hydrophobic Bond" between Tethered Hexadecane Molecules. *The Journal of Physical Chemistry B* **2006,** 110, (35), 17578-17583.

Rief, M.; Oesterhelt, F.; Heymann, B.; Gaub, H. E., Single molecule force spectroscopy on polysaccharides by atomic force microscopy. *science* **1997,** 275, (5304), 1295-1297.

Roach, P.; Farrar, D.; Perry, C. C., Interpretation of protein adsorption: surface-induced conformational changes. *J. Am. Chem. Soc.* **2005,** 127, (22), 8168-8173.

Rust, M. J., Bates, M. & Zhuang, X. W. Sub-diffraction-limit imaging by stochastic optical reconstruction microscopy (STORM). *Nat. Methods* **3**, 793-795, doi:10.1038/nmeth929 (2006).

Saffman, P.; DelbrÃ¼ck, M., Brownian motion in biological membranes. *Proceedings of the National Academy of Sciences* **1975,** 72, (8), 3111-3113.

Sanghvi, A. B., Miller, K. P. H., Belcher, A. M. & Schmidt, C. E. Biomaterials functionalization using a novel peptide that selectively binds to a conducting polymer. *Nat. Mater.* **4**, 496-502, doi:10.1038/nmat1397 (2005).

Schmidt, C.; Zimmermann, R.; Gaub, H., Multilayer adsorption of lysozyme on a hydrophobic substrate. *Biophys. J.* **1990,** 57, (3), 577-588.

Schütz, G. J.; Schindler, H.; Schmidt, T., Single-molecule microscopy on model membranes reveals anomalous diffusion. *Biophys. J.* **1997,** 73, (2), 1073-1080.

Schwierz, N.; Horinek, D.; Netz, R. R., Anionic and Cationic Hofmeister Effects on Hydrophobic and Hydrophilic Surfaces. *Langmuir* **2013,** *29*, 2602-2614.

Selle, C.; Rckerl, F.; Martin, D. S.; Forstner, M. B.; KÃ¤s, J. A., Measurement of diffusion in Langmuir monolayers by single-particle tracking. *Physical Chemistry Chemical Physics* **2004,** 6, (24), 5535-5542.

Sharonov, A. & Hochstrasser, R. M. Wide-field subdiffraction imaging by accumulated binding of diffusing probes. *Proc. Natl. Acad. Sci. U. S. A.* **103**, 18911-18916, doi:10.1073/pnas.0609643104 (2006).

Skaug, M. J.; Mabry, J.; Schwartz, D. K., Intermittent molecular hopping at the solid-liquid interface. *Physical Review Letters* **2013,** 110, (25), 256101.

Steinbach, P. J., Filtering artifacts from lifetime distributions when maximizing entropy using a bootstrapped model. *Analytical Biochemistry* **2012,** 427, (1), 102-105.

Steinbach, P. J.; Ionescu, R.; Matthews, C. R., Analysis of Kinetics Using a Hybrid Maximum-Entropy/Nonlinear-Least-Squares Method: Application to Protein Folding. *Biophys. J.* **2002,** 82, (4), 2244-2255.

Tamada, K.; Kim, S.; Yu, H., Lateral diffusion of a probe lipid in biphasic phospholipid monolayers: liquid/gas coexistence films. *Langmuir* **1993,** 9, (6), 1545-1550.

Tanaka, K.; Manning, P. A.; Lau, V. K.; Yu, H., Lipid lateral diffusion in Dilauroylphosphatidylcholine/Cholesterol mixed monolayers at the air/water interface. *Langmuir* **1999,** 15, (2), 600-606.

Tanaka, K.; Yu, H., Lipase activity on lipid/polymer binary monolayers: lateral diffusion-controlled enzyme kinetics. *Langmuir* **2002,** 18, (3), 797-804.

Thomas, A. S.; Elcock, A. H., Direct Observation of Salt Effects on Molecular Interactions through Explicit-Solvent Molecular Dynamics Simulations: Differential Effects on Electrostatic and Hydrophobic Interactions and Comparisons to Poisson-Boltzmann Theory. *J. Am. Chem. Soc.*

2006, *128*, 7796-7806.

Thomas, A. S.; Elcock, A. H., Molecular Dynamics Simulations of Hydrophobic Associations in Aqueous Salt Solutions Indicate a Connection between Water Hydrogen Bonding and the Hofmeister Effect. *J. Am. Chem. Soc.* **2007,** 129, (48), 14887-14898.

Thompson, N. L., Fluorescence correlation spectroscopy. In *Topics in fluorescence spectroscopy*, Springer: 1999; pp 337-378.

Ulman, A., Formation and structure of self-assembled monolayers. *Chemical Reviews* **1996,** 96, (4), 1533-1554.

Venables, J., Rate equation approaches to thin film nucleation kinetics. *Philosophical Magazine* **1973,** 27, (3), 697-738.

Venables, J.; Spiller, G.; Hanbucken, M., Nucleation and growth of thin films. *Reports on Progress in Physics* **1984,** 47, (4), 399.

Vezenov, D. V.; Noy, A.; Ashby, P., Chemical force microscopy: probing chemical origin of interfacial forces and adhesion. *Journal of Adhesion Science and Technology* **2005,** 19, (3-5), 313-364.

Walba, D. M.; Liberko, C. A.; Korblova, E.; Farrow, M.; Furtak, T. E.; Chow, B. C.; Schwartz, D. K.; Freeman, A. S.; Douglas, K.; Williams, S. D., Self-assembled monolayers for liquid crystal alignment: simple preparation on glass using alkyltrialkoxysilanes. *Liquid crystals* **2004,** 31, (4), 481-489.

Walder, R.; Honciuc, A.; Schwartz, D. K., Directed Nanoparticle Motion on an Interfacial Free Energy Gradient. *Langmuir* **2009,** 26, (3), 1501-1503.

Walder, R.; Honciuc, A.; Schwartz, D., Phospholipid Diffusion at the Oil-Water Interface. *Journal of Physical Chemistry B* **2010,** 114, (35), 11484-11488.

Walder, R.; Kastantin, M.; Schwartz, D. K., High throughput single molecule tracking for analysis of rare populations and events. Analyst 2012, 137, (13), 2987-2996.

Walder, R.; Nelson, N.; Schwartz, D. K., Single Molecule Observations of Desorption-Mediated Diffusion at the Solid-Liquid Interface. *Physical Review Letters* **2011,** 107, (15), 156102.

Walder, R.; Nelson, N.; Schwartz, D. K., Super-resolution surface mapping using the trajectories of molecular probes. *Nat Commun* **2011,** 2, 515

Walder, R.; Schwartz, D. K., Single Molecule Observations of Multiple Protein Populations at the Oil-Water Interface. *Langmuir* **2010,** 26, (16), 13364-13367.

Walder, R.; Schwartz, D. K., Dynamics of protein aggregation at the oil-water interface characterized by single molecule TIRF microscopy. *Soft Matter* **2011**.

Wu, D. M., Liu, Z. W., Sun, C. & Zhang, X. Super-resolution imaging by random adsorbed molecule probes. *Nano Lett.* **8**, 1159-1162, doi:10.1021/nl0733280 (2008).

Xu, H. *et al.* Microcontact Printing of Dendrimers, Proteins, and Nanoparticles by Porous Stamps. *Journal of the American Chemical Society* **131**, 797-803, doi:10.1021/ja807611n (2008).

Yamamoto, M. *et al.* Patterning Reactive Microdomains inside Polydimethylsiloxane Microchannels by Trapping and Melting Functional Polymer Particles. *Journal of the American Chemical Society* **130**, 14044-14045, doi:10.1021/ja804803s (2008).

Yamato, M.; Konno, C.; Utsumi, M.; Kikuchi, A.; Okano, T., Thermally responsive polymer-grafted surfaces facilitate patterned cell seeding and co-culture. *Biomaterials* **2002**, 23, (2), 561-567.

Yan, Y. Y.; Gao, N.; Barthlott, W., Mimicking natural superhydrophobic surfaces and grasping the wetting process: A review on recent progress in preparing superhydrophobic surfaces. *Advances in Colloid and Interface Science* **2011,** 169, (2), 80-105.

Yang, Q.; Zhao, J., Hofmeister effect on the interfacial dynamics of single polymer molecules. *Langmuir* **2011,** 27, (19), 11757-11760.

Yebra, D. M., Kiil, S. & Dam-Johansen, K. Antifouling technology - past, present and future steps towards efficient and environmentally friendly antifouling coatings. *Prog. Org. Coat.* **50**, 75-104, doi:10.1016/j.porgcoat.2003.06.001 (2004).

Zhang, S. G. Fabrication of novel biomaterials through molecular self-assembly. *Nat. Biotechnol.* **21**, 1171-1178, doi:10.1038/nbt874 (2003).

Zhang, Y.; Cremer, P. S., Interactions between Macromolecules and Ions: The Hofmeister Series. *Curr. Opin. Chem. Biol.* **2006,** *10*, 658-663.

Zhong, Z.; Lowry, M.; Wang, G.; Geng, L., Probing Strong Adsorption of Solute onto C18-Silica Gel by Fluorescence Correlation Imaging and Single-Molecule Spectroscopy under RPLC Conditions. *Analytical Chemistry* **2005,** 77, (8), 2303-2310.